

---


Electronic Theses and Dissertations, 2020-

---

2020

## Multi-Element Multi-Datastream Visible Light Communication Networks

Sifat Ibne Mushfique  
*University of Central Florida*

 Part of the [Computer Engineering Commons](#)  
Find similar works at: <https://stars.library.ucf.edu/etd2020>  
University of Central Florida Libraries <http://library.ucf.edu>

This Doctoral Dissertation (Open Access) is brought to you for free and open access by STARS. It has been accepted for inclusion in Electronic Theses and Dissertations, 2020- by an authorized administrator of STARS. For more information, please contact [STARS@ucf.edu](mailto:STARS@ucf.edu).

---

### STARS Citation

Ibne Mushfique, Sifat, "Multi-Element Multi-Datastream Visible Light Communication Networks" (2020). *Electronic Theses and Dissertations, 2020-*. 367.  
<https://stars.library.ucf.edu/etd2020/367>

MULTI-ELEMENT MULTI-DATASTREAM VISIBLE LIGHT COMMUNICATION  
NETWORKS

by

SIFAT IBNE MUSHFIQUE  
M.S. University of Central Florida, 2018

A dissertation submitted in partial fulfillment of the requirements  
for the degree of Doctor of Philosophy  
in the Department of Electrical and Computer Engineering  
in the College of Engineering and Computer Science  
at the University of Central Florida  
Orlando, Florida

Fall Term  
2020

Major Professor: Murat Yuksel

© 2020 Sifat Ibne Mushfique

## **ABSTRACT**

Because of the exponentially increasing demand of wireless data, the Radio Frequency (RF) spectrum crunch is rising rapidly. The amount of available RF spectrum is being shrunk at a very heavy rate, and spectral management is becoming more difficult. Visible Light Communication (VLC) is a recent promising technology complementary to RF spectrum which operates at the visible light spectrum band (400 THz to 780 THz) and it has 10,000 times bigger bandwidth than radio waves (3 kHz to 300 GHz). Due to this tremendous potential, VLC has captured a lot of interest recently as there is already an extensive deployment of energy efficient Light Emitting Diodes (LEDs). The advancements in LED technology with fast nanosecond switching times is also very encouraging. One of the biggest advantages of VLC over other communication systems is that it can provide illumination and data communication simultaneously without needing any extra deployment. Although it is essential to provide data rate at a blazing speed to all the users nowadays, maintaining a satisfactory level in the distribution of lighting is also important. In this work, we present a multi-element multi-datastream (MEMD) VLC architecture capable of simultaneously providing lighting uniformity and communication coverage in an indoor setting. The architecture consists of a multi-element hemispherical bulb design, where it is possible to transmit multiple data streams from the bulb using multiple LED modules. We present the detailed components of the architecture and formulate joint optimization problems considering requirements for

several scenarios. We formulate an optimization problem that jointly addresses the LED-user associations as well as the LEDs' transmit powers to maximize the Signal-to-Interference plus Noise Ratio (SINR) while taking an acceptable illumination uniformity constraint into consideration. We propose a near-optimal solution using Geometric Programming (GP) to solve the optimization problem and compare the performance of this GP solution to low complexity heuristics. To further improve the performance, we propose a mirror employment approach to redirect the reflected LED beams on the wall to darker spots in the room floor. We compare the performance of our heuristic approaches to solve the proposed two-stage optimization problem and show that about threefold increase in average illumination and fourfold increase in average throughput can be achieved when the mirror placement is applied which is a significant performance improvement. Also, we explore the use case of our architecture to provide scalable communications to Internet-of-Things (IoT) devices, where we minimize the total consumed energy emitted by each LED. Because of the non-convexity of the problem, we propose a two-stage heuristic solution and illustrate the performance of our method via simulations.

## **ACKNOWLEDGMENTS**

First and foremost, I would like to thank my advisor Dr. Murat Yuksel for his continuous support and mentoring for this work from start to finish. This would not have been possible without his valuable advices and inputs. Special thanks goes to Dr. Ahmad Alsharoa as well, who was a co-author in most of my publications. I would also like to thank my dissertation committee members, Dr. Kenle Chen, Dr. Yaser Fallah, Dr. Nazanin Rehnavard, and Dr. Kyle Renshaw for their valuable time and feedback for improving this thesis. Many thanks to my lab colleagues as well for their help and support whenever I needed them. Also, many thanks to Computer Engineering department of UCF for providing all technical and material support for my thesis work.

And at last but not least, my deepest gratitude towards my family members who are the most important part of my life; specially my beloved parents - who are far away in Bangladesh but it seems they are always near to me, my wife - who has been a true life partner of mine, and my little daughter Suhaila - the apple of our eyes. I always pray and hope to be blessed by you people for my whole life.

## TABLE OF CONTENTS

LIST OF FIGURES .....	xii
LIST OF TABLES .....	xvi
CHAPTER 1 : INTRODUCTION .....	1
1.1 Thesis Contribution .....	4
1.2 Thesis Organization .....	7
CHAPTER 2 : RELATED WORK .....	10
2.1 Improving Data Rates in VLC .....	10
2.2 Maintaining LOS Property in VLC .....	12
2.3 Modulation Schemes and Dimming Support in VLC .....	13
2.3.1 On-Off Keying (OOK) .....	14
2.3.2 Pulse Position Modulation (PPM) .....	14
2.3.3 Color Shift Keying (CSK).....	15
2.3.4 Orthogonal Frequency Division Multiplexing (OFDM).....	16

2.3.5	Dimming Support .....	17
2.4	Hybrid VLC Schemes .....	17
2.5	Categorization of Previous Works Based on the Number of Transmitters and Datastreams Involved .....	20
<b>CHAPTER 3 : MULTI-ELEMENT BULB ARCHITECTURE .....</b>		<b>24</b>
3.1	The Bulb .....	25
3.1.1	Design of the Bulb .....	25
3.1.2	Layered Bulb Structure and Placement of LEDs .....	28
3.2	Mobile Receiver Units .....	30
3.3	RF/FSO Hybrid LOS Management .....	31
3.3.1	Establishing the Link .....	32
3.3.2	Maintaining the Link .....	33
3.3.3	Terminating the Link.....	34
<b>CHAPTER 4 : OPTIMAL MULTI-ELEMENT BULB DESIGN FOR HIGH SIGNAL-TO-INTERFERENCE RATIO AND SMOOTH LIGHTING .....</b>		<b>35</b>
4.1	Parameters .....	35
4.2	Link Model and SIR Calculation .....	36
4.3	Optimization Objective .....	39



4.4	MAX_SIR: Maximum SIR Problem .....	41
4.5	MAX_SIR_LQ: Maximum SIR with Lighting Quality (LQ) Constraint .....	43
4.6	Heuristic Design for Nonlinearity .....	44
4.7	Simulation Results .....	45
4.7.1	Calculation Method .....	45
4.7.2	Solution for Best Bulb Configuration .....	47
4.7.3	Effect of Power Constraints .....	48
4.7.4	Effect of Divergence Angle .....	50
4.7.5	The Three-Region Behavior .....	53
4.8	Chapter Summary .....	55
CHAPTER 5 : OPTIMIZATION OF SINR AND ILLUMINATION UNIFORMITY IN MEMD VLC NETWORKS .....		56
5.1	System Model .....	57
5.1.1	Assumptions and Notation .....	57
5.1.2	LED-User Association .....	60
5.1.3	Channel Model .....	60
5.1.4	SINR Calculation .....	62
5.1.5	Illumination Uniformity .....	62

5.2	Problem Formulation . . . . .	63
5.2.1	NP-Completeness . . . . .	66
5.3	Near Optimal Solution . . . . .	69
5.3.1	Geometric Programming . . . . .	69
5.3.2	GP Standard Form Transformation . . . . .	72
5.4	Heuristic Solutions . . . . .	73
5.4.1	SINR First Approach (SFA) . . . . .	74
5.4.2	Uniformity First Approach (UFA) . . . . .	76
5.4.3	Computational and Memory Complexity . . . . .	80
5.5	Simulation Results . . . . .	81
5.5.1	UFA versus SFA . . . . .	84
5.5.2	GP Solution versus UFA . . . . .	84
5.5.3	Effect of Number of Users on UFA . . . . .	86
5.5.4	UFA with Different Room Sizes . . . . .	87
5.5.5	Effect of Divergence Angles with UFA . . . . .	88
5.5.6	Effect of Bulb Radius on UFA . . . . .	89
5.5.7	Heatmaps of the Transmit Power of LEDs with UFA and GP . . . . .	90
5.6	Chapter Summary . . . . .	91

CHAPTER 6 : MIRRORVLC: OPTIMAL MIRROR PLACEMENT FOR MULTI-ELEMENT VLC NETWORKS .....	92
6.1 System Model .....	93
6.1.1 VLC Channel Model .....	95
6.1.2 Illumination Uniformity .....	99
6.1.3 LED-User Association .....	99
6.1.4 SINR Calculation .....	100
6.2 Problem Formulation and Solution .....	100
6.2.1 Design Problem .....	101
6.2.2 Communication Problem .....	104
6.3 Simulation Results .....	109
6.3.1 Placement of Mirrors .....	110
6.3.2 Performance Comparison among Mirror Placement approaches .....	112
6.3.3 Comparison between NUA, SSA-LED and SSA-User .....	113
6.3.4 Effect of Divergence Angle .....	114
6.4 Chapter Summary .....	116
 CHAPTER 7 : RESOURCE OPTIMIZATION IN VISIBLE LIGHT COMMUNICATION FOR INTERNET OF THINGS .....	 117
7.1 System Model .....	118

7.1.1	Assumptions and Notation .....	118
7.1.2	LED-User Association .....	118
7.1.3	Channel Model .....	118
7.1.4	SINR Calculation .....	119
7.1.5	Illumination Uniformity .....	119
7.2	Problem Formulation .....	119
7.3	Problem Solution .....	120
7.3.1	Low Complexity Two-Stage Solution (TSS) .....	121
7.4	Simulation Results .....	124
7.4.1	Effect on Total Power Consumption of the System .....	125
7.4.2	Effect on Data Rate .....	127
7.4.3	System Analysis for different LED Divergence Angles .....	128
CHAPTER 8 : SUMMARY AND FUTURE DIRECTIONS .....		131
APPENDIX A : LIST OF ABBREVIATIONS .....		134
APPENDIX B : LIST OF SYMBOLS .....		137
LIST OF REFERENCES .....		141

## LIST OF FIGURES

Figure 1.1	Comparison between Single-datastream and Multi-datastream VLC architectures. . . . .	3
Figure 3.1	Sample design of a MEMD VLC architecture. . . . .	25
Figure 3.2	Placement of transmitters in the bulb. . . . .	26
Figure 3.3	Calculation of maximum number of layers in the bulb. . . . .	29
Figure 4.1	Transmitter and receiver angles. . . . .	38
Figure 4.2	Flow diagram of the optimization. . . . .	40
Figure 4.3	Nonlinearity of the obj. function: SIR against divergence angle and number of layers. . . . .	45
Figure 4.4	Convergence of $I_s$ values for $k_1 = 11$ , $k_2 = 14$ and $\theta_d = 26$ degrees. . . . .	46
Figure 4.5	$SIR$ and $I_s$ values versus power constraint for $MAX\_SIR$ and $MAX\_SIR\_LQ$ . . . . .	48
Figure 4.6	Objective function output versus power constraint. . . . .	49
Figure 4.7	Avg. SIR vs. divergence angle for two layers of LEDs. . . . .	50
Figure 4.8	Illumination variation vs. divergence angle for two layers of LEDs. . . . .	51

Figure 4.9	Obj. function output versus Divergence angle for different number of layers. . .	52
Figure 4.10	Effect of divergence angle comparison between 2 and 6 layers. . . . .	53
Figure 4.11	The 3-region behavior. . . . .	54
Figure 5.1	Transmitters and Receivers in a VLC channel model. . . . .	61
Figure 5.2	Comparison with minimum $v$ -cut problem. . . . .	66
Figure 5.3	A case of interference for an user: LEDs L1, L2 and L3 are assigned to user 1, 2 and 3 respectively. In this case, received power from L2 and L3 will be considered as interference at user 1 - since these LEDs are assigned to user 2 and user 3. . . . .	74
Figure 5.4	Effect of $\tau$ on throughput and uniformity for UFA. . . . .	78
Figure 5.5	Runtime vs. No. of users for UFA and GP. $M = 65$ . . . . .	79
Figure 5.6	Difference in signal strength across the room floor assuming the hemispherical bulb in the center of the ceiling. . . . .	81
Figure 5.7	Comparison between UFA and SFA. . . . .	85
Figure 5.8	Comparison between GP and UFA with $M = 65$ and $\theta_d = 50^\circ$ . . . . .	85
Figure 5.9	Throughput and Uniformity for many users for UFA. $M = 391$ and $\theta_d = 40^\circ$ . . . . .	87
Figure 5.10	Throughput and Uniformity for different room sizes. $M = 391$ and $\theta_d = 40^\circ$ . . . . .	87
Figure 5.11	Comparison between different divergence angles in UFA. $M = 391$ . . . . .	88
Figure 5.12	Comparison between different bulb radius in UFA. $M = 391$ and $\theta_d = 40^\circ$ . . . . .	89
Figure 5.13	Heatmaps of the transmit power of LEDs with UFA and GP. . . . .	90

Figure 6.1	System Model. . . . .	94
Figure 6.2	Comparison between an NLoS channel with mirror and LoS channel by using a mirror image of user $u$ to the wall from the same LED $m$ . . . . .	97
Figure 6.3	Figure explaining different values of $\chi_{mz}$ in a room wall. $\chi_{mz} = \xi_z$ when grid position $z$ is inside the reflection area of LED $m$ (marked in orange) and 0 otherwise. Grid positions with mirrors are marked in light blue. . . . .	98
Figure 6.4	A case of conflict for an user-by-user approach such as SSA-User: both User 1 and User 2 are getting strongest signal from LED L1, but since L1 is assigned to User 1 first, User 2 has to be assigned to L2, which provides the second strongest signal for User 2. . . .	107
Figure 6.5	Mirror placement heatmaps in four walls for different bulb radiuses and divergence angles. . . . .	110
Figure 6.6	Comparison between different mirror placement approaches for $NUA$ with $M = 391$ and $\theta_d = 30^\circ$ . . . . .	111
Figure 6.7	Comparison between different mirror placement approaches for $SSA - User$ with $M = 391$ and $\theta_d = 30^\circ$ . . . . .	112
Figure 6.8	Comparison between $NUA$ , $SSA - LED$ and $SSA - User$ with $M = 391$ and $\theta_d = 30^\circ$ . . . . .	114
Figure 6.9	Comparison between $NUA$ , $SSA - LED$ and $SSA - User$ for different divergence angle with 6 users. $M = 391$ and $R = 40cm$ . . . . .	115

Figure 7.1	Nearest User Assignment Approach in case of interference for an LED on the bulb. ....	121
Figure 7.2	Effect on Power Consumption of the System. ....	125
Figure 7.3	Average Transmit Power Decay Per User for $\theta_d = 20^\circ$ and $\theta_d = 80^\circ$ . ....	126
Figure 7.4	Effect on User Data Rate of the System. ....	127
Figure 7.5	System Analysis for different LED Divergence Angles. ....	128



## LIST OF TABLES

Table 4.1	Parameters .....	35
Table 4.2	Best results for MAX_SIR and MAX_SIR_LQ .....	47
Table 5.1	List of Key Symbols .....	59
Table 5.2	Simulation Parameters .....	83
Table 7.1	Simulation Parameters .....	124

# CHAPTER 1

## INTRODUCTION

In the past few decades, the worldwide demand for wireless broadband data has been increasing exponentially [1] because of the popularity of smart-phones, laptops, and tablets. As Light Emitting Diodes (LEDs) appropriation is on an ascent [2] it is expected that a large portion of the enlightenment will be by means of LEDs in the following 10-15 years. Utilizing these LEDs, Visible Light Communication (VLC) is expected to be one of the primary wellsprings of communication in the near future. This change is driven by several characteristics of VLC, such as non-interference with Radio Frequency (RF) signals, enhanced security (unlike RF signals, light can't pass through walls, and thus the chance of eavesdropping is virtually nonexistent), spatial reuse (with the help of highly directional light beams), safety (visible light does not have any health hazard unlike high frequency Infra-Red), energy efficiency (LEDs are highly controllable and energy efficient light sources as they typically use 80% less energy than the traditional incandescent lights and last 25 times longer [3]), easy implementation into existing infrastructure as LEDs are already getting widely deployed, and low cost since only a few upgrades of existing lighting infrastructure are needed rather than the initial set up cost of an entire communication system. In the current circumstances, LEDs are ending up being more accessible and solid-state circuitry to drive the LEDs is becoming lower in cost. Lighting is transitioning to solid-state lighting technologies and

visible light is offering an excellent opportunity for combining both lighting and mobile wireless communications, particularly at indoor settings [4, 5].

Most of the VLC literature can be categorized into four groups based on the number of transmitters and datastreams involved in the design. Two of them are single-datastream designs - *Single Element Single Datastream (SESD)* and *Multi Element Single Datastream (MESD)*. In single-element designs like SESD, the vast majority of the work has concentrated on diffuse optics [6] and diversity combining [7, 8] for downloading a datastream to devices in a room. In contrast to the diffuse optics, multi-element VLC in designs such as MESD enables different datastreams to be transmitted simultaneously with the help of several LED transmitters with narrow divergence angles. The existing work in the literature related to multi-element VLC are on expanding the Field-Of-View (FOV), range, and rate of communication, and significant advances have been attained in increasing what is possible with a single element, i.e., a transmitter (an LED), receiver (a Photo-Detector (PD)), or transceiver (an LED-PD pair) [9]. Coming to the comparison between single-datastream and multi-datastream designs, single-datastream designs like SESD or MESD have one major drawback - different data downloads cannot be sent at the same time from light source(s), which necessitates a time sharing. This single-datastream design approach, thus, cannot exploit spatial reuse possibilities. For instance, if there are multiple receivers in a room, since all light sources are working towards sending a single datastream at a time, another receiver cannot be sent a different data download simultaneously. The other two multi-datastream design types, *Single Element Multi Datastream (SEMD)* and *Multi Element Multi Datastream (MEMD)* are able to resolve this problem. Although SESD or MESD designs have the issue of unavailability of data

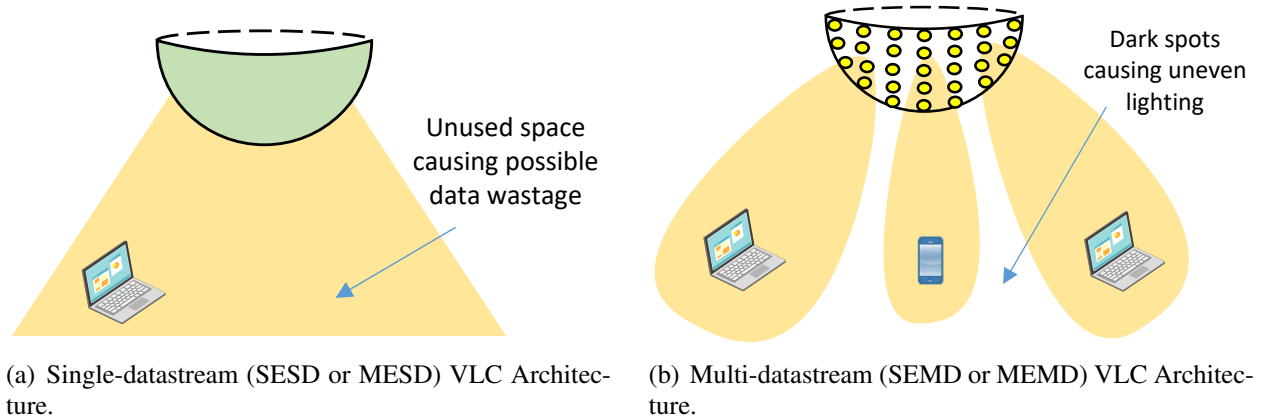


Figure 1.1: Comparison between Single-datastream and Multi-datastream VLC architectures.

to multiple receivers simultaneously, that can be handled by MEMD designs. Multi-element VLC modules in MEMD designs can significantly improve the efficiency of data transmission as they can take full advantage of directionality of light by modulating each LED transmitter with a different datastream. By designing these multi-element modules conformal to spherical shapes, one may also provide uniform light coverage across the room. Fig. 1.1 makes a visual comparison of single-datastream and multi-datastream VLC architectures.

Considering the limited functionality and efficiency of the single element VLC architecture, the goal of this work is to explore designs using many elements with narrow FOV. In particular, we use multi-element VLC modules for simultaneous transfer of multiple datastreams and attain higher spatial reuse in short ranges due to the dense grid formed by the narrow FOV LEDs. Unlike the works in the literature that focus on integrating multiple spotlighting mechanism into a single light source and creating an apparently large FOV, our research focuses on unicast datastream from individual spotlight at an overhead light source [10]. This approach will likely be more practical for

the emerging Internet-of-Things (IoT) applications that involve closely placed receivers accessing the VLC resources. Further, since most of these IoT receivers will not be highly mobile, handover across spotlights will not be prohibitively costly.

Despite their large potential in addressing wireless data provisioning to many IoT devices in dense and short-range settings, multi-datastream designs present two key challenges. First, since each LED can be assigned to a different receiver in the room, this assignment needs to be updated every time a receiver moves around. Second, due to the narrow LED beams (or spotlights as we called it above), uniformity of lighting in the room can deteriorate too much to the level that it becomes unacceptable for casual human life. Narrow light beams allow us to attain high spatial reuse but, in return, they bring the lighting uniformity problem. In this thesis, we address these two challenges and deal with the problem of optimizing the design of our MEMD VLC architecture so that we can have a decent overall communication quality for the receivers with as uniform lighting as possible across the room floor while dynamically associating/assigning LEDs to individual receivers to maximize the aggregate data rate being provided to the receivers inside the room. We formulate several optimization problems where we vary different system and room parameters, and study the multi-element VLC architecture under various contexts.

## **1.1 Thesis Contribution**

This thesis makes the following contributions and findings, some of which were published in our previous works [11, 12, 13, 14].

- We explore the trade-off between using small and large divergence angles in an MEMD VLC architecture with relatively narrow divergence angles. The bulb is supported with a LoS alignment protocol to steer the datastreams to individual or group of LED boards corresponding to a particular receiver in the room [15]. We formulate the LED placement on the bulb as an optimization problem under power constraints. Specifically, these constraints are applied as the maximum power that can be assigned to each LED.
- We analyze the performance of the multi-element bulb architecture based on several metrics such as the positions of the receivers, divergence angle of the transmitters with the help of this optimization problem which takes both uniformity of lighting and signal strength indicated by SIR across the room into consideration.
- Considering the power constraint on the bulb, we find out that no matter how much we increase the power constraint or the number of LEDs on the multi-element bulb, maximum SIR saturates after a certain point which is detailed in Section 4.7.3.
- We study the effect of divergence angle of the LEDs over the objective function of the optimization problem. Furthermore, we find out that based on the SIR, we can divide the room into three separate regions which demonstrate different communication characteristics. These discoveries are detailed in Section 4.7.
- We also formulate an optimization problem that jointly addresses the LED-user associations as well as the LEDs' transmit powers in order to maximize the SINR while taking an acceptable illumination uniformity constraint into consideration.

- In order to show the necessity of near-optimal / heuristic solution, we prove that our formulated optimization problem is NP-Complete.
- We propose a near-optimal solution using Geometric Programming (GP) to solve the optimization problem, and compare the performance of this GP solution to low complexity heuristic approaches.
- From our simulations, for reasonable assumptions about the LEDs and bulb size, we observe that one of our heuristic approaches can attain about 10 Mbps minimum throughput while keeping illumination uniformity higher than 0.7 for up to 20 receivers in a  $36m^2$  room.
- We also explore the capabilities of our MEMD VLC architecture for providing scalable communications to Internet-of-Things (IoT) devices by proposing an optimization problem aiming to minimize the total consumed energy emitted by each LED taking into consideration the LEDs power budget, users perceived quality of service (QoS), LED-user associations, and illumination uniformity constraints.
- Because of the non-convexity of the problem, we solve it in two stages: (1) We design an efficient algorithm for LED-user association for fixed LED powers, and (2) using the LED-user association, we find an approximate solution based on Taylor series to optimize the LEDs power. We devise a heuristic solution based on this approach and illustrate the performance of our method via simulations.

- We propose a mirror employment approach (MirrorVLC) in order to improve the SINR of the system and overall illumination uniformity of the room by redirecting the reflected LED beams on the wall to darker spots.
- We formulate a joint optimization problem for the mirror placement approach and propose a solution in two stages - one for illumination uniformity and another for SINR. For the solution of the second stage, we devise three heuristic approaches.
- We compare between our solutions based on the three heuristic approaches and also compare them with the typical approach without employing the mirrors via simulation. We show that up to threefold increase in average illumination and fourfold increase in average throughput can be achieved using a mirror placement approach.

## 1.2 Thesis Organization

The rest of the thesis is organized as follows:

Chapter 2 surveys the relevant work and describes the motivation behind our work on multi-element VLC systems. The related works on VLC are elaborated based on several things like improvement on data transmission speed, modulation schemes, maintaining LoS property, and hybrid RF-VLC architectures. We also categorize the related work in VLC based on the number of transmitters and data-streams in detail.



In Chapter 3, we propose a multi-element bulb and describe in detail about the components of the whole architecture. We also describe the proposed RF/FSO hybrid LoS management scheme.

In Chapter 4, we present a detailed discussion on the bulb design optimization problem based on LED divergence angle along with a detail formulation of the problem. We also describe the simulation setup with detail explanation of the results.

In Chapter 5, we formulate an optimization problem that jointly addresses the LED-user associations as well as the LEDs transmit powers in order to maximize the SINR while taking an acceptable illumination uniformity constraint across a room into consideration. We propose a near-optimal solution using GP to solve the optimization problem, and compare the performance of this GP solution to low complexity heuristics.

To further improve the performance, in Chapter 6, we propose a mirror employment approach to redirect the reflected LED beams on the wall to darker spots in the room floor. In order to maximize the average throughput and illumination, we formulate an optimization problem to obtain optimum mirror placement, power allocation and LED-user association. As the problem is NP-complete, we propose a two-stage solution to the optimization problem. As a part of the solution of the first stage, we introduce several mirror placement approaches and analyze their performance. To deal with heavy computation complexity in the second stage with the communication problem, we present multiple heuristic approaches to solve it with a detailed analysis on their performance. Our simulations indicate significant performance improvement with the mirror placement approach.

In Chapter 7, we explore the use case of our architecture to provide scalable communications to Internet-of-Things (IoT) devices, where our optimization problem aims to minimize the total consumed energy emitted by each LED taking into consideration the LEDs' power budget, users perceived quality of service, LED-user associations, and illumination uniformity constraints. Because of the non-convexity of the problem, we propose a two-stage heuristic solution and illustrate the performance of our method via simulations.

Finally, we summarize our work and discuss briefly about the current progress on the expansion plus lay out some possible future work plans in Chapter 8.

## **CHAPTER 2**

### **RELATED WORK**

Optical communication can be utilized in different structures to serve quick correspondence interfaces in remote areas. Fiber optic communication has the most acknowledgment as a wired innovation and it is able to do rapid transmission. Despite the fact that FSO communication frameworks utilize a similar convention and same type of transmitters and receivers, this innovation is as yet thought to be in its early childhood. In any case, years of research have been making this innovation one stride ahead to deploy it commercially. Related research works on VLC can be categorized on some important factor, which are described below.

#### **2.1 Improving Data Rates in VLC**

In the realm of communication, data rate of information transfer is an imperative factor. However, the data rate relies on many factors, such as transmission capacity, impacts, region of scope, impedance, adjustment and method of communication. In [16], the authors demonstrate a bidirectional 1.25 Gbits/sec indoor Home Access Network project using power line communication in the backbone and RF/VLC as front-end. In this case, the VLC is used as a broadcast medium to support multiple users. In [8], the receiver has three different elements directed in three direc-

tions, motivated from the concept of angle diversity to facilitate handover between the elements depending on signal strength. The implementation uses infra-red front end instead of LEDs, while the authors claim that the system is compatible with LEDs. The LOS system uses angle-diversity transceivers enabling discrete beam steering. Three transmitting and receiving elements are used in each transceiver giving an overall field of view of 25 x 8 degrees and a transmission range of 3 meters. Measurements show that the system can operate at a bit error rate below  $10^{-9}$  without channel coding and the handover between cells is 400 ns. A detailed demonstration of high-definition (HD) video embedded in gigabit Ethernet stream using this system is presented as well.

Speeds upto 1.28 Terabit/s has also been achieved using Wavelength-division Multiplexing (WDM) transmission techniques on laser beams [17]. A novel FSO framework is reviewed representing a noteworthy achievement in FSO communications. The framework incorporates a couple of novel terminals, which enable immediate and straightforward optical association with basic single mode fibers and incorporate a dedicated electronic control unit that adequately tracks the signal beam wandering because of atmospheric turbulence and mechanical vibrations. Assist change in the flag control adjustment is accomplished by methods for saturated Erbium-doped Fiber Amplifiers (EDFAs). These arrangements permit to understand another FSO framework, which is tried in a double pass FSO link between two towers in Pisa, Italy. At the point when the terminals are bolstered by normal WDM signals they permit enough power spending plan and edges to help a record high limit transmission (32 x 40 Gbits/sec), with a gigantic change of steadiness (six hours with no mistake burst). Amid day-long transmission, the framework conduct has been profoundly portrayed to associate any expansion of Bit Error Rate (BER) to the FSO control parameters.

All of these mentioned works are done on the basis of improving the data speed, although the architecture used in them is either single element with large FOV or the beams are highly directional like laser, so basically they neither consider simultaneous transmission of multiple data streams nor the uniformity of lighting across the room. Our work takes both of these into consideration and tries to optimize the design of the architecture based on that.

## **2.2 Maintaining LOS Property in VLC**

The LOS property of optical communication is a critical issue that needs to be addressed in any VLC system. In LOS communication, an optical link has to be established by aligning the transmitter and receiver and maintained to facilitate ongoing communication. We cover some of the mechanisms developed to address the LOS issue in this section. In [18], the authors propose two protocols: (i) a peer-to-peer protocol where the receiving elements provide a multi-hop path among them, and (ii) a peer-to-host protocol where the multi-hop path is provided within the base stations. The peer-to-peer protocol consists of a narrow beam and field of view from the proposed device and thereby can have good performance in terms of speed without a central host. The peer-to-host protocol, in contrast, is simpler and easy to implement; but, due to its diffuse link model and interference, it is less manageable for high data rates and requires an accessible host. The latter is proved better in a scenario with fewer number of user devices and the former in the scenario with more user devices.

Instead of using a light source with wide FOV, the work in [19] suggests using multiple spot light sources. According to the authors, the concept of ideal spot light results in an ideal cone of light which is focused and directed to provide both high data-rate VLC signal and bright light covering a small surface. It reduces multi-path distortion due to reflection of the signal off walls and objects. It is to be noted that these light sources are designed to be completely independent light sources. By focusing the light, large signal strength are obtained with fewer or smaller LEDs, which potentially simplifies the driver circuitry and reduces transmitter capacitance, leading to increased amount of bandwidth in result. The paper uses the concept that of a spotlight typically having all its LEDs in a small space, and if they are switched simultaneously, the LOS light from all the LEDs to all transmitter locations is synchronized, which is not case for uniform lighting. Joint optimization of illumination of communication has been studied in [20], where the authors compared two different LED driver schemes, analyzed the ripple effect on the filter of the receiver, and proposed two approximations to model the ripple interference. However, in our work, we emphasize on finding an optimum design for the multi-element architecture that is proposed for high spatial reuse.

### **2.3 Modulation Schemes and Dimming Support in VLC**

In VLC, the modulating signals can be used to switch LEDs at desired frequencies which contains information to be transmitted. Several modulation schemes are tried in VLC, which are discussed below -

### **2.3.1 On-Off Keying (OOK)**

On-off Keying (OOK) is one of the simplest modulation techniques used to switch an LED between a high (bit 1) and low (bit 0) transmit power levels to modulate data. Run-Length Limited (RLL) codes such as Manchester coding may be used for DC balance [21]. In Non-return-to Zero (NRZ) OOK, 0s and 1s are represented by positive and negative voltages. This technique had been widely used in VLC and can carry more information since there is no rest state. Fujimoto *et al.* demonstrated the simplest NRZ-OOK system with a single Red Green Blue (RGB) LED (only red to transmit) achieving a bit rate of 477 Mbits/sec [22] and also employed duo-binary technique with bandwidth enhancement (using transmitter and receiver equalization) to achieve 614 Mb/s. A single commercially available red LED is used with a low-cost PIN-PD by adopting a proposed practical LED driver with a basic pre-emphasis circuit. They have also confirmed 456 Mbits/sec error-free operation of the proposed simple and low-cost high-speed VLC system that requires a single LED drive circuit with a single RGB-type white LED and one optical receiver with a low-cost PIN PD and no optical filter.

### **2.3.2 Pulse Position Modulation (PPM)**

In L-Pulse Position Modulation (L-PPM), a pulse corresponding to a certain bit is transmitted in one of L time slots within a symbol period. The average power requirement for PPM is lower than OOK since it avoids the DC and lower frequency component of the spectrum, but it is less

bandwidth efficient. System complexity is increased on PPM compared with OOK, as it requires stricter bit and symbol synchronization at the receiver. Variable PPM (VPPM) and Multiple PPM (MPPM) are the schemes amongst PPM generally used for dimming control as well as transmitting data. In [23], an 80W smart LED module is used to integrate communication and power management functions. The luminaire provides high-efficiency programmable ambient lighting and can also act as a networked sensor node to gather a variety of local measurements, which leads to improved safety, comfort and efficiency in future lighting systems. A dimmable LED driver based on the Logic Link Control (LLC) resonant DC-DC converter topology is proposed using VLC. The digitally controlled LLC converter operates in constant-current burst mode, where the burst is sequenced to autonomously control the dimming and data transferring using the VPPM modulation scheme. A receiver circuit is designed to demodulate and decode the visible light signal. The 50 kbits/sec system is successfully demonstrated on a 308 LED luminaire with a digitally controlled LLC DC-DC converter.

### **2.3.3 Color Shift Keying (CSK)**

In the new IEEE 802.15.7 standards published in 2011, using multi-chip LEDs for VLC has been introduced. In the CSK modulation scheme, the color point for each symbol is generated by modulating the intensity of RGB chips. However, CSK cannot be used in a VLC system where the source is a pc-LED (which is one of the most common sources of light in an illumination system) and implementation of CSK requires a complicated circuit structure. In [24], some modifications



so as to include multiuser capabilities provided by a time-based multiplexing scheme are proposed with the modulation constellation symbols being adapted to encode data with the luminous powers of the red, green and blue color bands respectively. A simple and low-complexity time-based pulse signals structure is employed to separate the users data symbols, while a three-dimensional signal constellation design is merged to ameliorate the data throughput. To assess the performance of the architecture, numerical simulations are performed, and it is observed that the statistical properties of the transmitted RGB signals ensure dimming capabilities and that the illumination function is unaffected by flickering.

#### **2.3.4 Orthogonal Frequency Division Multiplexing (OFDM)**

Orthogonal Frequency Division Multiplexing (OFDM) is spectrally efficient, and is robust against channel dispersion. It is used extensively in RF applications such as Wi-Fi and Terrestrial Digital Video Broadcasting (DVB-T). Since VLC uses visible light to transfer data, a real and unipolar valued signal needs to be produced. Therefore, the conventional OFDM scheme used in RF communications should be modified. To achieve a real valued output signal, Hermitian symmetry is used on the parallel data streams into the Inverse Fast Fourier Transform (IFFT) input. In [25], an experimental demonstration of indoor VLC transmission at 1 Gb/s using MIMO OFDM is reported. The system consists of a four-channel MIMO link that uses white LED sources, each transmitting signals at 250 Mb/s using OFDM. A nine-channel imaging diversity receiver is used

to detect the signals, and an average bit error rate of  $10^{-3}$  is achieved at the room illumination level of approximately 1000 lux at 1m range.

### **2.3.5 Dimming Support**

Light dimming is an interesting indoor VLC application as described in [26]. The authors define the "lights off" mode as level that satisfies humans that the lighting is effectively "off". This is implemented by maintaining the surface area of the emitter large and the brightness of the emitter matching with current brightness of the room. The results show that the "lights off" mode can maintain data rates of several Nm/s with low light emission. Investing VLC with limits on transmit power, this result is an important step toward ensuring acceptance and adoption of VLC technology.

## **2.4 Hybrid VLC Schemes**

Optical communication was at first created as a substitution for constrained RF innovation. Be that as it may, hybrid RF/FSO communication frameworks has gotten to be a hot topic where the preferences of both technologies are integrated. The points of interest of RF incorporate non-requirement of Line Of Sight, more extensive range of coverage and multi-user support. On the other hand, advantages of VLC incorporate illumination and communication at the same time, secure communication in an indoor setting, cheaper, simple to setup and less in general control utilization compared to RF etc. As an illustration, a work by [27] includes utilizing a crossover

RF/FSO framework in backbone networks as FSO links give tall transmission capacity and security and RF links offer unwavering quality. They propose a directing system which empowers traffic engineering on the oncoming traffic by integrating traffic engineering and transfer speed administration at an off-line computing unit. This data is at that point utilized at ingress routers for traffic engineering and routing when the network is online.

Another recent study done on such a hybrid scheme showed that a hybrid system outperforms single standalone VLC system in terms of user connectivity and energy consumption [28]. It has analyzed the feasibility and possible benefits of using hybrid radio-optical wireless systems. Potential benefits are identified as service connectivity and energy efficiency of battery operated device in indoor environments. Moreover, cooperative communication using optical relays are also introduced in order to increase the coverage and energy efficiency of battery operated devices. The connectivity and energy efficiency of such hybrid radio-optical cooperative communications are characterized by optical LOS channel model, relay selection algorithm, mobility of user, semi angle at half power of the LED and the FOV of the photo detector. Simulations have been performed in order to evaluate the connectivity and energy efficiency performance of such homogeneous and hybrid networks. Simulation results reveal that user connectivity and energy efficiency depend on user density, coverage range ratio between single-hop and multi-hop, relay probabilities and mobility of the user. Finally, it has been claimed that hybrid radio-optical wireless systems have a positive impact on the performance of user connectivity and energy consumption. There have been some more recent studies on hybrid RF-VLC schemes. In [29], a hybrid Wi-Fi and FSO network consisting of femtocells is described a novel location-assisted coding technique is introduced,

based on which, the number of novel rate allocation algorithms is proposed to increase throughput and reduce interference for multiple users in a dense array of overlapped femtocells. In [30], a hybrid RF and VLC system is considered, where multiple RF and VLC access points are analyzed. The authors have proposed in order to improve the per usage data rate performance to support the standalone VLC network. It is assumed that the VLC system resources are fixed, and this paper quantifies the minimum spectrum and power requirements for a RF system. The hybrid RF/VLC system achieves certain per user rate coverage performances after the exposure to the VLC system. In another work [31], the authors have proposed and implemented two heterogeneous systems, one of which is a hybrid Wi-Fi/VLC system. It uses VLC for the downlink and Wi-Fi for the uplink. This approach helps to solve the optical uplink challenges and gets the benefit of the full-duplex VLC communication. The authors have shown theoretical proof of improvement on average system delay. The experiment result shows that the hybrid system performs better than conventional Wi-Fi in terms of throughput. In [32], the authors have proposed PLiFi, which is a hybrid VLC/Wi-Fi system using power line communication. It provides high speed interconnection between LEDs along with VLC/WiFi integration. The Wi-Fi access point connects to the power line using an Ethernet-PLC modem. For the downlink transmission, the packets received from the Internet are first forwarded to the power line network by the WiFi access point, and then to LED transmitters which deliver the packets to the end devices. On the uplink, the end-devices directly connect to the WiFi Access point. Preliminary results show that this PLC architecture provides sufficient data and coverage. An extension of ns3 network simulator is proposed in [33] in order to investigate the characteristics of hybrid RF/VLC networks. the VLC downlink and the RF (WiFi) uplink are

connected using the combination of the proposed ns3 VLC component and existing ns3 RF modules. Simulations show how this situation can be analyzed in terms of VLC signal to noise ratio (SNR) and bit error rate (BER) parameters, and in the resulting network performance measured as goodput. All these works consider that in the downlink, each user is served only by a single LED, while in the uplink, an RF technology such as WiFi is used for communication.

It can be observed from the previously mentioned works that most research goes into either improving the properties of VLC systems or working a way around to make communication feasible. Our research differs from the recent works in the integration of multiple spotlighting mechanism onto a single light source (base station), thereby creating an apparently large FOV which makes handover easier and also serves the purpose of illumination. Instead of developing a VLC-based broadcast system, our research focuses on specific data stream from individual spotlight from the overhead light source.

## **2.5 Categorization of Previous Works Based on the Number of Transmitters and Datastreams Involved**

*Single Element Single Datastream (SESD)* designs are where one LED sends one datastream to one receiver. SESD VLC systems were heavily studied, especially in the early stages of VLC research, with a focus on modulation and data rate. In [34], the authors were able to show high speed data transmission using a phosphorescent white LED. 40 Mb/s speed was reported using On-Off Keying (OOK) modulation and more than 100Mb/s speed using Quadrature Amplitude Modulation

(QAM), although the distance between the LED and photodiode was very small, i.e., 1cm. In a more practical setup demonstrated in [35], the authors were able to transmit data with a distance of 2.5m using off-the-shelf LEDs with 115Kb/s speed. In [36], performance of a novel LED lamp arrangement was investigated for reducing the Signal-to-Interference Noise Ratio (SINR) fluctuation from different locations in the room for multi-user VLC. They assumed that the illumination uniformity of the system would be maintained as the distribution of luminance had the same shape as that of the received optical power. This can be assumed only if the transmitters of the system have a fixed amount of source power in such a way that the received optical power in the room floor is uniform which is different from the case considered in this work. Another work [37] with emphasis on SINR proposed a coverage optimization model where genetic algorithm is used for optimizing LED arrangements. While maintaining the illumination requirement, a 75% improvement in communication coverage is attained. However, this work did not consider illumination uniformity though, and all the LEDs were assumed to have the same transmit power. In SESD designs, distance between the transmitter and the receiver plays a great role in data transmission speed.

*Single Element Multi Datastream (SEMD)* designs have one LED sending multiple datastreams to multiple receivers. Significant amount of work explored how to use a single light source to serve multiple receivers, mostly via techniques involving diffuse optics and sharing of the VLC link. In [38], an outdoor VLC system is considered with a powerful light source to serve a large number of users accommodated by a big area. The work focused on the problem of using VLC system resources based on Time Division Multiple Access (TDMA) technique while aiming to maximize

the spectral efficiency of the downlink fulfilling a Quality-of-Service (QoS) requirement. In [39], the authors analyzed a diffuse VLC Multiple-Input Multiple-Output (MIMO) system taking Line-Of-Sight (LOS) propagation into account. Their simulation indicated that the angular diversity detectors had better performance over vertical oriented receivers for the mobile optical receivers. Two separate channel coding techniques were analyzed in [40] considering a  $4 \times 4$  VLC MIMO setting where an effort of optimizing the LED positions to obtain uniform SNR for the desired BER in a given area. The channel coding techniques analyzed were Repetition Code (RC) and Spatial Modulation (SM), and the simulation results indicated that SM could offer better SNR when the spacing between the receivers was larger. To improve system performance, power requirements of the LEDs were optimized and uniform distribution of SNR in a given area was also calculated.

*Multi Element Single Datastream (MESD)* techniques employ multiple LEDs that send one datastream to one receiver. In order to increase the received light intensity at the receiver, MESD designs use multiple LED sources sending the same data to a single receiver. Availability of multiple transmitters in MESD designs allows cooperative transmission [41], where the time of arrival from all the LEDs can be used to improve the detection probability of data bits at the receiver, and hence reduce BER. By employing multiple photo-detectors at the receiver, MESD designs also allow MIMO modulation techniques. Such MIMO VLC designs were shown to maximize data rate well with a modified singular value decomposition [42] while maintaining certain illumination requirements.

*Multi Element Multi Datastream (MEMD)* designs recently emerged and used multiple LEDs sending multiple datastreams to multiple receivers. Due to the additional flexibility in the multiplicity of

elements and datastreams, more interesting MEMD VLC system combinations are possible based on LED placements and coverage of the illumination areas. The authors in [43] proposed a multi-cell VLC system for large area networks, where LED arrays in one cell can coordinate with LED arrays in the adjacent cells to cancel the inter-cell interference. In another recent work [44], Discrete Multi-Tone (DMT) modulation scheme has been shown to significantly improve the throughput of VLC in a room. In [45], the authors studied LED assignment problem in MEMD VLC systems taking proportional fairness and QoS requirement into consideration. They proposed suboptimal heuristic algorithms for LED assignment to receivers.

Illumination uniformity is an important factor to be considered in MEMD architecture where uniform light distribution needs to be considered as each LED's transmit power is being tuned. Otherwise, spotty lighting might emerge while the transmit powers of LEDs are being tuned for maximal SINR. Our work in this paper considers a more practical scenario than the previous works in the literature, where we jointly optimize the illumination uniformity with users' QoS. It is critical to ensure quality lighting in the room, while optimizing the LED assignment problem with a source power constraint on each LED. This type of MEMD architecture can improve the system performance as investigated in [46, 47].



## CHAPTER 3

### MULTI-ELEMENT BULB ARCHITECTURE

We focus on two main objectives of our multi-element VLC approach: 1) *high spatial reuse* by fully utilizing the directionality of LEDs, and 2) *seamless handling of mobility* of receivers by using software protocols that steer the data transmissions to mobiles.<sup>1</sup> Unlike the traditional design of LEDs/transmitters with large divergence angles, we propose to use narrow divergence angles and still perform an acceptable illumination by using a large number of LEDs on a “bulb”. In particular, our work - 1) presents an architecture with LEDs having narrow divergence angles to reap the rewards of high spatial reuse; 2) uses software protocols for efficiently tackling the mobility issues such as LOS discovery, alignment maintenance, and receiver association; and 3) utilizes software-based heuristic optimizations to solve interference problems between simultaneous VLC links, which is significantly different from the concepts described in [2, 48].

Even when we use hundreds of LEDs, we still have the problem of steering the data transmission to the corresponding LED when the mobile receiver is moving. We tackle this problem with a software-defined and enhanced version of electronic steering [4]. Our architecture takes advantage of spatial reuse and seamless steering which are untapped sources of efficiency in VLC. We detail the architecture in Figure 3.1 by describing three key components below.

---

<sup>1</sup>Most of the content on this chapter was published in proceedings [11].

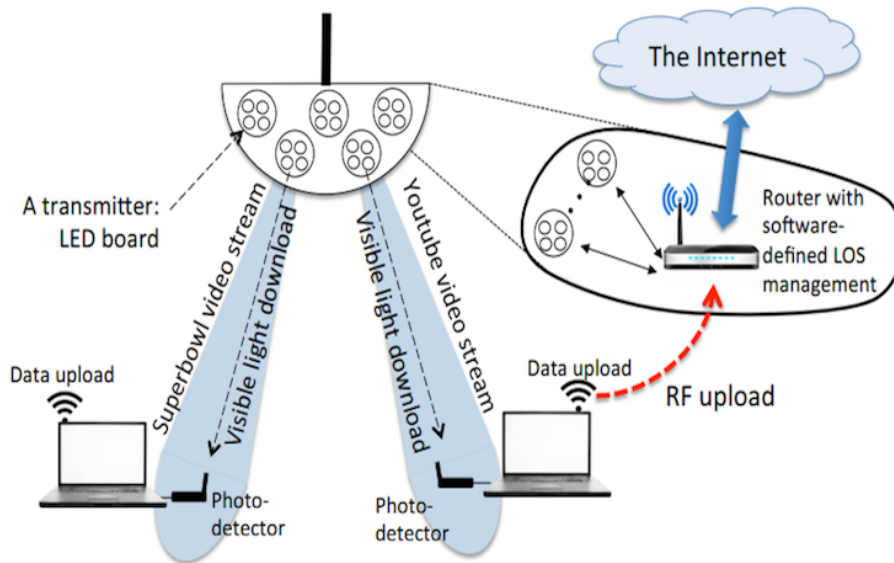


Figure 3.1: Sample design of a MEMD VLC architecture.

### 3.1 The Bulb

#### 3.1.1 Design of the Bulb

We consider a single hemispherical bulb for an indoor VLC system consisting of  $M$  LEDs serving  $U$  users. Each LED  $m$  transmits power equal to  $P_m$  Watt,  $\forall m = 1, \dots, M$ . We also consider that the hemispherical bulb structure with two functions: Illumination of the room and wireless download to mobile users by acting as an access point for the room. It consists of multiple transmitters (i.e., LEDs) to facilitate simultaneous downloads to multiple receivers (i.e., users) as shown in Fig. 3.2. These LEDs are attached to the surface of the bulb in several layers pointing towards different

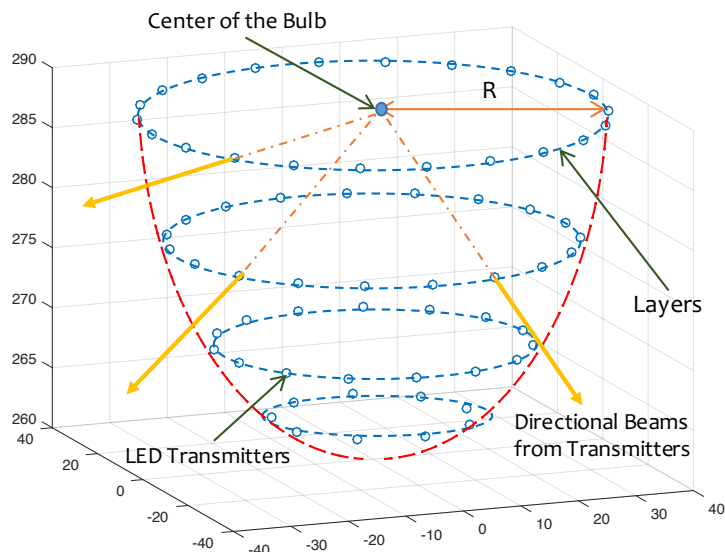


Figure 3.2: Placement of transmitters in the bulb.

directions so that they can illuminate different parts of the room. Furthermore, in addition to wireless communications, the LEDs are intended to provide light coverage in the room.

As the hemispherical bulb (which is the AP) has many transmitters attached to it, overall it has a broad coverage even in cases where each LED transmitter has a narrow beam. In fact, this is a key novelty of our work. We consider the cases where LEDs have narrow divergence angles which causes spotty lighting but attains pretty good throughput/SINR. Using smaller divergence angle for the transmitters decreases the chance of interference among multiple simultaneous data downloads as the overlapping of LED beams is less compared to the cases of larger divergence angles. To remedy the spotty lighting issue of our design, we make the illumination uniformity a key part of the optimization objective rather than just leaving it to a constraint which typically can be done as

the light intensity being greater at a particular location on the room floor as in some of the earlier works [37].

We envision mobile users equipped with a Photo-Detector (PD) or a collection of PDs conformal to the surface of the unit with additional apparatus like lenses as appropriate. These users also need the capability of uploading using legacy Radio Frequency (RF) transmitters. Each receive a separate datastream download from the LED(s) with which they are in LOS alignment. The design of these units requires joint work of solid-state device and packaging as well as communication protocols. For instance, multi-element conformal PDs can be designed to cover a smartphone's or a laptop's surface, or multiple PDs can be used to attain a large field-of-view (FOV) [49] at the user.

Given multiple mobile users each downloading a different datastream, our MEMD VLC system aims to attain high download speed for all users and smooth lighting across the room. To do so, the bulb structure will have to perform two tasks: (1) Partition LEDs to groups and assign each group to a user so that the user's download speed is maximized with minimal interference to the other downloads in the room, and (2) tuning transmit power of LEDs so as to maximize the illumination uniformity in the room. The ideal scenario would be to update the association and transmit power of the LEDs instantly, i.e. whenever there is a change in the position of any of the users, which is happening in our simulation as we are solving the optimization problem and calculating our objective function output based on several random sets of user coordinates. In a practical scenario, though, it would depend on the uplink speed of the RF transmitter of the user as the bulb will be able to start the process and update the association when it receives the

acknowledgement from the receivers responding to the search frames periodically coming from the LEDs. Given the current system delays in the association process (e.g., the frequency of search packets being sent from the bulb, transmission delay of the search packets, the receivers processing delay upon receiving the search packets, the transmission delay of the acknowledgments from the receivers, and processing delay of the acknowledgments at the bulb), we are expecting the frequency of updating the association and transmit powers to be in the order of tens of milliseconds. Note that doing the update at several hundreds of milliseconds is also acceptable since human movement happens at larger timescales.

### 3.1.2 Layered Bulb Structure and Placement of LEDs

We place the LEDs on the hemispherical bulb on  $l$  layers as shown in Fig. 3.2. Let  $L$  be the maximum possible number of layers, and  $K_i$  is the maximum possible number of LED in the  $i$ -th layer. Depending on the shape of the bulb and LED transmitters<sup>2</sup>,  $L$  and  $K$  can have different upper limits. To find the maximum number of layers  $L$ , we assume the LEDs to be spaced as closely as possible. First, we calculate how many LEDs can possibly be placed on the surface of any one half on the hemispherical bulb when looking from the  $x$ - $z$  plane ( $y=0$ ). So, each LED on the same layer will create the same angle with the center point of the bulb (since their radius is the same) which

---

<sup>2</sup>These LED transmitters may be composed of one or more LEDs. We assume that the transmitters are circular with a fixed radius  $r_l$ , which can be implemented by multiple LEDs placed in a circle. We will keep referring to these circular transmitters as ‘LEDs’ or ‘LED transmitters’.

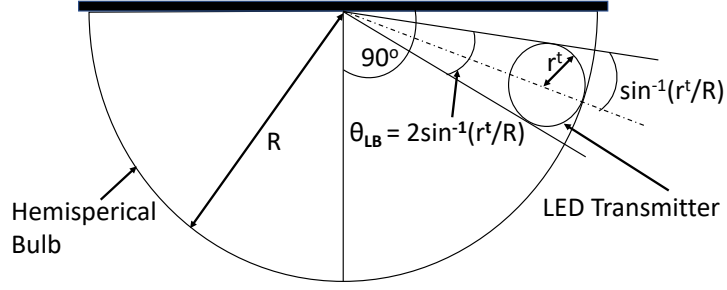


Figure 3.3: Calculation of maximum number of layers in the bulb.

can be defined as:

$$\theta_{LB} = 2 \sin^{-1} \left( \frac{r_t}{R} \right) \quad (3.1)$$

where  $r_t$  is the radius of an LED and  $R$  is the radius of the bulb. The factor 2 comes from the fact that we are using transmitter radius as our parameter for the calculation, and the angle the whole transmitter (with its diameter) creates with the center of the bulb is twice the angle it creates with its radius. Fig. 3.3 illustrates this more clearly. Then, the maximum number of layers for a particular  $r_t$  and  $R$  can be expressed as:

$$L = \left\lfloor \frac{90^\circ}{\theta_{LB}} \right\rfloor \quad (3.2)$$

where  $\theta_{LB}$  is measured in degrees.

Next, we calculate the upper limit of the number of LEDs in a particular layer  $i$ . If the angle between the  $i$ -th layer and the perpendicular normal is  $\theta_i$ , then the radius of circle created by the

LED boards in the  $i$ -th layer will be:

$$r_{li} = R \cos \theta_i \quad (3.3)$$

Then, the angle created by each LED with the center of this circle will be:

$$\theta_{li} = 2 \sin^{-1} \left( \frac{r_t}{r_{li}} \right) \quad (3.4)$$

Lastly, the maximum number of possible LEDs in the  $i$ -th layer can be calculated as:

$$K_i = \left\lfloor \frac{360^\circ}{\theta_{li}} \right\rfloor \quad (3.5)$$

where  $\theta_{li}$  is measured in degrees. In our earlier work [11], we designed techniques to optimize the number of LEDs in each layer (i.e.,  $k_i$ ) up to these maximum values (i.e.,  $K_i$ ) for their corresponding layer. The key insight was to place more LEDs at the lower layers of the bulb as they contribute more for the achievable throughput. Thus, in this paper, we place the LEDs at the lower layers first and go up if more LEDs are available.

### 3.2 Mobile Receiver Units

The receiver unit can be mobile and needs to be equipped with a PD. It is assumed that the PD(s) are conformal to the surface of the unit with additional apparatus like lenses as appropriate (something

like in [50]). These mobiles also need the capability of uploading using legacy RF transmitters. We are assuming that these mobile devices have one PD receiver and one RF transmitter such as WiFi. They receive the download data from the transmitter(s) with which they are in LOS alignment. The design of these units requires joint work of solid-state device and packaging as well as communication protocols. For example, multi-element conformal PDs can be designed so that they cover the surface of a smart-phone or laptop.

### **3.3 RF/FSO Hybrid LOS Management**

We are using a hybrid RF/FSO approach in our architecture, as bidirectional VLC can cause significant interference near the bulb. In hybrid RF/FSO approach the data download is administered through FSO/VLC and upload is handled using RF. This approach considerably reduces the collision that can be caused by bidirectional VLC communication. Also, we are using RF - the slower communication between the two - for data uploading as typically there is much less traffic in case of data uploading compared to data downloading. In our hybrid architecture, the multi-element bulb follows a software-defined approach to find the best receiver-transmitter link. In order to achieve this, we firstly establish the optical link and then maintain this link taking into consideration the receiver mobility. For this, establishing an optical link by associating transmitter(s) to a receiver and maintaining this link with mobility of the receiver across the room is needed. The controller device also has to partition the transmitters so that multiple transmitters can serve a receiver, and cease the optical link once the receiver is off-line. The transmitters located close to each other



(that are in the same partition) are assigned to the same receiver and transmit the same data stream. When a receiver moves slightly, a handover will not be immediately necessary as it will still be receiving the data signal from the neighboring transmitters in the same partition. Thus, this design will require a handover (or a redoing of the receiver-transmitter association) only when the receiver makes abrupt movements, which is unlikely inside a room. This protocol allows smooth and continuous mobility for the receivers by electrically steering the data transmission in accordance with the position of the receiver. We group these functionality into three basic bulb-mobile association mechanisms as detailed below.

### **3.3.1 Establishing the Link**

To search for new receivers in the room, the bulb periodically sends SEARCH frames via its transmitter LEDs. Each LED on the bulb has a local ID,  $k$ , which is included in the SEARCH frames being sent from that LED  $k$ . These SEARCH frames are like Ethernet's RTS messages, with a key difference that they are augmented with the local ID of the LED they are being sent from. A mobile receiver  $i$ , entering the room, receives these SEARCH frames. The receiver might receive multiple of the SEARCH frames depending on its position with respect to the bulb. We assume that the receivers have the capability to filter the SEARCH frame with strongest light intensity. A measure of the received signal strength indication (RSSI) can be fed into the controller where the decision is made over which input has the strongest signal. [51]

Once the receiver receives the SEARCH frame, it sends back an ACK frame (like a CTS in Ethernet) via its RF transmitter. This ACK includes the Ethernet / MAC address of the receiver and the local ID  $k$  of the LED from which the SEARCH frame was received. The ACK verifies to the bulb that  $i$  is aligned with the transmitter LED  $k$ . After receiving the ACK from  $i$ , the bulb assigns the LED  $k$  or a group of LEDs around the LED  $k$  to  $i$ , and maintains this information as an LED-receiver association table (LED-RAT). When there are multiple receivers in the room, the bulb partitions the LEDs and associates each partition (see Section ??) to a separate receiver. The LED-RAT needs to be updated accordingly. For every data frame to be sent, the bulb does a reverse lookup to the LED-RAT, with the Ethernet address the frame is destined to. In this manner, the bulb steers the data stream destined for receiver  $i$  onto the transmitters that just got associated to  $i$ . The partitioning of the LEDs across the receivers will be crucial in the overall performance of the spatial reuse.

### 3.3.2 Maintaining the Link

Once an optical link is established between the receiver and the LEDs on the bulb, it is maintained by periodic exchange of SEARCH-ACK messages as described in the previous subsection. When there is a change in the LED-receiver association, the bulb will need to update LED-RAT and re-partition the LEDs. Since such changes can happen frequently, it is crucial to keep the complexity of the LED-RAT update and partitioning of LEDs small. Furthermore, the re-partitioning operation

should be performed in a manner independent of the number of LEDs, as there will be hundreds of LEDs on the bulb.

### 3.3.3 Terminating the Link

When a receiver leaves the room or powers down, the controller in the bulb needs to update LED-RAT and re-partition the LEDs. There are two possibilities for achieving this:

- *Graceful Leave*: The receiver  $i$  lets the bulb know that it is powering down by sending a CLOSE frame via its RF transmitter.
- *Ungraceful Leave*: The receiver  $i$  simply leaves the room without informing the bulb about its departure. Then, the bulb will keep sending its SEARCH frames, and will timeout on  $i$  after  $N_t$  SEARCH frames without an ACK from  $i$ .  $N_t$  actually indicates the number of search frames without acknowledgement from a receiver after which the bulb will consider the connection between that receiver and itself is timed out. Therefore,  $N_t$  can be changed under various circumstances.

# CHAPTER 4

## OPTIMAL MULTI-ELEMENT BULB DESIGN FOR HIGH SIGNAL-TO-INTERFERENCE RATIO AND SMOOTH LIGHTING

### 4.1 Parameters

In this chapter, we optimize the multi-element bulb design with respect to the *divergence angle of the LEDs* ( $\theta_d$ ) and the *number of LED Boards in each layer* ( $k_1, k_2, \dots, k_i$ ).<sup>1</sup> All the needed parameters for the model are described in table 4.1.

Table 4.1: Parameters

Parameter Name	Symbol
Visibility (km)	$V$
Optical signal wavelength (nm)	$\lambda$
Particle distribution constant	$q$
Coefficient of absorption and scattering	$\sigma$
Divergence angle (radian)	$\theta_d$
Transmitter radius (cm)	$r_t$
Radius of the bulb (cm)	$R$

---

<sup>1</sup>Most of the content on this chapter was published in proceedings [11] and magazine [12].

<b>Parameter Name</b>	<b>Symbol</b>
Layer $i$ 's angle with the normal (radian)	$\theta_i$
Vector between $i$ th LED board on the bulb and its normal point on the floor	$\vec{LP}_i$
Vector of the central LED facing down	$\vec{LP}_0$
Power on the normal for LEDs in $i$ -th layer (W)	$P_L(i)$
Receiver radius (cm)	$r_r$
Slanted normal length for LEDs in $i$ -th layer (cm)	$H_i$
Number of receivers in the room	$N_{rcv}$
Array of LED count in each layer	$k_{i=1..l}$
Source power of each LED (W)	$P_{LED}$
Total power generated by the bulb (W)	$P_{total}$

## 4.2 Link Model and SIR Calculation

The placement of layers and LEDs in the bulb is already described in section 3.1. We assume that the transmitters on the bulb are grouped into sections so that each section is associated with a particular receiver. For example, if there are two receivers in the room, the LED boards (or transmitters) are grouped into two sections each corresponding to one of the receivers. So, we assume that the transmitters are grouped such that they are associated with the receiver closest to

(or in the best LOS alignment with) their Lambertian beam. Given this, the normal component of the power generated by LED board  $i$  will be [9]:

$$P_L(i) = P_{LED} + 10\log(e^{-\sigma H_i}) + 20\log\left(\frac{r_r}{r_t + 200H_i\theta_i}\right) \quad (4.1)$$

where  $P_{LED}$  is the source power of each LED,  $\sigma$  is the atmospheric absorption and scattering coefficient. The expression for  $\sigma$  is:

$$\sigma = \left(\frac{3.91}{V}\right)\left(\frac{\lambda}{550}\right)^{-q} \quad (4.2)$$

Here  $q$  is particle distribution constant, where:

$$q = \begin{cases} 1.6, & \text{if } V > 50km \\ 0.5, & \text{if } V \geq 6km \text{ and } V \leq 50km(1) \\ 0.585V^{1/3} & \text{if } V < 6km \end{cases}$$

with visibility  $V = 0.5km$  and optical wavelength  $\lambda = 600nm$  [52]. And, after the grouping of the transmitters is complete, if a receiver  $i$  is located at partition  $j$  and the number of LED boards in partition  $j$  is  $N_j$ , then the average signal received by that receiver from that partition is:

$$S_{ij} = \sum_{m=1}^{N_j} P_L(m) \cos \phi_m \quad (4.3)$$

where  $m$  refers to the IDs of LEDs in partition  $j$ . Similarly, the average power of the signals received by that receiver from a partition other than  $j$  (which will be treated as interference) is:

$$S_{il} = \sum_{m=1}^{N_l} P_L(m) \cos \phi_m \quad (4.4)$$

where  $P_L$  is the received power at the normal of the layer of the respective LED boards of that particular partition.

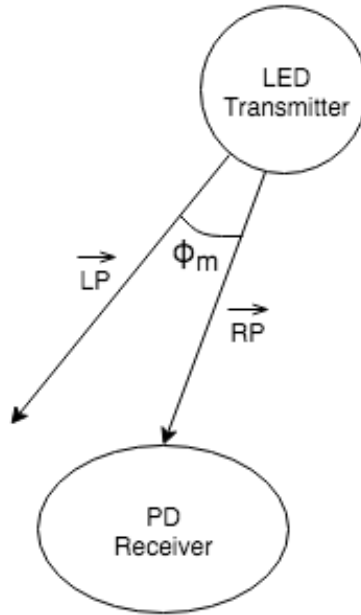


Figure 4.1: Transmitter and receiver angles.

Further, the angle between the LED board's normal and the normal of the receiver's field-of-view (FOV),  $\phi_m$ , is defined as:

$$\phi_m \implies \tan^{-1} \left( \frac{|\vec{RP} \times \vec{LP}|}{\vec{RP} \cdot \vec{LP}} \right) \quad (4.5)$$

where  $\vec{RP}$  is the distance vector from the origin point of the LED board to the receiver point in the X-Y plane, and  $\vec{LP}$  is the LED vector for that particular LED board. Essentially,  $\phi_m$  is the angle between  $\vec{RP}$  and  $\vec{LP}$  in Figure 4.1. Then, for receiver  $j$ , the average Signal-to-Interference Ratio (SIR) is

$$SIR_j = \frac{S_{ij}}{\frac{1}{N_s - 1} \sum_{l=1..N_s, l \neq j} S_{il}} \quad (4.6)$$

Finally, the average SIR of the system will be:

$$SIR_a = \frac{1}{N_{rcv}} \sum_{j=1}^{N_{rcv}} SIR_j \quad (4.7)$$

Our main goal is to maximize this average SIR with minimum costs. The result of the optimization is the bulb configuration values (e.g., bulb radius, number of LED boards, divergence angle of LEDs, and radius of the transmitters) that maximize SIR under certain constraints.

### 4.3 Optimization Objective

The goal of this work is to optimize the SIR of the system while considering the illumination quality at an indoor settings. So, the optimization objective could be formulated as to maximize SIR while taking into consideration the illumination quality and aggregate power consumption. We explore optimum bulb configurations for a particular number of layers by varying the number



of LED boards in each layer to see which combination produces the maximum SIR under an aggregate power constraint.

We also used the divergence angle of the LEDs as another variable parameter for the optimization problem. Then, we update the optimization problem by adding a constraint on the illumination quality, which is defined by the standard deviation of luminance on the room floor, referred as illumination variation. We, then, compare the two results to analyze the effect of the illumination requirement on the overall optimization problem. The flow diagram with input parameters, intermediate values to calculate the SIR and the illumination variation, and the output parameters are shown in Figure 4.2.

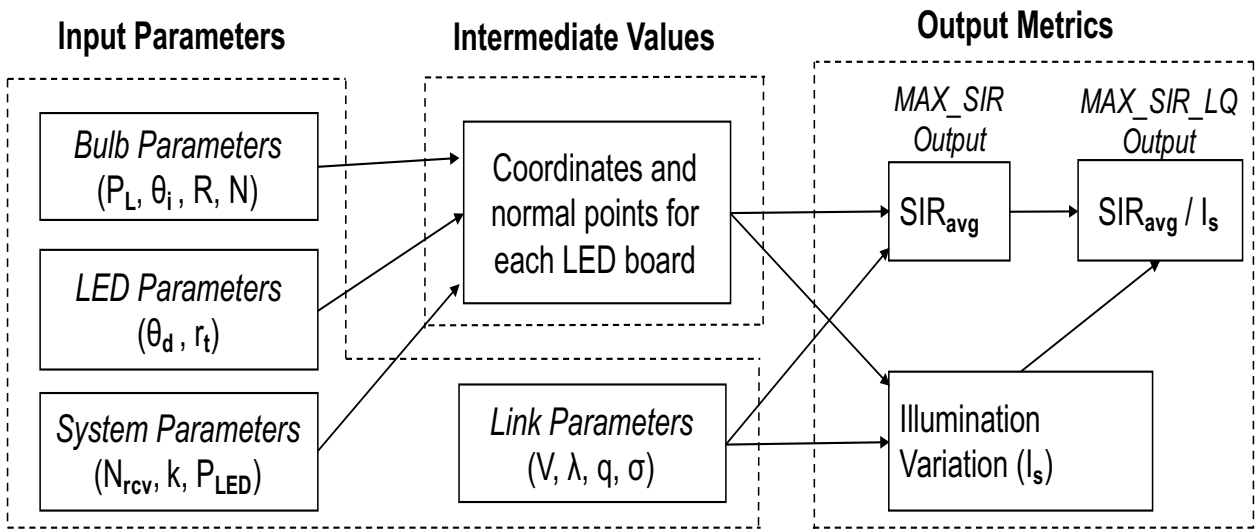


Figure 4.2: Flow diagram of the optimization.

#### 4.4 MAX\_SIR: Maximum SIR Problem

We first formulate the problem of finding maximum SIR under a power constraint, i.e., the MAX\_SIR problem. At a high level, MAX\_SIR aims to find the best placement of LED boards on each layer of the bulb and the best divergence angle for the LEDs. We detail the variable and fixed parameters below:

##### Variable Parameters:

- $k_i$ , *Number of Transmitters in Layer  $i$* : Intuitively, given a fixed number of LED boards, they can be placed in layers in many different ways, depending on the size of the LED boards and the bulb radius. Considering all the parameters involved, we vary the number of LED boards per layer by adjusting the spacing between them on each layer.
- $\theta_d$ , *Divergence Angle of LEDs*: Divergence angle of the LED is one of the key factors in the source power and illumination quality. While large divergence angles yield better lighting (small variation of the illumination across the room floor), narrow ones are beneficent for increasing the spatial reuse and higher SIR. Thus, we try different divergence angles (in degrees) to find the configurations yielding maximum SIR.

**Fixed Parameters:** We assume that the following parameters are constant:

- *Room Size*: We are assuming a fixed room dimension of 6m x 6m x 3m for width, length and height, respectively.
- *R, Radius of the Hemispherical Bulb*: 40cm

- $r_t$ , Radius of the LED/Transmitter: 3.5cm
- *Number of Layers*: Depending on  $R$  and  $r_t$ , different number of layers are possible in the hemispherical bulb. Given  $R$  and  $r_t$ , we calculate the maximum possible number of layers in the bulb. We are considering the minimum number of layers to be 2. For a specific number of layers between this minimum and maximum value, we have varied the number of LED boards in each layer to find the optimum layering combination.

Now, we formulate the MAX\_SIR problem as follows:

$$\max_{k, \theta_d} SIR_{avg}(k, \theta_d) \quad (4.8)$$

subject to

$$2 \leq k_i \leq K_i \quad (4.9)$$

$$P_{LED} \sum_{i=1}^l k_i \leq P_{total} \quad (4.10)$$

$$l \leq L \quad (4.11)$$

where  $l$  is the number of layers in the bulb,  $L$  is the maximum possible number of layers, and  $K_i$  is the maximum possible number of LED boards in the  $i$ -th layer. Further,  $k = k_1, k_2, \dots, k_L$  is the array of the number of LED boards in each layer.  $P_{LED}$  is the source power of a single LED board and  $P_{total}$  in (4.10) is the total power constraint, which we have assumed to be 25 Watts unless otherwise said.

#### 4.5 MAX\_SIR\_LQ: Maximum SIR with Lighting Quality (LQ) Constraint

Although the communication quality has been considered to be the major goal in VLC, recent studies point to potentially significant health concerns of solid-state lighting. Both link quality metrics such as SIR and lighting quality must be considered in future designs. The hallmark of our multi-element design is the relatively smaller divergence angles of LEDs (to attain higher spatial reuse). But, these narrow angles can cause uneven lighting in the room. Thus, we focused on maximizing SIR while keeping the illumination variation on the floor,  $I_s$  under a limit.

We update the MAX\_SIR problem (by scaling the  $SIR_{avg}$  with respect to  $I_s$  and adding a constraint on  $I_s$ ) and define the MAX\_SIR\_LQ problem as follows:

$$\max_{k, \theta_d} SIR_{avg}(k, \theta_d) / I_s \quad (4.12)$$

subject to

$$2 \leq k_i \leq K_i \quad (4.13)$$

$$P_{LED} \sum_{i=1}^l k_i \leq P_{total} \quad (4.14)$$

$$l \leq L \quad (4.15)$$

$$0 < I_s \leq I_s^{max} \quad (4.16)$$

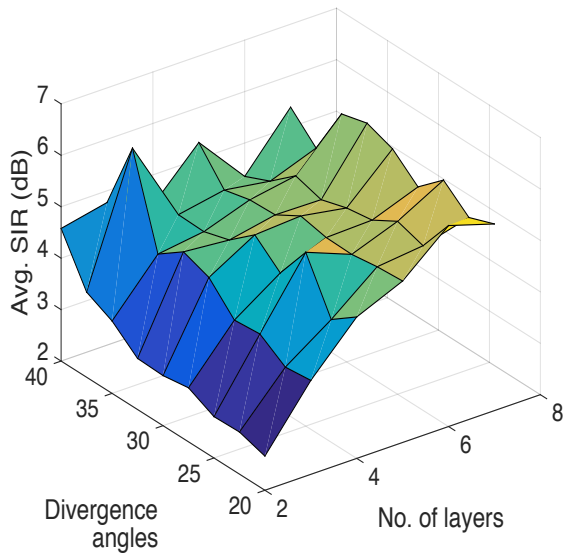
where  $I_s^{max}$  is the maximum allowed  $I_s$ .

The updated objective (4.12) and the additional constraint (4.16) significantly change the dimension and complexity of the problem, as there might be designs which can produce a better SIR but an uneven lighting. For simplicity, we are using  $I_s^{max} = 5$ , which could be varied for better exploration in future studies.

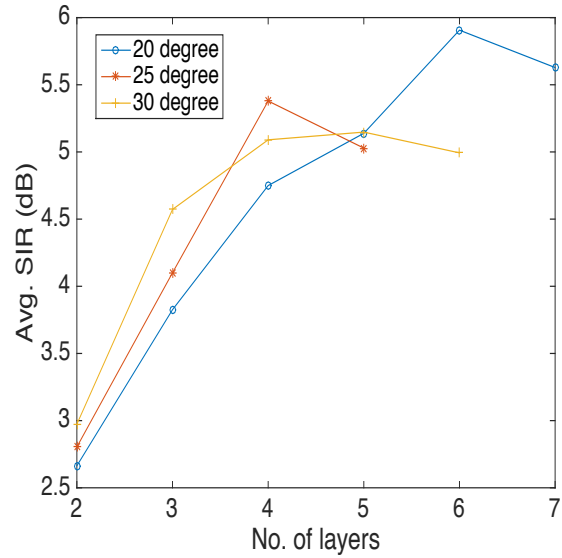
#### 4.6 Heuristic Design for Nonlinearity

To observe the overall effects and the complexity of the search space, we calculated  $SIR_{avg}$  against the divergence angle and the number of layers – placing as many LED boards as possible in each layer. Both the line plot and the surface plot are shown in Figure 4.3(a) and Figure 4.3(b). The line plot is done for 3 divergence angles, and as expected, in all the cases after a certain point, the average SIR decreases, which indicates non-linearity, as it increases in the beginning.

From the surface plot we can also observe the nonlinear nature of the problem as several local maxima and minima can be spotted from the surface. Since the search space is pretty large for finding an optimum bulb configuration (detailed in Subsection 4.7.2), we followed a heuristic similar to Recursive Random Search [53]. In particular, we started the optimizer at 20 different random points and took the best local maxima resulting from these searches. Then we centered the search space around the best local maxima and shrunk it by halving each parameter range. We



(a) SIR against divergence angle.



(b) SIR against number of layers.

Figure 4.3: Nonlinearity of the obj. function: SIR against divergence angle and number of layers.

repeated this step until majority of the local maxima pointed to the same result, which we assumed to be the best result.

## 4.7 Simulation Results

### 4.7.1 Calculation Method

To find solutions to the MAX\_SIR problem, we used MATLAB's mixed nonlinear constrained optimizer. Before calling the optimizer, we first fixed the number of layers  $l$ . We called the optimizer with variable parameters  $k = k_1, k_2, \dots, k_l$  and  $\theta_d$ . Then, the optimizer called our user-

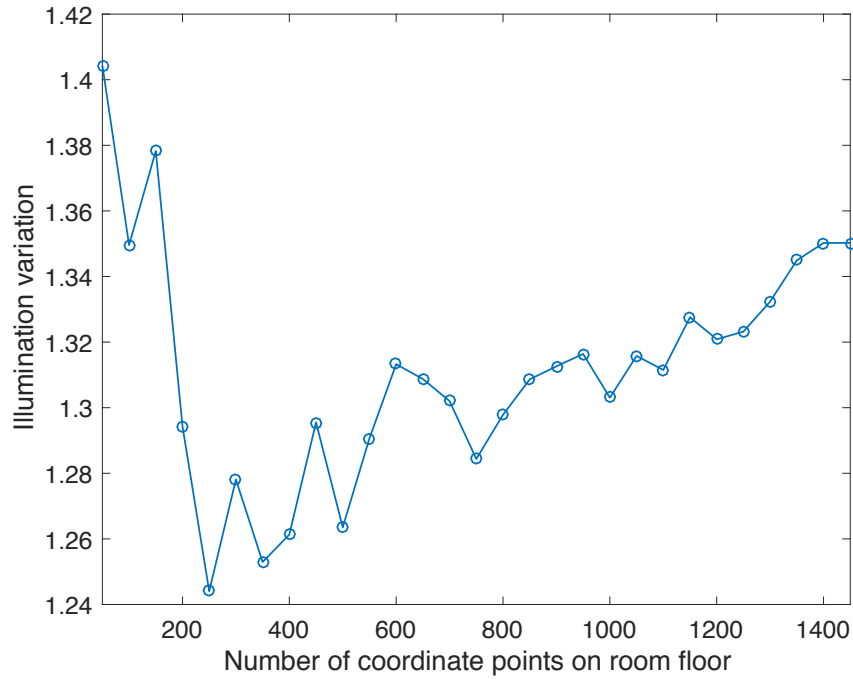


Figure 4.4: Convergence of  $I_s$  values for  $k_1 = 11$ ,  $k_2 = 14$  and  $\theta_d = 26$  degrees.

defined objective function  $SIR_{avg}$  with different combinations of  $k$  and  $\theta_d$  to search for the bulb configuration maximizing SIR.

Each time  $SIR_{avg}$  is called, the optical power received at each coordinate of the room floor needs to be calculated in order to calculate  $I_s$ , the illumination variation across the floor.

To reduce the computation time, we have chosen random points on the floor and calculated  $I_s$  for those random coordinates, and then iteratively added more random points to the previous ones until the  $I_s$  value becomes stable, that is, the value of  $I_s$  in the current iteration is within one percent of the value in the previous iteration. Figure 4.4 shows such a convergence in the case of  $k_1 = 11$ ,  $k_2 = 14$  and  $\theta_d = 26$  degrees.

Table 4.2: Best results for MAX\_SIR and MAX\_SIR\_LQ

<b>Objective</b>	$l$	$k_1$	$k_2$	$k_3$	$\theta_d$
MAX_SIR	2	19	2	–	$39.5^\circ$
	3	16	26	2	$47.2^\circ$
MAX_SIR_LQ	2	6	28	–	$16^\circ$

Further, upon each call to  $SIR_{avg}$ , two random points on the room floor are chosen for receivers, which are assumed to have a radius of 3.75cm and be facing upwards.

We then use these receiver locations to calculate the SIR for the two receivers. We repeated this random selection of locations for pairs of receivers 100 times to calculate the average SIR.

#### 4.7.2 Solution for Best Bulb Configuration

We ran our heuristic to solve various cases of MAX\_SIR and MAX\_SIR\_LQ. Table 4.2 shows the results for 2 and 3 layers cases. We observe that, in MAX\_SIR, the best bulb configuration has much fewer LED boards in the higher layer. This is expected since the normal points for the LED boards in the higher layers go outside of the boundary of the room floor, so they contribute much less towards the SIR. When lighting quality is considered, in MAX\_SIR\_LQ, the best bulb configuration places more LED boards to the higher layers with the goal of attaining even lighting across the floor. Putting more LED boards to bottom layers would result in a high SIR spot in the center of the room but have dark areas towards to corners. As expected, MAX\_SIR\_LQ balances this tradeoff.



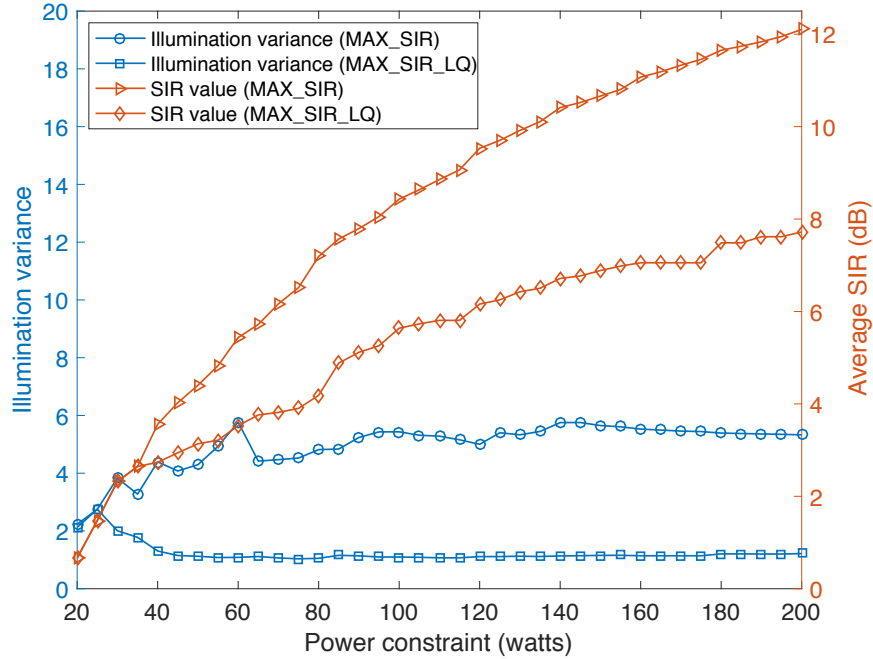


Figure 4.5:  $SIR$  and  $I_s$  values versus power constraint for  $MAX\_SIR$  and  $MAX\_SIR\_LQ$ .

### 4.7.3 Effect of Power Constraints

We also looked at the effect of the power constraints on the results. Figure 4.5 shows optimum  $SIR$  versus the total power constraint, which shows a rise at the beginning, but as expected, the best achievable  $SIR$  saturates as the power constraint increases.

It is also observed that the optimum  $SIR$  is significantly lower when there is an illumination constraint, again confirming our expectations. For the illumination variation, in case of  $MAX\_SIR\_LQ$  it gradually decreases as the power constraint increases, since better configurations are possible at higher power constraints. As we can see from the figure, the value of illumination variation is much lower in case of  $MAX\_SIR\_LQ$ , which results in higher objective function for lower  $SIR$  values. In Figure 4.6, the objective function also gets saturated; because, when

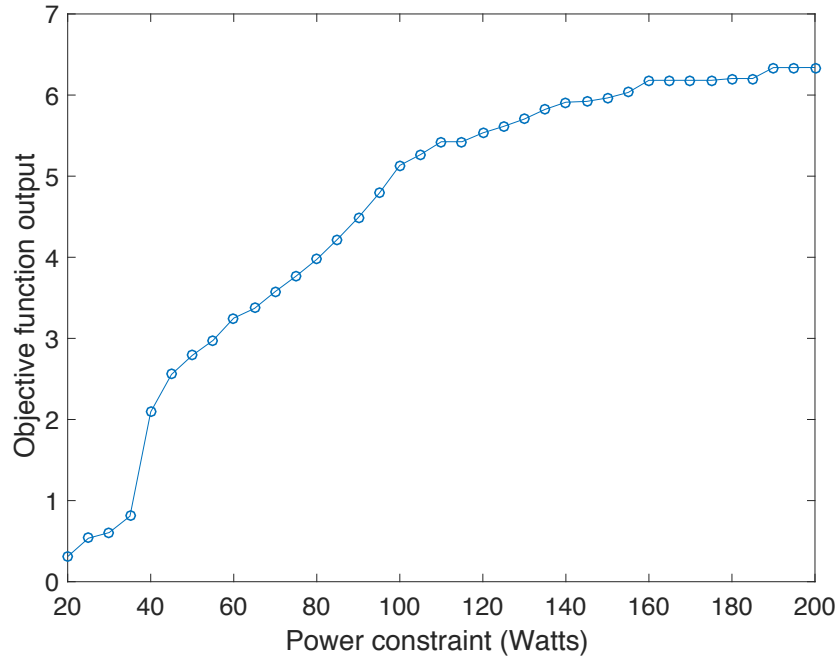
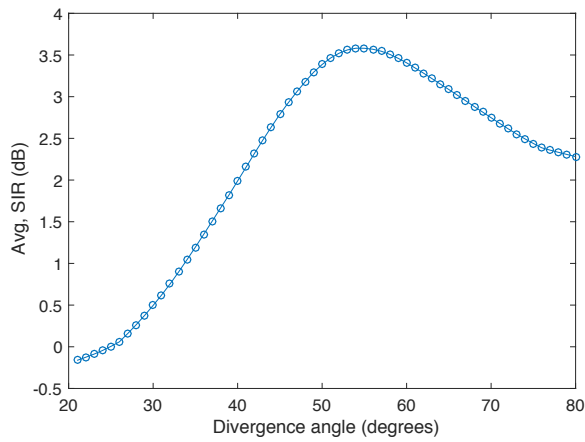


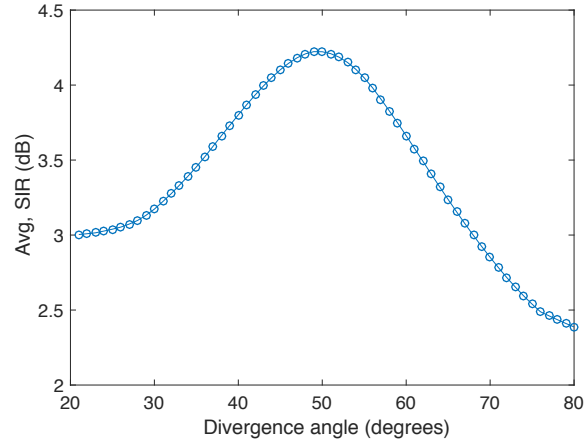
Figure 4.6: Objective function output versus power constraint.

the power constraint is increased (i.e., the number of LED boards in a configuration can be increased), it means that the signal strength also increases. Since we cannot have unlimited number of transmitters on the bulb, after a certain value of the power constraint, we cannot get any more improvement in the SIR. Even with maximum possible number of LED boards in each layer, we cannot achieve the best SIR because of higher interference coming into action. Therefore, after that threshold value the objective function value remains the same.

Since the main objective is to find a good balance between the SIR and the lighting quality, this is clearly evident from Figure 4.5. We can see that from every value of the power constraint, SIR considering the illumination constraint is lower than the SIR without considering the constraint



(a) Avg. SIR vs.  $\theta_d$  for  $k_1 = 12$  and  $k_2 = 15$ .



(b) Avg. SIR vs.  $\theta_d$  for  $k_1 = 19$  and  $k_2 = 31$ .

Figure 4.7: Avg. SIR vs. divergence angle for two layers of LEDs.

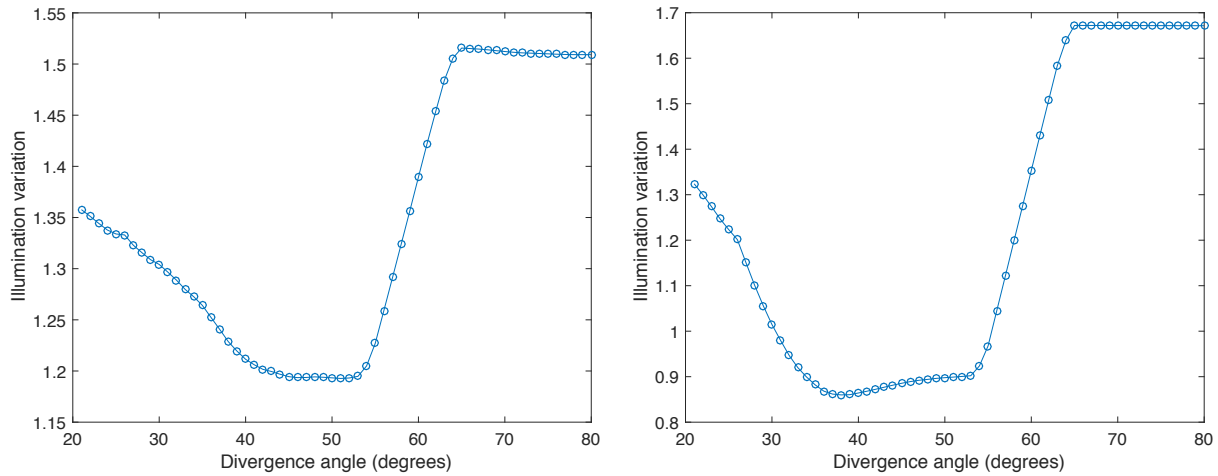
because of the low value of the variation (which indicates better quality of lighting), and that is why the value of objective function is the highest.

To observe the more interactions between the power constraint and the number of layers, more layers must be considered similar to the results in Figure 4.3(a) and Figure 4.3(b).

#### 4.7.4 Effect of Divergence Angle

We have observed the effect of divergence angle of the LEDs on the objective function for two layers of LEDs in the bulb.

From the simulation we found the values of  $K_1$  and  $K_2$  as  $K_1 = 19$  and  $K_2 = 31$ . Within this bound, we have plotted objective function vs. divergence angle for different combinations of  $k_1$



(a) Illumination variation vs.  $\theta_d$  for  $k_1 = 12$  and  $k_2 = 15$ . (b) Illumination variation vs.  $\theta_d$  for  $k_1 = 19$  and  $k_2 = 31$ .

Figure 4.8: Illumination variation vs. divergence angle for two layers of LEDs.

and  $k_2$ . Figure 4.8(a) shows the plot for  $k_1 = 12, k_2 = 15$  and Figure 4.8(b) shows the plot for  $k_1 = 19, k_2 = 31$ . In both cases, we can see that the optimum value of divergence angle (for which the objective function value is the highest) is at around 53 degrees. For lower values of angles, the objective function is lower because of the overall low signal reception for the receivers, and for higher values of angles the objective function is lower as well because of the increased amount of interference. Also in Figure 4.7 and Figure 4.8, where we have plotted SIR and illumination variation respectively, we can see the best value of divergence angle at around the same region.

We have also studied this effect for more number of layers in the bulb. In Figure 4.9, plots of objective function versus divergence angle for 2,3,4,5 and 6 layers are shown. As expected, with increasing number of layers, the optimum value for divergence angle decreases as more LEDs are

placed in the bulb for more number of layers which can result the best communication coverage and uniformity of illumination across the room.

As we can see the optimum divergence angle value is lower in case of more number of layers, we wanted to see whether a higher SIR value (better spatial reuse) or a lower  $I_s$  value is the reason behind this.

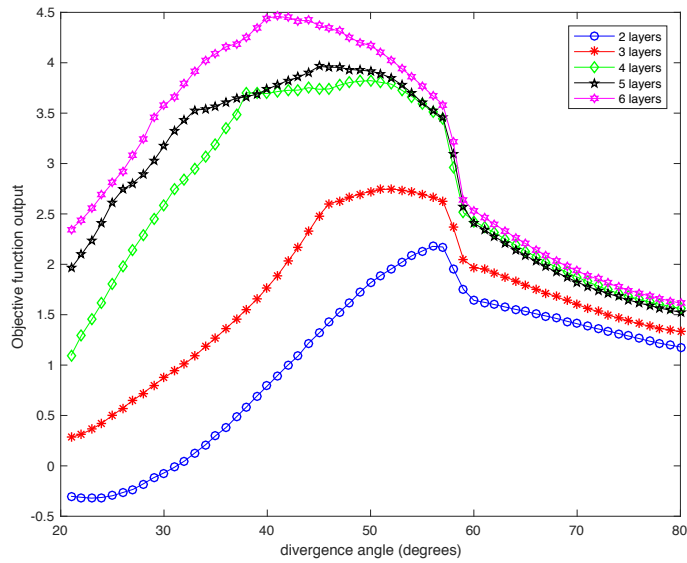
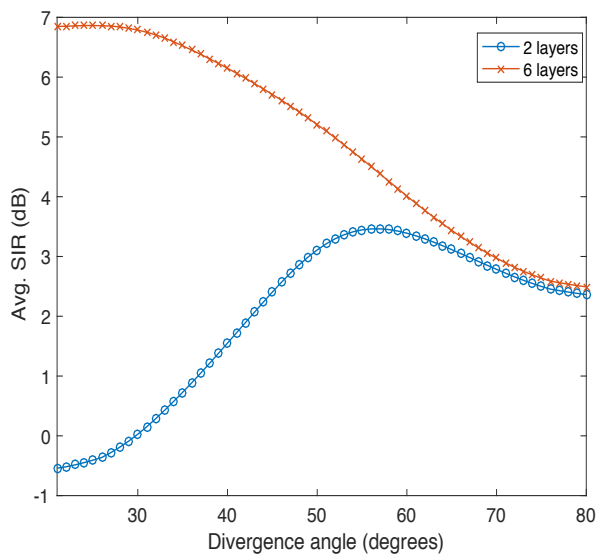
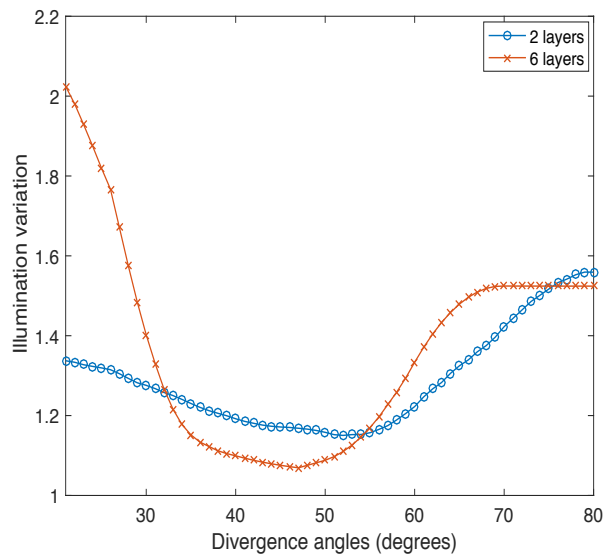


Figure 4.9: Obj. function output versus Divergence angle for different number of layers.

To observe this, we plot both SIR and  $I_s$  against the divergence angle for 2 and 6 layers cases which is shown in Figure 4.10. We can see that optimum divergence angle value is lower for 6 layers case in both plots, but the difference is more significant in the plot of SIR against divergence angle. So, the higher SIR value is the main reason behind the lower value of optimum divergence angle in the case of more layers of LEDs.



(a) SIR against divergence angle for 2 and 6 layers.



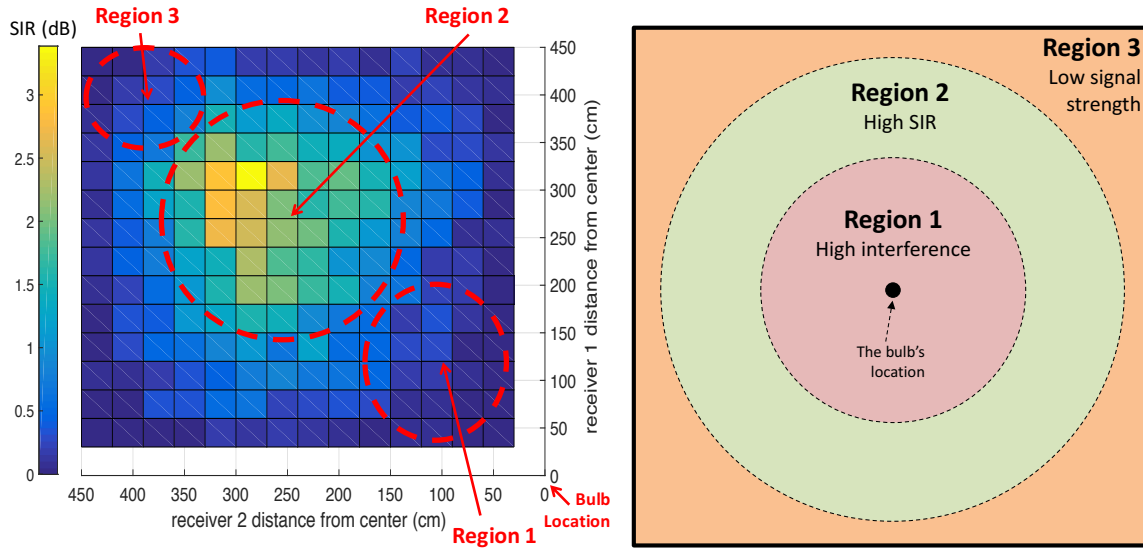
(b)  $I_s$  against divergence angle for 2 and 6 layers.

Figure 4.10: Effect of divergence angle comparison between 2 and 6 layers.

#### 4.7.5 The Three-Region Behavior

Figure 4.11(a) shows the contour plot of average SIR of receivers 1 and 2 (i.e.,  $\frac{1}{2}(\gamma_1 + \gamma_2)$ ) versus distance between each of the two receiver laptops and the floor center, which shows an interesting behavior. The SIRs are averaged over a large number of user locations, each of which satisfy the considered Euclidean distances to the center of the room as in Figure 4.11(a).

If the laptops are placed in region 1 (the center region of the room) then the distances between them and the center of the room floor is small, and if we place them in region 3 (in the corners), then this distance has to be large. In the surface plot we can see relatively low values of SIR for small and large distances between the laptops and the center of the room floor and higher values



(a) Contour plot of SIR.  $k_1 = 11$ ,  $k_2 = 17$ ,  $\theta_d = 45^\circ$ .

(b) Top view of the room floor.

Figure 4.11: The 3-region behavior.

for the medium distances, so this indicates region 2 (the middle region between the center and the corner) to be the most favorable one. In the regions shown in Figure 4.11(b), it is assumed that both of the laptops are inside that region. The areas outside the red dotted circles in Figure 4.11(a) indicate cases where one receiver is close to the room center and the other is distant, which also produce low SIR.

The top view of the surface plot is shown in Figure 4.11(a) which more vividly points out the 3 regions (the red dotted circles), since the blue squares indicate low values and the yellow/green squares indicate high values of SIR. The 3 regions in the room floor are shown in Figure 4.11(b). Also in Figure 4.11(b) which illustrates the 3-region behavior in the SIR distribution across the room surface, it can be observed that SIR in the high interference region 1 reduces much slower

than the floor area, and in region 3, SIR decreases along with the floor size. This behavior can act as a useful guide in organizing the room layout for the placement of the receivers.

## 4.8 Chapter Summary

In this chapter, we have optimized a multi-element bulb design for both illumination and communication quality of VLC in a room by varying the number of LEDs in the bulb in each layer and the divergence angle of the LEDs. The framework enables optimizing the placement of LED boards/transmitters on the bulb for maximizing the signal-to-interference ratio (SIR) while respecting the evenness of the lighting on the room floor. We also considered a power constraint on the bulb and observed that maximum SIR saturates as the power constraint as well as the number of layers and LED boards on the bulb increase. Furthermore, we find out that based on the SIR, we can divide the room into three separate regions which demonstrate different communication characteristics. The presented framework can serve as a basis for future studies for better understanding and further improvement.



## **CHAPTER 5**

# **OPTIMIZATION OF SINR AND ILLUMINATION UNIFORMITY IN MEMD VLC NETWORKS**

In this chapter, we consider a downlink VLC architecture which is capable of providing simultaneous lighting and communication coverage across an indoor setting.<sup>1</sup> We design a multi-element hemispherical bulb which transmits multiple data streams from its LEDs to mobile receivers. The architecture employs a LOS alignment protocol to tackle the hand-off issue caused by the mobility of the receivers in the room. We formulate an optimization problem that jointly addresses the LED-user associations as well as the LEDs' transmit powers in order to maximize the SINR while taking into consideration an acceptable illumination uniformity constraint across the room. We propose a near-optimal solution using Geometric Programming (GP) to solve the optimization problem, and compare the performance of this GP solution to low complexity heuristics.

---

<sup>1</sup>Most of the content on this chapter was published in journal [14].

## 5.1 System Model

We consider a single hemispherical bulb for an indoor VLC system consisting of  $M$  LEDs serving  $U$  users. The design of the bulb and placement of layers and LEDs in the bulb are already described in Section 3.1.

### 5.1.1 Assumptions and Notation

For this chapter, we make the following assumptions:

- Each mobile user inside the room has one PD receiver and one RF transmitter, and is capable of extracting the desired signal from the optical transmitters.
- Locations of the mobile users are known to the access point, i.e., the bulb structure.
- There are  $N$  fixed light sensors assumed to be distributed uniformly inside the room. These sensors are not equipped with decoders and only used to ensure the illumination uniformity. Further, these sensors are not purposed for providing illumination, but rather for measuring illumination, and we do not need to employ them in a real scenario. We are solving this optimization problem for a multi-element VLC bulb whose dimensions are known and the room dimensions are fixed as well. These  $N$  sensors are used in our simulations in order to calculate the illumination level at the points on the floor, hence the illumination uniformity of the room. As far as the value of  $N$  is concerned, the larger it is, the more accurately we

can calculate the illumination uniformity of the room. But after a certain point, it is not worthy to increase  $N$  for a larger runtime as we can reach a near perfect accuracy. From our experimentation, we found 100 sensors to be sufficient for the room size we consider.

- LoS is always maintained between a user and the LED assigned to it. However, the users should be aware of the fact that temporary blockage by objects such as their own hands can disrupt data transmission, and in those cases data downloading medium switches back to the traditional RF communication.

To ease the rest of the discussion in the paper, we summarize our notation in Table 5.1.

Table 5.1: List of Key Symbols

<b>Notation</b>	<b>Description</b>
$M$	Number of LEDs
$U$	Number of users
$B$	Communication bandwidth
$P_m$	Transmit power of LED $m$
$\bar{P}$	Maximum LED's transmit power
$\varepsilon_{mu}$	Association between LED $m$ and user $u$
$h_{mu}$	Channel gain between LED $m$ and user $u$
$A_u$	User PD area
$d_{mu}$	Distance between LED $m$ and user $u$
$\varphi_{mu}, \phi_{mu}$	Irradiance and incidence angles, respectively
$\phi_c$	FOV angle of the PD
$Q_0(\varphi_{mu})$	Lambertian radiant intensity
$q$	The order of Lambertian emission
$\varphi_{1/2}$	The transmitter semiangle at half power
$\Gamma_u$	SINR at user $u$
$\vartheta$	Illumination uniformity
$\alpha_0$	The luminous efficiency
$\mu$	Minimum acceptable illumination uniformity

### 5.1.2 LED-User Association

Let us introduce a binary variable  $\varepsilon_{mu}$  that indicates the association between LED  $m$  and user  $u$ , and is given as follows:

$$\varepsilon_{mu} = \begin{cases} 1, & \text{if LED } m \text{ is associated with user } u. \\ 0, & \text{otherwise.} \end{cases} \quad (5.1)$$

Following the MEMD model, we assume that user  $u$  can be associated to many LEDs at the same time. In contrary, any LED is not allowed to associate with more than one user simultaneously. Thus, the following constraint should be respected:

$$\sum_{u=1}^U \varepsilon_{mu} \leq 1, \forall m. \quad (5.2)$$

### 5.1.3 Channel Model

In our channel model, we assume that the multipath propagation resulting from reflections and refractions is neglected and only LOS channel model is considered [54]. Therefore, the downlink communication channel between LED  $m$  and user  $u$  can be expressed as [55].

$$h_{mu} = \begin{cases} \frac{A_u}{d_{mu}^2} Q_0(\varphi_{mu}) \cos(\phi_{mu}) & , 0 \leq \phi_{mu} \leq \phi_c \\ 0 & , \phi_{mu} \geq \phi_c \end{cases} \quad (5.3)$$

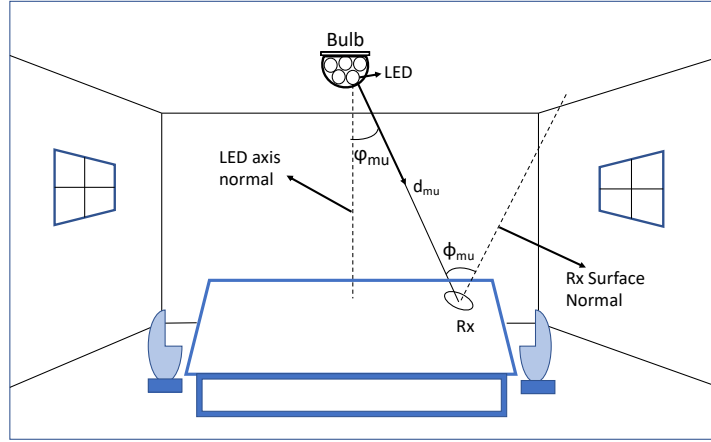


Figure 5.1: Transmitters and Receivers in a VLC channel model.

where  $A_u$  is the user PD area and  $d_{mu}$  is the distance between LED  $m$  and user  $u$ .  $\varphi_{mu}$  and  $\phi_{mu}$  are the irradiance and incidence angles, respectively (shown in Fig. 5.1).  $\phi_c$  is the FOV angle of the PD. We have assumed that no optical filter is used.  $Q_0(\varphi_{mu})$  is the Lambertian radiant intensity and expressed as

$$Q_0(\varphi_{mu}) = \frac{(q+1)}{2\pi} \cos^q(\varphi_{mu}), \quad (5.4)$$

where  $q = -\ln(2)/\ln(\cos(\varphi_{1/2}))$  is the order of Lambertian emission and  $\varphi_{1/2}$  is the transmitter semi-angle at half power.

Because of the nature of our system design (hemispherical bulb in the center of the room ceiling) the beams coming out from most of the LEDs in the bulb do not experience significant reflection. Beams coming from only a few number of LEDs in the higher layers of the bulb experience reflection from the side walls of the room. For this minimal effect of reflection, we do not consider it in our channel model to cut down the running time of our simulations.

#### 5.1.4 SINR Calculation

We assume that each LED is either associated with one user or used for lighting only. Therefore, SINR at user  $u$  can be expressed as

$$\Gamma_u = \frac{\beta_{uu}^2}{N_0 B + \sum_{\substack{k=1 \\ k \neq u}}^U \beta_{ku}^2} \quad (5.5)$$

where  $\beta_{iu} = \sum_{m=1}^M \epsilon_{mi} h_{mu} P_m$ .  $\beta_{iu}$ ,  $B$  and  $N_0$  are the total power received by user  $i$  from its assigned LEDs, the communication bandwidth and the spectral density of the Additive White Gaussian Noise (AWGN), respectively. Here, AWGN includes the noise coming from external light sources such as sunlight and other artificial light sources including fluorescent lamps, incandescent lamps etc.

#### 5.1.5 Illumination Uniformity

Another important factor to be considered is illumination intensity distribution across the room floor. Specifically, the illumination uniformity,  $\vartheta$ , can be defined as the ratio between the minimum and the average illumination intensity [56] among all  $N$  sensors, and is expressed as

$$\vartheta = \frac{\min(\sigma_n)}{\frac{1}{N} \sum_{n=1}^N \sigma_n} \quad (5.6)$$

where  $\sigma_n = \sum_{m=1}^M \alpha_0 P_m h_{mn}$  is the received total power at sensor  $n$ ,  $\alpha_0$  is the luminous efficiency that depends on the LED color wavelength,  $h_{mn}$  is the channel between LED  $m$  and sensor  $n$  and  $\min(\cdot)$  is the minimum function. It should be noted that the illumination uniformity is based only on the illumination generated by the LEDs on the bulb which is  $P_m$  for a particular, LED  $m$  and the channels between  $M$  LEDs and  $N$  sensors which is  $h_{mn}$  for a particular  $m$  and  $n$ . It does not have any relation with the number of users  $U$ .

## 5.2 Problem Formulation

The approach of maximizing the total data rate which is known in the literature as Max C/I [57], promotes users with favorable channel and interference conditions by allocating to them most of the resources, whereas users suffering from higher propagation losses and/or interference levels will have very low data rates. Therefore, due to the unfairness of total sum data rate utility, the need for more fair utility metrics arises. For this reason, we choose to use Max-Min utility of the SINR. The Max-Min utilities are a family of utility functions attempting to maximize the minimum SINR in a network [58]. By increasing the priority of users having lower SINR, Max-Min utilities lead to more fairness in the network.

The key goal of our approach is to find solutions that balance illumination uniformity as well as communication efficiency, i.e., high SINR. As one of the key novelties in our work is considering the narrow beams from the LED transmitters which can cause uneven lighting in the room, we have placed illumination uniformity inside the objective function of our optimization problem. This



ensures a more general approach to solve the problem of finding the best possible combination of illumination and communication. In this section, we formulate an optimization problem aiming to maximize the product of minimum SINR of all users ( $\min_u(\Gamma_u)$ ) and the illumination uniformity by taking into consideration the association and illumination intensity constraints. The optimization problem can be expressed as

$$\underset{\varepsilon_{mu} \in \{0,1\}, P_m \geq 0}{\text{maximize}} \quad \min_u(\Gamma_u) \vartheta \quad (5.7)$$

subject to:

$$P_m \leq \bar{P}, \quad \forall m, \quad (5.8)$$

$$\sum_{u=1}^U \varepsilon_{mu} \leq 1, \quad \forall m, \quad (5.9)$$

$$\vartheta \geq \mu, \quad (5.10)$$

where constraints (5.8) and (5.9) represent the power and association constraints, respectively. Constraint (5.10) is to ensure that the illumination uniformity is above a certain threshold, where  $\mu$  is the minimum acceptable illumination uniformity for an indoor setting [56].

We consider the communication signal for LED  $m$  to be carried on the background DC light intensity with power  $P_m$ . And, for the case of only illumination, we assume that all LEDs are providing the same background light intensity with power  $P_m$ . This power can be adjusted to achieve the best possible SINR and lighting distribution in both the cases considered here. Basically,  $P_m$  is considered as the DC power when the LED is providing illumination only, and  $P_m$  is considered

the average power when it is providing both illumination and communication. Similar assumptions can also be found at [45, 59].

In order to simplify the problem, we define new decision variables for minimum illumination  $I_{\min}$  and minimum SINR  $\Gamma_{\min}$ , respectively, as

$$I_{\min} = \min_n(\sigma_n), \quad (5.11)$$

$$\Gamma_{\min} = \min_u(\Gamma_u). \quad (5.12)$$

Using these new variables, our optimization problem becomes

$$\begin{array}{l} \text{maximize} \\ \varepsilon_{mu} \in \{0,1\} \\ P_m, I_{\min}, \Gamma_{\min} \geq 0 \end{array} \quad \frac{\Gamma_{\min} I_{\min}}{\frac{1}{N} \sum_{n=1}^N \sigma_n} \quad (5.13)$$

subject to:

$$\sigma_n \geq I_{\min}, \quad \forall n, \quad (5.14)$$

$$\frac{\beta_{uu}^2}{N_0 B + \sum_{\substack{k=1 \\ k \neq u}}^U \beta_{ku}^2} \geq \Gamma_{\min}, \quad \forall u. \quad (5.15)$$

and (5.8), (5.9), (5.10).

Notice that, the formulated optimization problem in (5.13)-(5.15) is a mixed-integer non-linear problem (MINP).

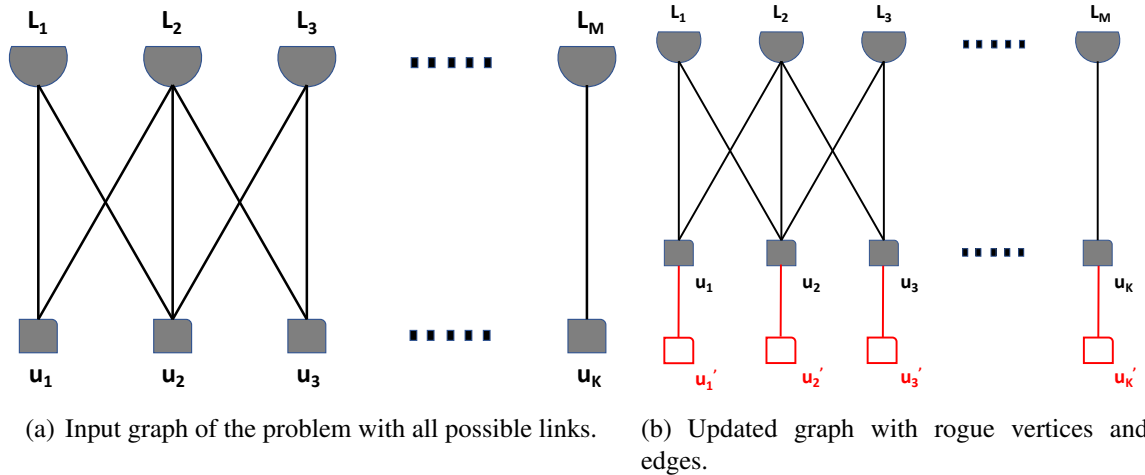


Figure 5.2: Comparison with minimum  $v$ -cut problem.

### 5.2.1 NP-Completeness

We have found our optimization problem to be NP-complete by reducing it to the Minimum  $v$ -cut problem, a well known NP-complete problem [60]. In Minimum  $v$ -cut, the input is a weighted undirected graph,  $G(V, E)$  from which a set of edges  $E^*$  needs to be removed such that the graph  $G$  becomes a set of  $v$  connected components and the total weight of the removed edges  $E^*$  is minimum. Formally, let  $MINIMUMvCUT(G, v)$  be a routine solving the Minimum  $v$ -Cut problem and returning the set of edges  $E^* \subset E$  to be removed from  $G$ .

Now, if we consider every possible link between each transmitter and receiver in our MEMD VLC system (only considering the links where the receiver falls in the coverage area of the transmitter) then the collection of all these edges are similar to the input graph in the Minimum  $v$ -cut problem. This is shown in Figure 5.2(a), where  $M$  LEDs on the bulb are named as  $L_1, L_2, \dots$  and  $L_M$ , and  $K$  receivers are named as  $u_1, u_2 \dots$  and  $u_K$ . To make our problem comparable with

---

**Algorithm 1** LED-User association problem: Reduction to Minimum  $v$ -cut

---

- 1: Input:  $\mathbf{J}_m$ , LED positions;  $\mathbf{W}_k$ , user positions.
  - 2: Output:  $\varepsilon$ , association of LEDs to users.
  - 3: Define vertex set  $V^l = L_1, L_2, \dots, L_M$  that has a vertex for each LED.
  - 4: Define vertex set  $V^u = u_1, u_2, \dots, u_K$  that has a vertex for each user
  - 5: Construct graph  $G(V, E)$  with  $V = V^l \cup V^u$  and  $E = \{(u, l) : u \in V^u, l \in V^l, h_{ul} \neq 0\}$ .
  - 6: **for** each edge  $(l_m, u_k) \in E$  **do**
  - 7:   Using inputs  $\mathbf{J}_m$  and  $\mathbf{W}_k$ , calculate  $h_{mk}$
  - 8:   Set weight  $w_{mk}$  to  $h_{mk}$
  - 9: **end for**
  - 10: Initialize set of rogue vertices  $V^* = \emptyset$ .
  - 11: Set  $V^{u*} = \{u'_k\}, k = 1, 2, \dots, K$ . // Construct rouge vertex for each user vertex.
  - 12:  $V^* \leftarrow V^* \cup V^{u*}$ .
  - 13:  $G(V, E) \leftarrow G(V \cup V^{u*}), E \cup \{(u, v) : u \in V^u, v \in V^{u*}\}$  // Graft  $G$  with rogue vertices  $V^{u*}$ .
  - 14:  $w_{max} = \sum_{u, v: (u, v) \in E} w_{uv}$ . // Calculate the total weight of all edges, including the grafted edges.
  - 15: Set weights  $w_{uu'} : u \in V^u, u' \in V^{u*}$  to  $w_{max}$ .
  - 16:  $E^* \leftarrow MINIMUMvCUT(G, K)$ .
  - 17:  $G(V, E) \leftarrow G(V \setminus V^*, E \setminus E^*)$  // Remove  $E^*$  and rogue vertices  $V^*$  from  $G$ .
  - 18: Set  $\varepsilon_{uv}$  to 1 for all  $u \in V^u$  and  $v \in V^v$  such that  $(u, v) \in E$ .
  - 19: **return**  $\varepsilon$ .
- 

$MINIMUMvCUT(G, v)$ , we define a simplified version of the input graph  $G(V, E)$  by assuming weight of these edges as the received signal strength from the LED to its assigned receiver, so the objective function described in (5.13) is dependent on these edges.

If we solve this simplified version of the problem as if it is  $MINIMUMvCUT(G, v)$ , then some edges from the input graph will be removed so that the overall cost is the minimum. The  $v$  vertices in  $MINIMUMvCUT(G, v)$  is comparable with the number of receivers, and the  $v$  connected components in the graph can be compared with the partitions in the bulb for the optimum assignment. Thus, this very simplified version of the problem is NP-complete whereas the actual problem is even more difficult to solve as each link is dependent on the other links in most of the cases. This is due to the fact that, when calculating SINR for each receiver, signal coming from the transmitters

other than the assigned one are treated as interference. Also, the illumination uniformity constraint (5.10) is another factor to consider in our original problem.

We show that the LED-user association problem is NP-Complete by doing a polynomial-time reduction in Algorithm 1. For  $M$  LEDs and  $K$  users, we construct the graph  $G(V, E)$  with all possible links considering the coverage area of the LEDs. After that, we set the weight of each link with the channel value between corresponding user and LED (lines 5-9). Next, we add rogue vertices to each user vertex and connect them to their corresponding user vertices in  $G$  with the highest possible value of edge weight, which we calculate as the sum of all weights in the existing graph  $G$  (lines 10-16). These new vertices and edges are shown in Fig. 5.2(b) in red color. Finally, we call  $MINIMUMvCUT(G, K)$  with the updated graph  $G$  as input, which gives us  $K$  connected components such that sum of weights on the cut edges is minimum.

The Minimum  $v$ -cut on the updated graph also corresponds to the optimal association of every user vertex to an LED vertex. It is evident from the  $K$  connected graphs that they will: 1) not be consisted of only LED vertices as they are not connected to each other; 2) have to include at least one user vertex  $u_k$  since the Minimum  $v$ -cut can't cross the edges (i.e. edges in 5.2(b)) between user vertices  $u_k$  and their rogue vertices  $u'_k$ , because the  $(u_k, u'_k)$  edges have the largest total weight  $w_{max}$  as there will be cuts smaller than  $w_{max}$ ; and 3) not have more than one user vertex  $u_k$  since there are only  $K$  such vertices in  $G$ . These conditions guarantee that Minimum  $v$ -cut will cross the edges in  $G$  such that LED vertices in each connected graph will be grouped with only one pair of user vertices  $(u_k$  and  $u'_k)$ . After getting the output graph from Minimum  $v$ -cut, we can remove the rogue vertices to obtain the optimal LED-user association.

### 5.3 Near Optimal Solution

In order to simplify the problem (5.7), we propose to approximate the joint optimization problem using Geometric Programming (GP). To do this, we first relax the variable  $\varepsilon_{mu}$  and make it continuous, i.e.,  $0 \leq \varepsilon_{mu} \leq 1$ . After obtaining an optimal value of  $\varepsilon_{mu}$ , we propose an efficient way to recover the best and closest upper integer value. We apply a successive convex approximation (SCA) approach to transform the non-convex problem into a sequence of relaxed convex subproblems that follows GP formulation [61].

#### 5.3.1 Geometric Programming

GP deals with a class of nonlinear and non-convex optimization problems that can be solved after converting them to nonlinear but convex problems [62]. The standard form of GP is defined as the minimization of a posynomial function subject to inequality posynomial constraints and equality monomial constraints as given below

$$\underset{b}{\text{minimize}} \quad f_0(b) \tag{5.16}$$

subject to:

$$f_l(b) \leq 1, \quad \forall l = 1, \dots, L, \tag{5.17}$$

$$\tilde{f}_{\tilde{l}}(b) = 1, \quad \forall \tilde{l} = 1, \dots, \tilde{L}, \tag{5.18}$$

where  $f_l(b)$ ,  $l = 0, \dots, L$  are posynomials and  $\tilde{f}_{\tilde{l}}(z)$ ,  $\tilde{l} = 1, \dots, \tilde{L}$  are monomials. A monomial is defined as a function  $f : \mathbf{R}_{++}^n \rightarrow \mathbf{R}$  as follows:

$$f(b) = \check{a} b_1^{a_1} b_2^{a_2} \dots b_Z^{a_Z}, \quad (5.19)$$

where the multiplicative constant  $\check{a} \geq 0$ , and the exponential constants  $a_z \in \mathbb{R}$ ,  $z = 1, \dots, Z$ . A posynomial is a non-negative sum of monomials.

In general, GP in its standard form is a non-convex optimization problem, because posynomials and monomials functions are non-convex functions. However, with a logarithmic change of the variables, objective function, and constraint functions, the optimization problem can be turned into an equivalent convex form using the property that the logarithmic sum of exponential functions is convex (see [62] for more details). Therefore, the GP convex form can be formulated as

$$\underset{c}{\text{minimize}} \quad \log f_0(e^c) \quad (5.20)$$

subject to:

$$\log f_l(e^c) \leq 0, \quad \forall l = 1, \dots, L, \quad (5.21)$$

$$\log \tilde{f}_{\tilde{l}}(e^c) = 0, \quad \forall \tilde{l} = 1, \dots, \tilde{L}, \quad (5.22)$$

where the new variable  $c$  is a vector that consists of  $[c_z] = [\log b_z]$ . It can be noticed that (5.13)-(5.15) can be transformed to the GP standard form easily. In order to convert the optimization problem formulated in (5.13)-(5.15) to a GP standard form, we propose to apply approximation

for constraint (5.14) and constraint (5.15). The single condensation method is employed to convert this constraint to posynomial as described below:

**Definition 1.** *The single condensation method for GP involves upper bounds on the ratio of a posynomial over a posynomial. It is applied to approximate a denominator posynomial  $g(b)$  to a monomial function, denoted by  $\tilde{g}(b)$  and leaving the numerator as a posynomial, using the arithmetic-geometric mean inequality as a lower bound [61]. Given the value of  $b$  at the iteration  $r - 1$  of the SCA  $b^{(r-1)}$ , the posynomial  $g$  that, by definition, has the form  $g(b) \triangleq \sum_{j=1}^J \mu_j(b)$ , where  $\mu_j(b)$  are monomials, can be approximated as:*

$$g(b) \geq \tilde{g}(b) = \prod_{j=1}^J \left( \frac{\mu_j(b)}{\tilde{\mu}_j(b^{(r-1)})} \right)^{\tilde{\mu}_j(b^{(r-1)})}, \quad (5.23)$$

where  $\tilde{\mu}_j(b^{(r-1)}) = \frac{\mu_j(b^{(r-1)})}{g(b^{(r-1)})}$ .  $J$  corresponds to the total number of monomials in  $g(b)$ .

In order to convert constraints (5.14) and (5.15) to posynomials, we propose to apply the single condensation method given in Definition 1 to approximate the denominator posynomial to a monomial function, where in this case  $J = M$  and  $J = M(M + 1)/2$  for constraints (5.14) and (5.15), respectively. Therefore, constraints (5.14) and (5.15) can be expressed respectively as

$$\frac{I_{\min}}{\tilde{g}_1 \left( P_m^{(r)} \right)} \leq 1, \forall n, \quad (5.24)$$

$$\frac{\Gamma_{\min} \left( N_0 B + \sum_{\substack{k=1 \\ k \neq u}}^U \beta_{ku}^2 \right)}{\tilde{g}_2 \left( P_m^{(r)}, \boldsymbol{\varepsilon}_{mu}^{(r)} \right)} \leq 1, \quad \forall u. \quad (5.25)$$



### 5.3.2 GP Standard Form Transformation

By considering the approximations of (5.24) and (5.25), we can formulate the GP approximated subproblem at iteration  $r$  of the SCA as

$$\begin{aligned} & \text{minimize} && \frac{\frac{1}{N} \sum_{n=1}^N \sum_{m=1}^M \alpha_0 P_m^{(r)} h_{mn}}{\Gamma_{\min}^{(r)} I_{\min}^{(r)}} && (5.26) \\ & \varepsilon_{mu}^{(r)}, P_m^{(r)}, && && \\ & \Gamma_{\min}^{(r)}, I_{\min}^{(r)} \geq 0 && && \end{aligned}$$

subject to:

$$\frac{I_{\min}^{(r)}}{\tilde{g}_1 \left( P_m^{(r)} \right)} \leq 1, \forall n, \quad (5.27)$$

$$\frac{\Gamma_{\min} \left( N_0 B + \sum_{\substack{k=1 \\ k \neq u}}^U \beta_{ku}^{(r)2} \right)}{\tilde{g}_2 \left( P_m^{(r)}, \varepsilon_{mu}^{(r)} \right)} \leq 1 \quad \forall u, \quad (5.28)$$

$$\frac{P_m^{(r)}}{\bar{P}} \leq 1, \quad \forall m, \quad (5.29)$$

$$\sum_{u=1}^U \varepsilon_{mu}^{(r)} \leq 1, \forall m, \quad (5.30)$$

$$\frac{\frac{\mu}{N} \sigma_n^{(r)} h_{mn}}{I_{\min}} \leq 1 \quad (5.31)$$

The optimization problem given in (5.26)-(5.31) can be transformed to a convex form as given in (5.20)-(5.22). Therefore, each iteration of the SCA can be solved optimally as described in Algorithm 2 using any standard optimization methods [63]. Each GP in the iteration  $r$  loop (lines 3-5) tries to improve the accuracy of the approximations to a particular minimum in the original feasible region. This is performed until no improvement in the objective function is made. A pa-

parameter,  $\xi \rightarrow 0$ , is introduced to control the accuracy of the algorithm convergence of the objective function as follows:  $|\chi^{(r)} - \chi^{(r-1)}| \leq \xi$ .

---

**Algorithm 2** SCA Algorithm

---

- 1: Select feasible initial values  $b^0 = [\epsilon_{mu}^{(0)}, P_m^{(0)}, \Gamma_{\min}^{(0)}, I_{\min}^{(0)}]$ .
  - 2:  $r=1$
  - 3: **while** Convergence ( $|\chi^{(r)} - \chi^{(r-1)}| \leq \xi$ ) **do**
  - 4:   Approximate the denominators using the arithmetic geometric mean as indicated in (5.23) using  $b^{(r-1)}$ .
  - 5:   Solve the optimization problem using the interior-point method to determine the new approximated solution  $b^{(r)} = [\epsilon_{mu}^{(r)}, P_m^{(r)}, \Gamma_{\min}^{(r)}, I_{\min}^{(r)}]$ .
  - 6:   Update  $r = r + 1$
  - 7: **end while**
- 

## 5.4 Heuristic Solutions

Since *PARTITION\_WU* is an NP-Complete problem, we try to design heuristics with low complexity in terms of computation and memory. The users in the MEMD VLC system will be mobile and ad hoc. The existing users will move around in the room or leave the room, and new users will enter the room. These events will require the re-partitioning and re-assignment of LEDs to users and re-tuning of their transmit powers so as to keep the joint optimization objective high. Thus, it is crucial to minimize the time it takes to re-optimize the optimization parameters, which is the reason for us to design heuristics. We present two heuristics in this section and, later, compare them to the GP approximation by simulations.

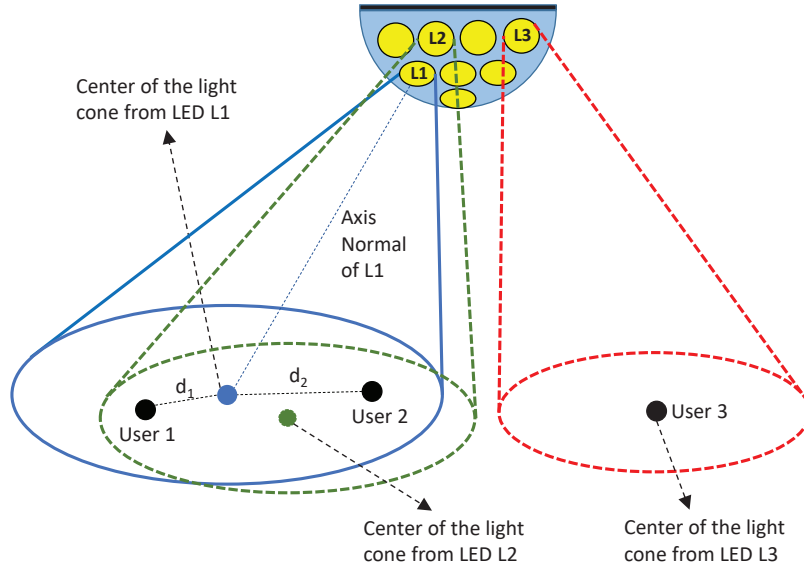


Figure 5.3: A case of interference for an user: LEDs L1, L2 and L3 are assigned to user 1, 2 and 3 respectively. In this case, received power from L2 and L3 will be considered as interference at user 1 - since these LEDs are assigned to user 2 and user 3.

#### 5.4.1 SINR First Approach (SFA)

In this approach, we propose to solve our optimization problem using a two-step iterative approach given the location coordinates of all users. In the first step, we optimize the LED-user association and the LED transmit powers that maximize the SINR. Then in the second step, by keeping the association fixed from the first step, we adjust only the LEDs' power level in order to achieve maximum objective function in (5.15) which is a function of SINR and illumination uniformity. The details of the proposed algorithm are as follows:

##### 1. Maximize SINR

- (a) We set a maximum power value,  $P_{max}$ , that can be assigned to an LED. We use  $P_{max} = 100$  mW.

- (b) We assign LED  $m$  to the closest user to its beam projection if the user lies in the cone of LED  $m$ .
- (c) If there is no user in the cone, then also  $P_{max}$  is allocated to LED  $m$  initially and it is not assigned to any of the users.
- (d) If there is more than one user in the cone of LED  $m$ , then we assign this LED to the user which is nearest to the center of the cone of the LED, but with fractional power, since there will be interference in this case. For simplicity, we calculate this fraction by taking the distances of the nearest and second nearest user from the center of the LED cone into account. For example, if the distance of the nearest user from the center of the cone is  $d_1$  and the distance of the second nearest user from the center of the cone is  $d_2$  then the allocated power to LED  $m$  would be,  $P_m = P_{max}(1-d_1/d_2)$  (shown in Fig. 5.3). When the second nearest user is much closer to the nearest user, the ratio of  $d_1$  and  $d_2$  is higher, and that makes the value of  $P_m$  to be lower to minimize the effect of interference.

After assigning all  $M$  LEDs in this fashion (which focuses on SINR) we try to improve the illumination uniformity in the next step.

## 2. Maximize Uniformity

- (a) We set four discrete power levels (i.e.,  $P_{max}$ ,  $P_{max}/2$ ,  $P_{max}/3$ ,  $P_{max}/4$ ) which can be allocated to the LEDs that are unassigned instead of allocating them the full power. We

allocate these discrete power levels to the LEDs which are unassigned and equipped with full power.

- (b) We then recalculate the illumination uniformity using (5.6) and select the discrete power values for the LEDs that gives the maximum uniformity.

This heuristic gives a lower priority to the illumination uniformity and aims to maximize SINR with low complexity while trying to achieve an acceptable illumination uniformity.

#### **5.4.2 Uniformity First Approach (UFA)**

In SFA, we try to maximize the SINR by assigning as much power as possible to the LEDs which have only one user in their cones, then try to improve the illumination uniformity. In the UFA, we do the opposite - we try to find the allocated power values of the LEDs for the best possible illumination uniformity, then we modify these power values to improve the SINR. The approach is described below:

1. We formulate a quasi-convex optimization problem that can be solved efficiently using bisection [62] to obtain the allocated power values for the LEDs for maximum possible uniformity, where the optimal solution is obtained for a fixed SINR value, i.e.,  $\Gamma_{\min}$  is constant.

This problem can be formulated as

$$\underset{P_m, I_{\min} \geq 0}{\text{minimize}} \quad \frac{\frac{1}{N} \sum_{n=1}^N \sigma_n}{\Gamma_{\min} I_{\min}} \quad (5.32)$$

subject to (5.8), (5.14).

We denote the resulting  $P_m$  values as intermediate power values which are  $P_{1i}, P_{2i}, \dots, P_{Mi}$  for M LEDs.

2. When there is only one or no user in LED  $m$ 's cone, then we proceed like Step 1(c) in SFA but with a little difference. Instead of allocating maximum power to LED  $m$ , we allocate  $\max(P_{mi}(1 + \tau), P_{max})$ . We try different values for  $\tau$ , from 0.1 to 0.7 which is a measurement of how much we can deviate the allocated power to LED  $m$  from its intermediate value  $P_{mi}$ .
3. Then, we proceed like Step 1(d) in SFA but with a little difference. The equation for the allocated power to LED  $m$  will be  $P_m = P_{mi}(1 - d_1/d_2)$ . We also make sure that  $P_m$  is within the tolerance limit we set, thus  $P_m \geq P_{mi}(1 - \tau)$ .

This approach gives more priority to the illumination uniformity and makes sure that the minimum uniformity constraint in (5.10) is satisfied as  $\tau$  gets closer to 0. A larger tolerance limit  $\tau$  allows UFA to deviate from the uniformity-satisfying transmit power values for a higher throughput. In essence,  $\tau$  can be used as a knob to tune UFA between optimizing for uniformity and throughput. Tuning  $\tau$  enables flexibility in our approach to solve the joint optimization problem. The designer of the VLC system could tune  $\tau$  in our formulation in order to attain solutions

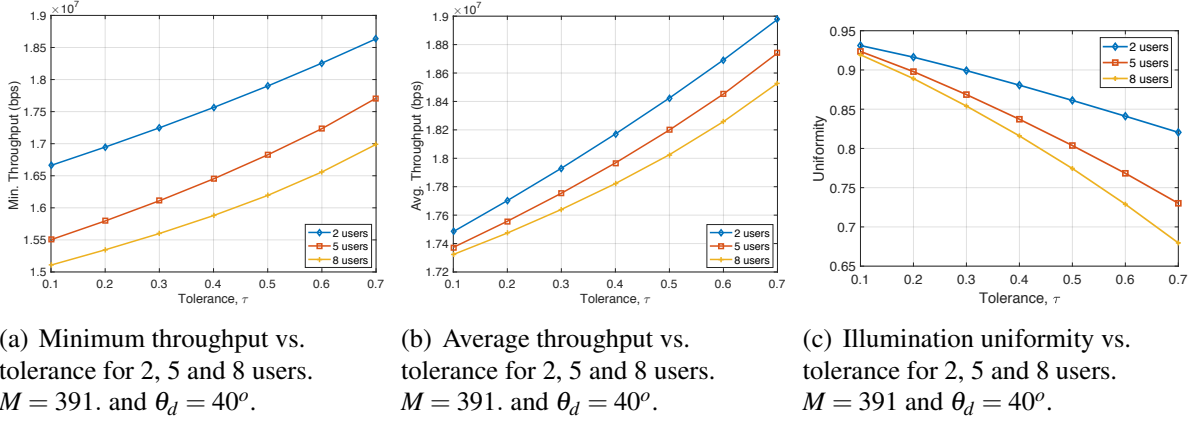


Figure 5.4: Effect of  $\tau$  on throughput and uniformity for UFA.

favoring higher throughput or more uniform illumination while still satisfying the minimum illumination constraint followed by the previous studies in the literature. This effect of  $\tau$  can be seen in Fig. 5.4, where we plot minimum throughput, average throughput and illumination uniformity vs. the tolerance value  $\tau$  for 2, 5 and 8 users cases. As described earlier, minimum and average throughput gradually increase while uniformity gradually decreases for higher value of  $\tau$ .

A critical design issue to consider in our problem is the dynamic nature of the VLC system in terms of the number of users, since it can change at any time with arrival or departure of users. In order to find solutions attaining higher SINR than what our approach finds, it may be possible to solve a traditional VLC SINR maximization problem[37] by feeding an appropriate minimum illumination constraint to the optimizer, e.g., approximately 0.925 for an attained minimum throughput of 15.2 Mbps from Fig. 5.4). However, this minimum illumination threshold changes depending on the user count and positions in the system. Thus, it would be necessary to find the appropriate illumination threshold before using the SINR maximization approach. Our approach allows a more flexible framework. The tolerance variable  $\tau$  enables us to run a fast heuristic to find a good

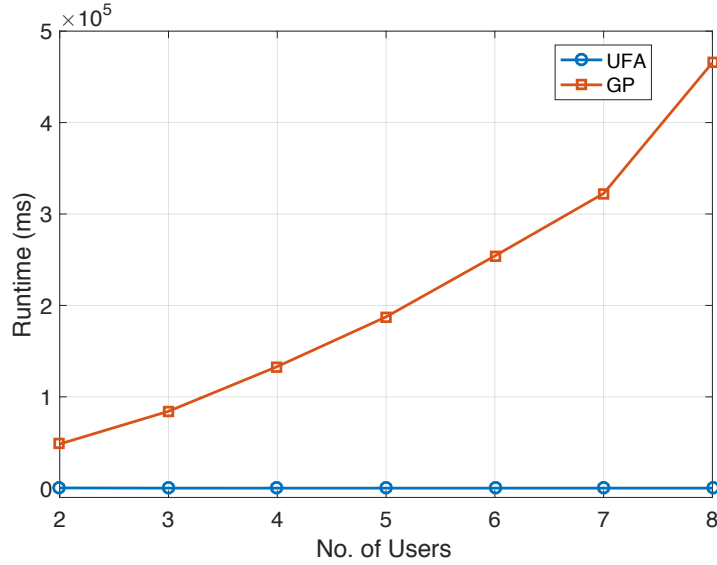


Figure 5.5: Runtime vs. No. of users for UFA and GP.  $M = 65$ .

solution when the number of served users or positions change. Further, using our approach, the designer of the VLC system can get the highest possible illumination uniformity with zero tolerance, and then improvement of the minimum throughput (SINR) is possible in two ways:

First, the designer can increase  $\tau$  up to 1 while making sure the threshold of minimum allowable illumination uniformity is maintained (which is the constraint (5.10) in our formulation) in search of a higher SINR.

Second, with  $\tau > 0$ , the designer can quickly find a good solution to learn the minimum illumination uniformity for that solution and then solve a traditional VLC SINR maximization problem [37] with the learned illumination uniformity threshold to search for a higher SINR.

Although in the second approach we may be able to find a higher SINR, we will need to run the optimizer for each of these  $\tau$  values and for each time the total number of users is changed - which is highly time-consuming. This is where the approach presented in our paper is most useful



as we will need to run the optimizer only once - which can be to find the maximum illumination uniformity for a particular bulb configuration, and then from that we can find SINR for different  $\tau$  values, and user count and positions. Thus, this approach takes less time overall while it is yet capable of obtaining a near optimal SINR if required.

### 5.4.3 Computational and Memory Complexity

We are assuming  $M$  total LEDs and  $N$  total sensors in our problem. In both UFA and SFA, we check each of the LEDs to allocate source power and assign it to a user if needed. This effectively takes  $O(M)$  time. The majority of the time is needed in calculating  $h_{mu}$  and  $h_{mn}$ , which take  $O(MU)$  and  $O(MN)$ , respectively.  $h_{mn}$  is only calculated once since user coordinates do not affect the communication channel between the LEDs and sensors. So, we can ignore the  $O(MN)$  complexity from the  $h_{mn}$  calculation as it will only be done when the VLC system is initialized. Thus, the overall running time complexity of both SFA and UFA is  $O(MU)$ .

Regarding the memory complexity, in both approaches we have to store the coordinates of  $M$  LEDs to calculate  $h_{mu}$  and  $h_{mn}$ . We store the value of  $h_{mu}$  and  $h_{mn}$  too, which takes space of  $O(MU)$  and  $O(NU)$  respectively. SINR and illumination uniformity variables takes space of  $O(U)$  and  $O(N)$ , respectively. So, overall the memory complexity of SFA and UFA is  $O((M + N)U)$ .

Calculating the complexity of the GP solution is not very straightforward as we use the 'fmincon' command of MATLAB in order to get the solution of our constrained nonlinear multi-variable objective function. In order to compare the GP solution with UFA in terms of running time, we the

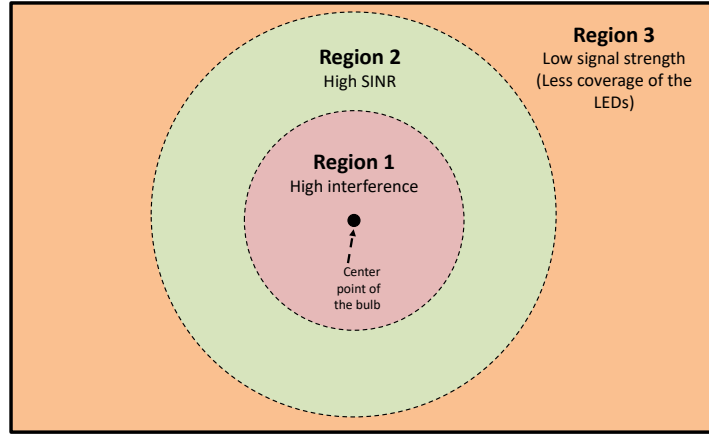


Figure 5.6: Difference in signal strength across the room floor assuming the hemispherical bulb in the center of the ceiling.

runtime versus number of users plot to observe the growth with respect to the growing number of users, which is shown in Fig. 5.5. We can clearly see that even for a small number of user range (2 to 8) the running time for GP starts to grow very quickly whereas for UFA it remains almost the same. This is the most important advantage of UFA over GP.

## 5.5 Simulation Results

In this section, we provide simulation results to study the performance of our MEMD VLC system model. Our aim is to see if the SFA and UFA heuristics can attain performance close enough to the GP solution, and identify any notable outcomes emerging from our designs. We focus on two metrics: *Minimum throughput* among the users and illumination *uniformity*. To compare our proposed methods (SFA, UFA, and GP), we use exact same input parameters for all of them. We randomly placed the users on the room floor with their receiver's FOV normal looking towards

the ceiling. We report the average of the minimum throughout and illumination uniformity results among these randomly generated cases. To gain confidence in our results, we repeated the simulation experiments 300 times for all the results.

Table 5.2: Simulation Parameters

Parameter	Value
Room Size	6m x 6m x 3m
Radius of the hemispherical bulb, $R$	40cm
Number of LEDs on the bulb, $M$	391
Radius of an LED transmitter, $r_t$	1.5cm
Divergence angle of the LEDs, $\theta_d$	40°, 50°
Maximum transmit power of the LEDs, $\bar{P}$	0.1W
Radius of a PD receiver*2, $r_r$	3.75cm
Number of users, $U$	2-8
Number of sensors, $N$	100
Visibility, $V$	0.5km
Optical signal wavelength, $\lambda$	650nm
AWGN spectral density, $N_0$	$2.5 \times 10^{-20}$ W/Hz
Modulation bandwidth, $B$	20MHz
Minimum uniformity, $\mu$	0.7

We use white LEDs with luminous efficiency  $\alpha_0 = 60$  lumen/watt [64]. The default values of the remaining input parameters used in our simulations are given in Table 5.2. For placing LEDs on the bulb, we followed the method in Section 3.1.2. In particular, for a bulb with  $R = 40$ cm radius, we place  $M = 391$  LEDs on 20 layers with  $k_{1..20} = [1, 6, 12, 15, 19, 26, 30, 37, 43, 33, 30,$

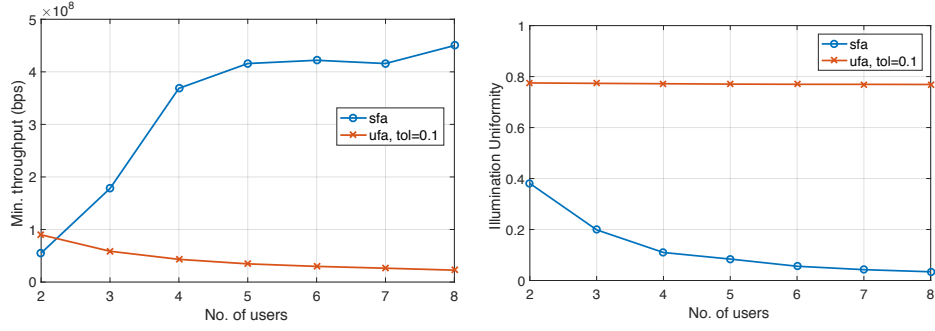
28, 25, 21, 16, 13, 11, 10, 9, 6]. The throughput and uniformity results we will present are likely to be attained by fewer LEDs; however, we want to observe the potential performance our heuristic and use a high number of LEDs in the simulation experiments.

### **5.5.1 UFA versus SFA**

First, we compare the two heuristic approaches, UFA and SFA to see whether one performs significantly better. We have compared both minimum throughput among the users and illumination uniformity for 2 to 8 users for these two approaches, as seen in Fig. 5.7(a) and Fig. 5.7(b). As we can see, minimum throughput and uniformity decrease for both approaches with increased number of users. Also, as expected, UFA gives better uniformity and SFA gives better minimum throughput. Although SFA gives a higher minimum throughput compared to UFA, the uniformity is poor and practically unacceptable, as typically the illumination uniformity of an indoor setting should be at least close to  $\mu=0.7$ . UFA is able to maintain this uniformity target even for 8 users. So, from this point on, we choose UFA to be the preferred heuristic solution as it is able to maintain an acceptable uniformity value although it has produced lower minimum throughput.

### **5.5.2 GP Solution versus UFA**

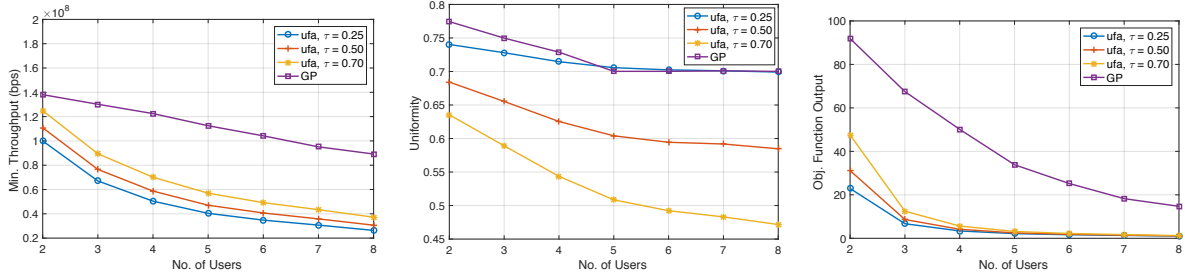
In order to understand how close our heuristics can get to our near-optimal solution via GP, we compare it to our preferred heuristic solution, UFA, with different tolerance values. An impediment



(a) Minimum throughput vs. No. of users.  $\theta_d = 50^\circ$ .

(b) Illumination uniformity vs. No. of users.  $\theta_d = 50^\circ$ .

Figure 5.7: Comparison between UFA and SFA.



(a) Minimum throughput vs. No. of users. (b) Illumination uniformity vs. No. of users. (c) Objective function value vs. No. of users.

Figure 5.8: Comparison between GP and UFA with  $M = 65$  and  $\theta_d = 50^\circ$ .

is the time complexity of the GP solution. Since it takes too long to run GP, we reduce the LED count  $M$  on the bulb to make it tractable with our computation capabilities. Following the method in Section 3.1.2, we place  $M = 65$  LEDs on 7 layers with  $k_{1..7} = [1, 11, 14, 17, 10, 7, 5]$ .

In Fig. 5.8(a) and 5.8(b), we observe that GP solution obtains much better minimum throughput compared to UFA but the uniformity is a little lower in some cases where  $\tau = 0.25$ , as it tries to put more balance in the objective function output towards throughput. It is clear from Fig. 5.8(c) that, for the objective function, the GP beats UFA for all tolerance values. Although GP has a higher objective function output in all the cases, UFA can come close in terms of minimum throughput

for higher  $\tau$  values and in terms of uniformity for lower  $\tau$  values. This is verifying our intuitions that  $\tau$  can be used to tune UFA's balance between throughput and uniformity.

### 5.5.3 Effect of Number of Users on UFA

Although UFA yields lower objective function output values in comparison to GP, a huge advantage of it is a much lower complexity. With GP, it becomes even more time-consuming to calculate the minimum throughput or uniformity in case of a high number of users (8 and above) whereas it can be done relatively quickly using UFA. Thus, we analyze how the throughput and uniformity changes when more users are added to the system. As shown in Fig. 5.9, the minimum throughput continues to decrease for higher number of users as expected, and a good uniformity value is maintained by UFA even for a very high number of users. Although marginal reduction in the minimum throughput is large early on (e.g., going from 2 to 3 users causes about a 3-fold decrease in minimum throughput), it is notable that UFA maintains a high minimum throughput even when the room is crowded. For instance, even though the number of users in the room increases by a 10-fold, the reduction in minimum throughput is also by 10-fold (from  $\approx 10^8$  Bits/s to  $\approx 10^7$  Bits/s). Further, we observe that higher tolerance does not yield much improvement on the minimum throughput as seen in Fig. 5.9(a).

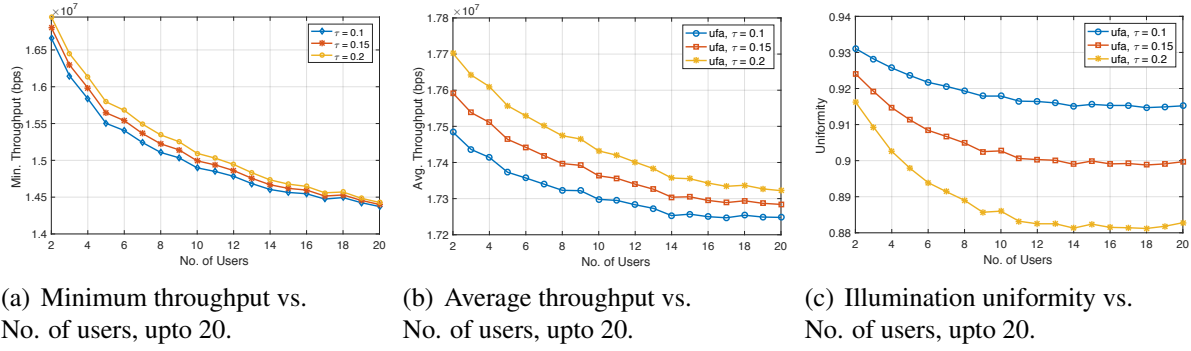


Figure 5.9: Throughput and Uniformity for many users for UFA.  $M = 391$  and  $\theta_d = 40^\circ$ .

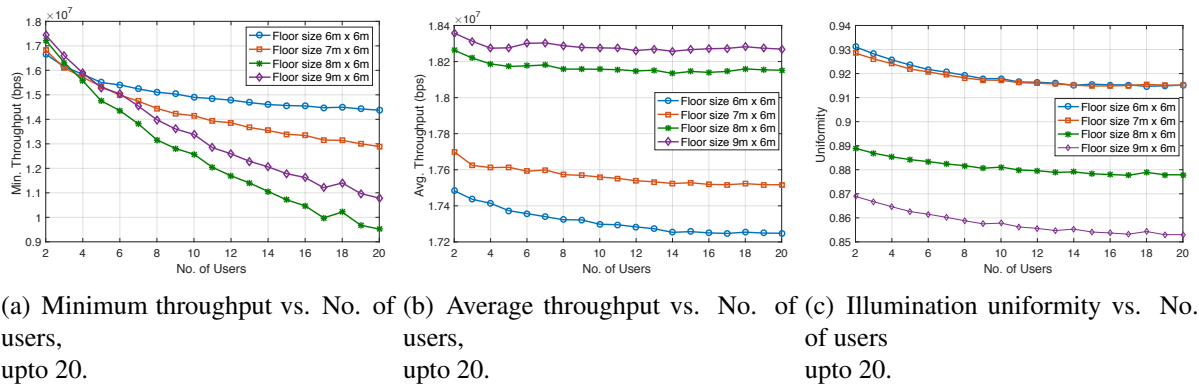
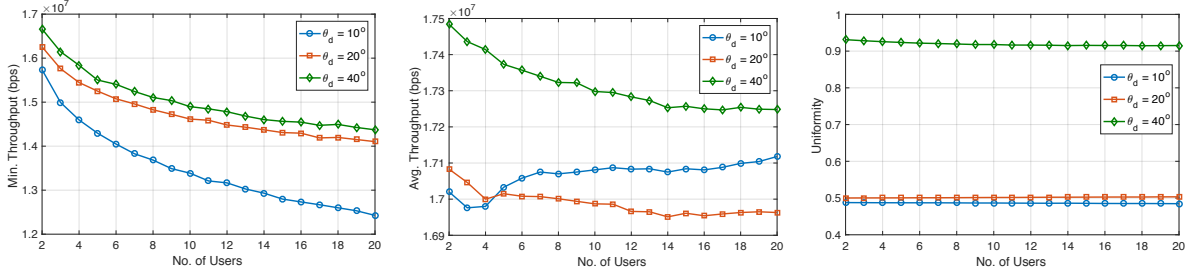


Figure 5.10: Throughput and Uniformity for different room sizes.  $M = 391$  and  $\theta_d = 40^\circ$ .

### 5.5.4 UFA with Different Room Sizes

We also look at how minimum throughput and uniformity is affected by different room sizes and shapes, e.g., the room gets more rectangular. To observe this, we keep increasing the width of the room by 1m at a time and keep the length of the room constant. Results are seen in Fig. 5.10. As the room floor gets more rectangular, spaces are more at both sides, so the chances of the users being more scattered increases, which means there are less chances of interference. But, with higher number of users, interference is going to be more likely, thus the throughput decreases. In the case of uniformity, it becomes increasingly difficult to maintain balanced lighting with the





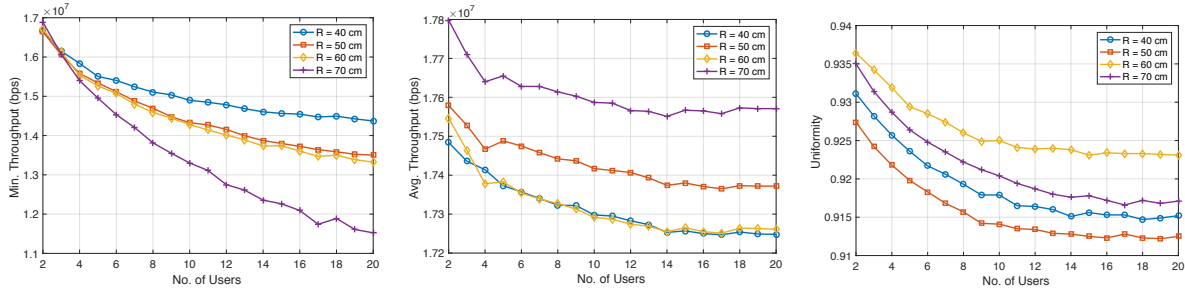
(a) Minimum throughput vs. No. of users for different divergence angles. (b) Average throughput vs. No. of users for different divergence angles. (c) Illumination uniformity vs. No. of users for different divergence angles.

Figure 5.11: Comparison between different divergence angles in UFA.  $M = 391$ .

width of the floor being significantly greater than the length, which explains the dip in uniformity for more rectangular room floors (Fig. 5.10(b)). Although, in case of small number of users, we can see the opposite scenario in Fig. 5.10(a). Whenever we are making the room more rectangular, it decreases the possibility of interference as they are going to be more scattered, but at the same time it increases the possibility of a user being in a 'low signal strength' region where there is much less transmitter coverage (these regions are shown in Fig. 5.6). After a particular number of users in the system the second possibility becomes more dominant over the first one, which explains the transitions in Fig. 5.10(a).

### 5.5.5 Effect of Divergence Angles with UFA

We also look at the effect of divergence angle of the LEDs with UFA. We use 3 divergence angle values =  $10^\circ$ ,  $20^\circ$  and  $40^\circ$ . In Fig. 5.11(a), 5.11(b), and 5.11(c), we observe minimum throughput, average throughput and uniformity, respectively. As we can see, throughput for  $10^\circ$  and  $20^\circ$  is



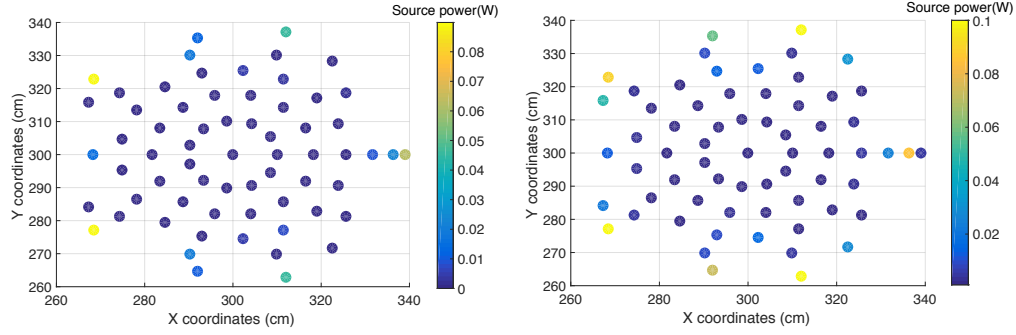
(a) Minimum throughput vs. No. of users for different bulb radius. (b) Average throughput vs. No. of users for different bulb radius. (c) Illumination uniformity vs. No. of users for different bulb radius.

Figure 5.12: Comparison between different bulb radius in UFA.  $M = 391$  and  $\theta_d = 40^\circ$ .

higher because of less interference since the beams are too directional, but this hampers the uniformity a lot as well. The average throughput for  $10^\circ$  goes higher than  $20^\circ$  for more than 4 users, as we see in Fig. 5.11(b). When the number of users are less than or equal to 4, the possibility of high interference with higher divergence angle is dominant enough to keep the throughput higher, but after that, the effect of interference becomes too high, making the throughput better for lesser divergence angle. Performance in the case of  $40^\circ$  is the best among these cases since a very balanced lighting is obtained with the ability to cover more users, as a result not hampering the average throughput too much.

### 5.5.6 Effect of Bulb Radius on UFA

We try to see the effect of different bulb radius on the system for UFA. As shown in Fig. 5.12, we plot minimum and average throughput as well as uniformity versus the number of users for  $R = 40cm, 50cm, 60cm$  and  $70cm$ . We can see that the decline of minimum throughput is the least in the case of 40 cm bulb radius, the value we have typically used. Uniformity is almost the same



(a) Heatmaps of the transmit power of LEDs with UFA.  $M = 65$ .  
 (b) Heatmaps of the transmit power of LEDs with GP.  $M = 65$ .

Figure 5.13: Heatmaps of the transmit power of LEDs with UFA and GP.

for all cases though a little better for higher bulb radius, as the LED beams can cover a little more space in the corner of the room floor. Average throughput is a little higher for greater bulb radius as the more expanded beam distribution is the cause of relatively less interference. We can see a small transition like Fig. 5.10(a) in Fig. 5.12(a), as the possibility of a particular user being in a 'less coverage' area is low for a small number of users, so higher bulb radius gives just a little better throughput in this case. But the mentioned possibility is significant enough in the case of more than 3 users, which makes the minimum throughput value lower for the higher bulb radius.

### 5.5.7 Heatmaps of the Transmit Power of LEDs with UFA and GP

To explore how the transmit powers of the LEDs are allocated with our proposed algorithms, we plot the projection point from the top of each LED on the floor using different colors, where the color of a particular projection point of an LED indicates the amount of transmit power of that LED. Like subsection 5.5.2, The higher the LEDs are in the bulb, the more outwards their projections

points are in floor. As we can see in Fig. 5.13, transmit power of the LEDs in the higher layers are more than those of the lower layers in the bulb. This is to maintain a good uniformity as the LEDs in the higher layers cover the corner (darker) spots in the room.

## 5.6 Chapter Summary

In this chapter, we explored in a multi-element multi-datastream (MEMD) VLC architecture where VLC is used for downlink and RF for uplink. For the downlink, we have formulated the problem of resolving tuning LED transmit powers and LED-user association as an optimization problem. The optimization problem takes the users' throughput and illumination uniformity into consideration and handles dynamic assignment of the transmitters to react to the mobility of users. We showed the problem is NP-Complete.

For the MEMD VLC downlink and access optimization, we proposed a near-optimal approximation solution and two suboptimal heuristic solutions, i.e., SINR First Approach (SFA) and Uniformity First Approach (UFA). We have analyzed the performance of the two heuristic solutions and found that UFA is significantly better. We, then, compared UFA with the near-optimal solution and found out that it is not far away from the near-optimal approach. A key insight is that one can design low complexity heuristics for the MEMD VLC downlink problem. From our simulations, for reasonable assumptions about the LEDs and bulb size, we observed that UFA can attain about 10Mbps minimum throughput while keeping illumination uniformity higher than 0.7 for up to 20 receivers in a 36m<sup>2</sup> room.

## **CHAPTER 6**

# **MIRRORVLC: OPTIMAL MIRROR PLACEMENT FOR MULTI-ELEMENT VLC NETWORKS**

In this chapter, we present a novel approach of using mirrors to enhance the illumination uniformity and throughput of an indoor multi-element VLC system architecture.<sup>1</sup>. In this approach, we improve the Signal-to-Interference plus Noise Ratio (SINR) of the system and overall illumination uniformity of the room by redirecting the reflected LED beams on the walls to darker spots with the use of mirrors. We formulate a joint optimization problem focusing on maximization of the SINR while maintaining a reasonable illumination uniformity across the room. We propose a two-stage solution of the optimization problem with optimization of illumination in the first stage and SINR at the second stage. We propose three different heuristic solutions for the second stage and analyze the performance of them, which demonstrates the advantages of each heuristic for different possible scenarios. We also show that about threefold increase in average illumination and fourfold increase in average throughput can be achieved when the mirror placement is applied which is a significant performance improvement.

---

<sup>1</sup>Most of the content on this chapter was published in a submitted work for a journal [65].

## 6.1 System Model

We consider a VLC downlink system model in an indoor setting consisting of a single hemispherical bulb containing  $M$  directional LED transmitters in  $L$  layers to serve  $U$  mobile users using power of  $P_m$  Watt,  $\forall m = 1, \dots, M$  which is already described in section 3.1. The bulb is a hemispherical structure with two goals: i) achieve uniform lighting illumination within the room, and ii) provide high speed wireless download to mobile users. We assume that the LEDs in the bulb are placed in different layers in order to cover different locations in the room. In order to improve the illumination uniformity and download speed to mobile users, we consider placing mirrors to the walls into the room's wall aiming to utilize NLoS beams from the LEDs. We divide each wall into an  $X \times Y$  grid. We assume that in each grid element, one mirror can be placed at most. We call this mirror as a 'grid mirror'. We anticipate that these grid mirrors in the walls will reflect the NLoS signals and thus potentially enhance the performance of the multi-element VLC network. The optimal placement of the mirrors, among other factors, will depend on the direction of the incident lights from the LEDs to the walls. We consider that a user's Photo-detector (PD) gain depends on the light intensity from three main directions: 1) the LoS beams directly coming from LEDs, 2) strong reflections of the LoS light beams from the grid mirrors, and 3) weak-reflected light from the regular walls as shown in Fig 6.1. Since there are four walls and each one is divided as  $X \times Y$  sized grid, we visualize the scope of mirror placement as a  $4X \times Y$  grid, where four walls are assumed to be placed side-by-side. Each cell of the grid can be defined with index  $z$  where  $z = 1, 2, 3, \dots, Z$ , here  $Z = 4XY$ .

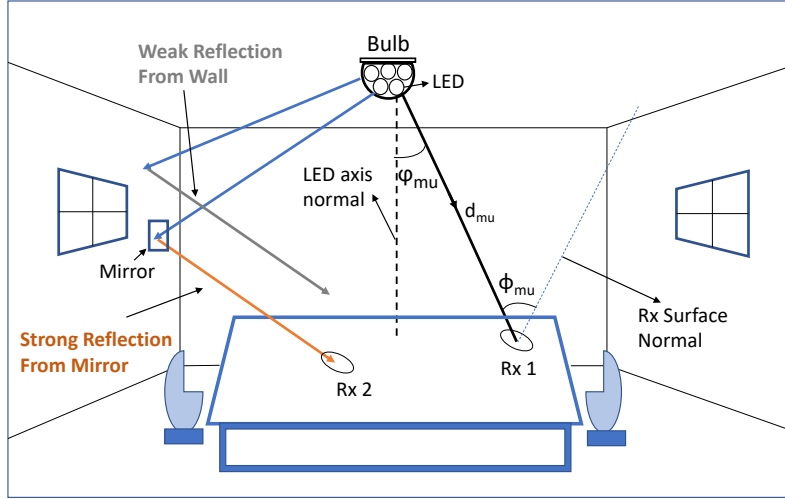


Figure 6.1: System Model.

To compute the illumination uniformity in our simulated environment, we consider  $N$  fixed sensing points uniformly distributed inside the room. The light intensity received at these points determine how uniform the lighting is inside the room. It is possible to place these points at a place of interest, however, we assume that they are uniformly distributed in a lattice placement pattern, to the room floor.

We also consider that each mobile user is equipped with a single PD to receive the downlink light beams. It is assumed that the location of the mobile users in the room can be predicted. On the other hand, we assume that the mobile users are equipped with an RF transmitter such as Wi-Fi for uplink transmission. In this work, we focus on downlink transmissions only and assume that the uplink transmission speed is not a bottleneck which is also the case for typical wireless access at an indoor setting.

To compute the illumination uniformity in our simulated environment, we consider  $N$  fixed sensing points uniformly distributed inside the room. The light intensity received at these points

determine how uniform the lighting is inside the room. It is possible to place these points at a place of interest, however, we assume that they are uniformly distributed in a lattice placement pattern, to the room floor.

We also consider that each mobile user is equipped with a single PD to receive the downlink light beams from the LEDs and the grid mirrors. It is assumed that the location of the mobile users in the room are known. On the other hand, we assume that the mobile users are equipped with an RF transmitter such as Wi-Fi for uplink transmission.

## 6.1.1 VLC Channel Model

### 6.1.1.1 LoS Channel

The LoS channel model between LED  $m$  and receiver node  $l$  ( $l \in \{u \text{ for users}, n \text{ for sensing points}\}$ ) can be expressed as [66]:

$$h_{ml}^{\text{LoS}} = \begin{cases} \frac{A_l}{d_{ml}^2} Q_0(\varphi_{ml}) \cos(\varphi_{ml}) & , 0 \leq \varphi_{ml} \leq \varphi_c \\ 0 & , \varphi_{ml} \geq \varphi_c \end{cases} \quad (6.1)$$

where  $A_l$  is the receiver node's PD area and  $d_{ml}$  is the distance between LED  $m$  and node  $l$ .  $\varphi_{ml}$  and  $\phi_{ml}$  are the irradiance and incidence angles, respectively, as shown in Fig. 6.1.  $\varphi_c$  is the FOV angle of the PD. We have assumed that no optical filter is used.  $Q_0(\varphi_{ml})$  is the Lambertian radiant intensity and expressed as

$$Q_0(\varphi_{ml}) = \frac{(q+1)}{2\pi} \cos^q(\varphi_{ml}), \quad (6.2)$$



where  $q = -\ln(2)/\ln(\cos(\varphi_{1/2}))$  is the order of Lambertian emission and  $\varphi_{1/2}$  is the transmitter semi-angle at half power.

### 6.1.1.2 NLoS Channel

There can be two types of reflection in the scenario we are considering - strong specular reflections from the mirrors and weak diffuse reflections from the walls. As light is greatly absorbed by concrete walls with lesser reflectivity, the effect of diffuse reflection is negligible compared to the specular reflection from mirrors unlike in the RF communication [67, 68]. For these reasons, we consider only the strong reflections of the LoS light beams for computing the NLoS channel model to avoid complexity. In a scenario where the light from LED  $m$  is coming to user  $u$  through a grid mirror located at  $\xi_z$  (i.e.,  $\xi_z = 1$ ), the NLoS channel model between LED  $m$  and node  $l$  can be expressed as [69]:

$$h_{ml}(z)^{\text{NLoS}} = \frac{\eta A_l}{\hat{d}_{ml}(z)^2} Q_0(\varphi_{ml}) \cos(\phi_{ml}) \quad (6.3)$$

where  $\eta$  is the reflectivity of a grid mirror and  $\hat{d}_{ml}(z)$  is the distance between  $m$  and  $l$  via the mirror located at index  $z$  of the grid  $\xi$ . This is explained in Fig. 6.2 where we compare the NLoS channel between LED  $m$  and user  $u$  with a channel between  $m$  and  $u'$  which is a mirror image of  $u$  with respect to the wall. We can see that the distance between  $m$  and  $u'$  is same as the total distance between  $m$  and  $u$  via the mirror. So, we can express the NLoS channel between  $m$  and  $u$  as the LoS channel between  $m$  and  $u'$  with one thing in consideration - the NLoS channel strength will be reduced by a factor as there is a mirror in its path, and this factor is dependent on  $\eta$ , the reflectivity

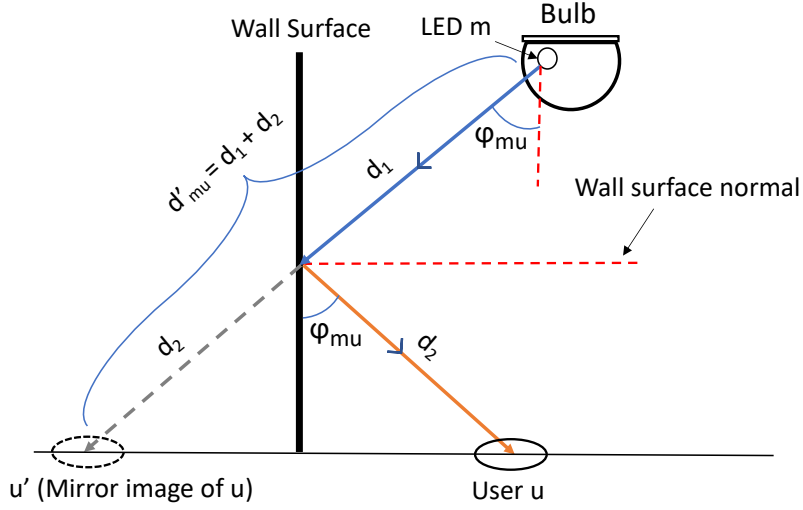


Figure 6.2: Comparison between an NLoS channel with mirror and LoS channel by using a mirror image of user  $u$  to the wall from the same LED  $m$ .

of the mirror. Same expression can be derived for the sensing points as well, thus we present the general expression for node  $l$  in (6.3).

### 6.1.1.3 Total Channel

Now, we can express the total channel model as the combination of LoS and NLoS channels as below:

$$H_{ml} = h_{ml}^{\text{LoS}} + \sum_{z=1}^{4XY} \chi_{mz} h_{ml}(z)^{\text{NLoS}} \quad (6.4)$$

such that

$$\begin{aligned} \chi_{mz} &= \xi_z, & \text{if } z \in \Upsilon_{zm}, \\ \chi_{mz} &= 0, & \text{otherwise.} \end{aligned} \quad (6.5)$$

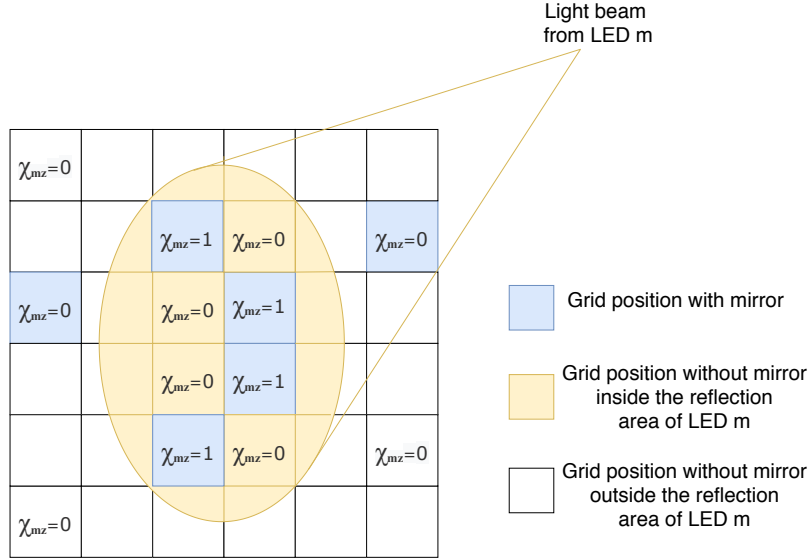


Figure 6.3: Figure explaining different values of  $\chi_{mz}$  in a room wall.  $\chi_{mz} = \xi_z$  when grid position  $z$  is inside the reflection area of LED  $m$  (marked in orange) and 0 otherwise. Grid positions with mirrors are marked in light blue.

To explain the above channel clearly, we define *reflection area* of LED  $m$  as the wall area being covered by the beam coming from LED  $m$ .  $\Upsilon_{zm}$  in eq. 6.5 is the set of  $z$  indices corresponding to the reflection area of LED  $m$ .  $\xi_z = 1$  if a grid mirror is placed at the cell located at index  $z$  of the grid  $\xi$  and  $\xi_z = 0$  otherwise. Further,  $\chi_{mz}$  is a binary variable that expresses whether or not a NLoS component from LED  $m$  via grid location  $z$  will be accumulated in the channel. Note that  $\chi_{mz}$  cannot be 1 if the grid location  $z$  is not within the reflection area of LED  $m$ . However, if the grid location  $z$  is within the reflection area of LED  $m$ , then it can be 0 or 1 depending on the existence of a grid mirror at  $z$  which is expressed by  $\xi_z$ . Fig. 6.3 explains different values for  $\chi_{mz}$ .

Although the above explained model seems a bit complex primarily because of the inclusion of an extra dependent variable  $\chi_{mz}$ , a designer of a VLC system can enjoy much more flexibility because of this. By bringing different combinations of  $\chi_{mz}$  into the overall search space, proba-

bility of finding a near optimal solution becomes much higher as we can control the contribution of every small fractions of each LED beam to either illumination only, or both illumination and communication.

### 6.1.2 Illumination Uniformity

An important factor to be considered in VLC is illumination intensity distribution across the room floor. Specifically, the illumination uniformity,  $\vartheta$ , can be defined as the ratio between the minimum and the average illumination intensity among all  $N$  sensors and is given as [56]

$$\vartheta = \frac{\min_n \left( \sum_{m=1}^M \alpha_0 P_m H_{mn} \right)}{\frac{1}{N} \sum_{n=1}^N \sum_{m=1}^M \alpha_0 P_m H_{mn}} \quad (6.6)$$

where  $\alpha_0$  is the luminous efficiency that depends on the LED color wavelength, e.g.  $\alpha_0 = 60$  lumen/watt for white LED [64].  $\min(\cdot)$  is the minimum function.

### 6.1.3 LED-User Association

We use a binary variable  $\varepsilon$  that indicates the association between LED  $m$  and user  $u$  which is given as follows:

$$\varepsilon_{mu} = \begin{cases} 1, & \text{if LED } m \text{ is associated with user } u. \\ 0, & \text{otherwise.} \end{cases} \quad (6.7)$$

We assume that user  $u$  can be associated with multiple LEDs at the same time. However, it is assumed that each LED can be associated with one user at most during the same time. Therefore, the following conditions should be respected:

$$\sum_{u=1}^U \epsilon_{mu} \leq 1, \forall m = 1, \dots, M. \quad (6.8)$$

#### 6.1.4 SINR Calculation

We assume that each LED is either associated with one user or used for lighting only. Therefore, SINR at user  $u$  can be expressed as [45]

$$\Gamma_u = \frac{\left( \sum_{m=1}^M \epsilon_{mu} H_{mu} P_m \right)^2}{N_0 B + \sum_{\substack{k=1 \\ k \neq u}}^U \left( \sum_{m=1}^M \epsilon_{mk} H_{mk} P_m \right)^2} \quad (6.9)$$

where  $B$  and  $N_0$  are the communication bandwidth and the spectral density of the Additive White Gaussian Noise (AWGN), respectively.

## 6.2 Problem Formulation and Solution

In a nutshell, the problem we are considering to solve is to optimize the combination of SINR and illumination uniformity based on mirror placement on the wall ( $\xi_z$ ), LED-user assignment ( $\epsilon_{mu}$ )

and source power for each of the  $m$  LEDs ( $P_m$ ). Although it is possible to re-optimize the objective value by updating  $\varepsilon_{mu}$  whenever a user changes its position, it is not feasible to do so for the mirrors. For this reason, we have divided the problem in two separate optimization problems. First, we find the optimal mirror placements and LED source powers which maximize the illumination uniformity, and after that, we look for the best LED-user association along with tuning the LED source powers to maximize the combination of SINR and illumination uniformity using the results from the first problem. We think that this staging makes the optimal mirror placement more practical. In particular, the solution to the first problem will yield the best places to set up the grid mirrors so that high illumination uniformity is attained. Then, the second problem can be solved on-the-fly as users are moving in the room, yielding the best LED transmit powers and LED-user association depending on the user movements.

In this section we formulate these two optimization problems defined as mirror design problem and communication problem.

### **6.2.1 Design Problem**

The main goal of this problem is to achieve the best illumination quality by optimizing not only the mirror placements but also the LEDs' transmit powers. Therefore, the mirror design optimization

can be formulated as follows:

$$\underset{\xi_z, \chi_m \in \{0,1\}, P_m}{\text{maximize}} \quad \min_n \left( \sum_{m=1}^M \alpha_0 P_m H_{mn} \right) \quad (6.10)$$

subject to (6.5) and:

$$P_{min} \leq P_m \leq \bar{P}, \quad \forall m, \quad (6.11)$$

$$\frac{\min_n \left( \sum_{m=1}^M \alpha_0 P_m H_{mn} \right)}{\frac{1}{N} \sum_{n=1}^N \sum_{m=1}^M \alpha_0 P_m H_{mn}} \geq \mu \quad (6.12)$$

$$\phi_2 \leq \sum_{m=1}^M \alpha_0 P_m H_{mn} \leq \phi_1, \quad \forall n, \quad (6.13)$$

where  $P_{min}$  and  $\bar{P}$  are the minimum and maximum source power respectively that can be allotted to an LED and  $\mu$  is the minimum acceptable illumination uniformity for an indoor setting [56].  $\chi_m$  is a dependent variable here, i.e. it is directly related to the values of  $\xi_z$ .  $\phi_1$  and  $\phi_2$  are the maximum and minimum levels of total illumination allowed at a particular sensing point. These are introduced to ensure that the room is illuminated at a minimum level and also it does not go beyond a level where it can be harmful to human eye.

We aim to solve the above design optimization problem optimally. In order to do this, we first linearize the objective function (6.10) and constraint (6.13) by introducing a new decision variable  $\phi$  as follows:

$$\phi = \min_n \left( \sum_{m=1}^M \alpha_0 P_m (h_{mn}^{\text{LoS}} + \sum_{z=1}^Z \chi_{mz} h_{mn}^{\text{NLoS}}(z)) \right). \quad (6.14)$$

Equation (6.14) can be re-written as follows:

$$\phi = \min_n \left( \sum_{m=1}^M \alpha_0 P_m h_{mn}^{\text{LoS}} + \sum_{z=1}^Z \alpha_0 \rho_{mz} h_{mn}^{\text{NLoS}}(z) \right), \quad (6.15)$$

where  $\rho_{mz} = \chi_{mz} P_m$ , which is introduced as another decision variable to linearize the product of binary variable  $\chi_{mz}$  and real decision variables  $P_m$ . Indeed maximizing the objective function given in (6.10) is equivalent to maximizing  $\phi$  given that  $\phi \leq \sum_{m=1}^M \alpha_0 P_m H_{mn}, \forall n$ . With the introduction of  $\rho_{mz}$ , the following inequalities also have to be respected:

$$\begin{aligned} 1) \quad & P_m \geq \rho_{mz} \geq 0, \forall m, \forall z \\ 2) \quad & \rho_{mz} \geq \bar{P}_m \chi_{mz} - \bar{P}_m + P_m, \forall m, \forall z \\ 3) \quad & \rho_{mz} \leq \bar{P}_m \chi_{mz}, \forall m, \forall z. \end{aligned} \quad (6.16)$$

The first two inequalities ensure that  $\rho_{mz}$  value is between  $\chi_{mz}$  and  $P_m$ . The third inequality guarantees that  $\rho_{mz} = 0$  if  $\chi_{mz} = 0$ , and  $\rho_{mz} = P_m$  if  $\chi_{mz} = 1$ . Therefore, the optimization problem



can be reformulated as binary linear optimization problem as follows:

$$\begin{aligned} & \underset{\substack{\xi_z, \chi_{mz}, P_m \\ \phi, \rho_{mz}}}{\text{maximize}} \quad \phi & (6.17) \end{aligned}$$

subject to (6.5), (5.8), (6.16), (6.13) and:

$$\phi \geq \frac{\mu}{N} \sum_{n=1}^N \sum_{m=1}^M \alpha_0 \left( P_m h_{mn}^{\text{LoS}} + \sum_{z=1}^Z \rho_{mz} h_{mn}^{\text{NLoS}}(z) \right) \quad (6.18)$$

$$\phi \leq \sum_{m=1}^M \alpha_0 \left( P_m h_{mn}^{\text{LoS}} + \sum_{z=1}^Z \rho_{mz} h_{mn}^{\text{NLoS}}(z) \right), \forall n \quad (6.19)$$

It can be noticed that the solution for such binary linear optimization problem can be determined optimally using on-the-shelf software such as Gurobi/CVX interface [70].

## 6.2.2 Communication Problem

Now that we have solved the mirror placement problem, we move on to the communication problem where we want to maximize the SINR of the system to ensure the best possible data rate to the users. We choose to use Max-Min utility of the SINR. The approach of maximizing the total data rate which is known in the literature as Max C/I [57], promotes users with favorable channel and interference conditions by allocating them most of the resources, whereas users suffering from higher propagation losses and/or interference levels will have very low data rates. Therefore, due to the unfairness of total sum data rate utility, the need for more fair utility metrics arises. The Max-Min utilities are a family of utility functions attempting to maximize the minimum SINR in

a network [58]. Our goal is to induce more fairness in the network by increasing the priority of users having lower SINR using the Max-Min utility. Thus, we formulate an optimization problem aiming to maximize the minimum SINR of all users by taking the association and illumination intensity constraints into consideration. This optimization problem can be expressed as

$$\begin{aligned} & \underset{\epsilon_{mu} \in \{0,1\}, P_m \geq 0}{\text{maximize}} && \Gamma_{min} && (6.20) \\ & \text{subject to} && (6.8), (5.8) \text{ and } (5.10). \end{aligned}$$

where  $\Gamma_{min} = \min_u(\Gamma_u)$  is the minimum SINR among all users.

### 6.2.2.1 NP-Completeness

As the number of LEDs  $M$  being considered can be quite large, the number of ways to assign these LEDs to multiple users can be very large and it is practically infeasible to obtain an optimal solution as the users might move frequently inside the room, and the problem is needed to be solved again whenever any of the user coordinates is updated. In fact, this LED assignment problem in consideration is proven to be NP-Complete as elaborated in section 5.2.1, so we propose three low complexity heuristic solutions to solve it.

### 6.2.2.2 Heuristic Approaches

We describe each of our proposed heuristic approaches in this subsection.

*Nearest User Assignment (NUA)*: We denote the resulting  $P_m$  values from the solution of (6.17) as intermediate power values  $P_1^{prev}, P_2^{prev}, \dots, P_M^{prev}$  for  $M$  LEDs, and assign LED  $m$  to the closest user to its beam projection if the user lies in the cone of LED  $m$ . If there is one or no user in the cone, then we allocate  $\min(P_m^{prev}(1 + \tau), \bar{P})$  where  $\tau$  is a measurement of how much we can deviate the allocated power to LED  $m$  from its intermediate value  $P_m^{prev}$ . We use 0.3 as the value for  $\tau$  in our simulations. If there is more than one user in the cone of LED  $m$ , then we assign this LED to the user which is nearest to the center of the cone of the LED, but with fractional power, since there will be interference in this case as shown in Fig. 5.3. More details on this heuristic algorithm can be found in section 5.4 where it was introduced for the first time.

*Strongest Signal-based Assignment with User-first Approach (SSA-User)*: An LED-by-LED assignment approach is implemented in the *NUA* algorithm. In contrast, in this approach, we do a user-by-user assignment. We inspect each user one by one and check the user in consideration is under how many LED beams, either via LoS or via NLoS. There are three possible scenarios -

- 1) If there is no incoming LED beam towards this user, then we do not assign any LED to it.
- 2) If there is only one incoming LED beam, then we follow similar approach to *NUA* and assign the user with source power  $\min(P_m^{prev}(1 + \tau), \bar{P})$ .
- 3) If there are more than one incoming LED beams, then we take total channel model values between each of these LEDs and this particular user into consideration. There are two possible

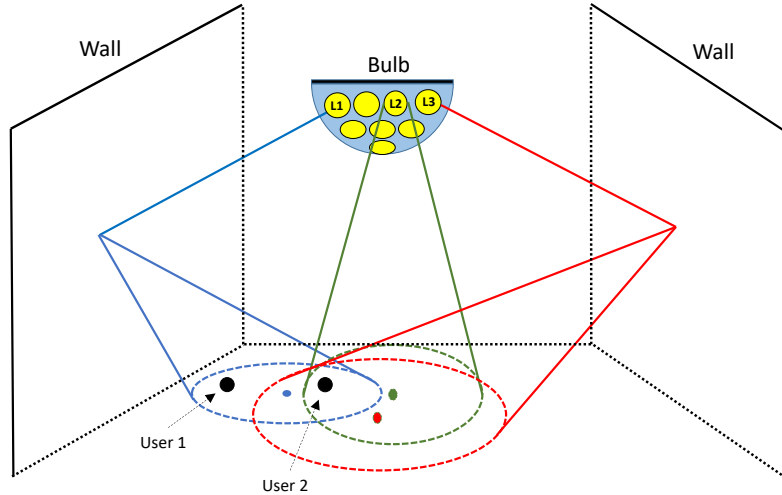


Figure 6.4: A case of conflict for an user-by-user approach such as SSA-User: both User 1 and User 2 are getting strongest signal from LED L1, but since L1 is assigned to User 1 first, User 2 has to be assigned to L2, which provides the second strongest signal for User 2.

cases in this scenario - i) There is no incoming LED which is already assigned to another user, which means no possible interference - and ii) There is one or more LED(s) which are already assigned to other user(s), which creates interference. In the first case, since there is no chance of interference from any other user, we assign all the incoming LEDs to the user in consideration. However, a much more careful approach is needed for the second case, which is shown in Fig. 6.4. Here we assign all the incoming LED beams, or simply ‘incoming LEDs’, to the current user which are not already assigned to other user(s). We calculate the fraction,  $\kappa$ , as the ratio of maximum channel value of all the incoming LEDs including those also which are already assigned to other user(s) denoted as  $H_{m_j u_i}$  assuming  $m_j$  is the one among these LEDs with strongest channel value with the current user  $u_i$  - and maximum of the channel values between all the incoming LEDs to the current user which are still unassigned, denoted as  $H_{m_i u_i}$  assuming  $m_i$  is the one among these

LEDs with strongest channel value with  $u_i$ . It can be expressed as  $\kappa = \frac{H_{m_j u_i}}{H_{m_i u_i}}$ . Finally, we allot the LED  $m_i$  with the source power of  $\max(P_m^{prev}(1 - \kappa), P_m^{prev}((1 - \tau)))$ .

*Strongest Signal-based Assignment with LED-first Approach (SSA-LED)*: This approach is a blend of the previous two approaches - the scanning procedure is LED-by-LED like *NUA* and the assignment is based on channel strength like *SSA – User*. For each LED  $m$  in the bulb, this approach checks whether there is any user inside it's coverage, either directly or via the mirror. We allocate  $\min(P_m^{prev}(1 + \tau), \bar{P})$  amount of source power when there is no or one user is covered by this LED. Now, if there are more than one user covered, we do not assign the current LED  $m$  to any user. This is done to reduce the effect for interference when multiple users are being covered by the same LED. We give fraction of  $P_m^{prev}$  to the current LED with a ratio  $\kappa = \frac{H_{m u_j}}{H_{m u_i}}$ , where  $u_i$  and  $u_j$  respectively is the user with strongest and second strongest channel value with the current LED  $m$ . Thus the power allocated to LED  $m$  is  $\max(P_m^{prev}(1 - \kappa), P_m^{prev}((1 - \tau)))$ .

Each of the above described approaches has its own advantages and disadvantages. *NUA* has the simplest approach, although it is the worst-performing one which is elaborated further in Section 5.5. *SSA – User* is suitable for the scenarios where the users in the room are prioritized in some manner as it is an user-by-user approach which provides the best service to the user which is chosen first. But this is the most expensive approach considering the time complexity as many of the LEDs are needed to be examined multiple times if they cover more than one user. *SSA – LED* can be considered as a balance between *NUA* and *SSA – User* since it is less complex than *SSA – User* and obtains better performance than *NUA*. It also provides fairness to all the users in the system.

### 6.2.2.3 Computational Complexity

We are assuming  $M$  total LEDs and  $U$  total users in our problem. In both *NUA* and *SSA – LED*, we check each of the LEDs to allocate source power and assign it to a user if needed. This effective runtime of checking this is  $O(M)$ . Calculating the channel values for all users will take  $O(MU)$  time which is the most dominant component, so the overall runtime for both *NUA* and *SSA – LED* is  $O(MU)$ .

For *SSA – User*, we take an user-by-user approach, and there may be cases when there is a conflict while assigning an LED to a particular user. In the worst case, this will be  $O(M^2)$  when but on average this will be  $O(M \log M)$  as this situation is similar as the Quick Sort algorithm. Combining this with the running time  $O(MU)$  to calculate the channel values, we find the overall time complexity of the *SSA – User* approach to be  $O(M(U + \log M))$ .

## 6.3 Simulation Results

In this section, we provide simulation results to study the performance of our MEMD VLC system model. Our aim is to make comparison between the three heuristics we proposed in terms of the *minimum throughput* and the *average throughput* of the system. To compare our proposed methods (*NUA*, *SSA-LED*, and *SSA-User*), we use exact same input parameters for all of them. We randomly placed the users on the room floor with their receiver's FOV normal looking towards the ceiling. We report the average of the minimum throughput and illumination uniformity re-

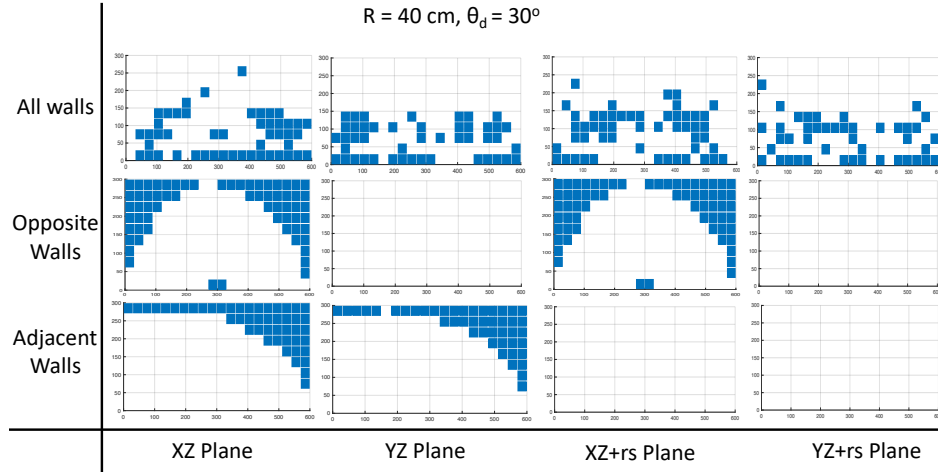


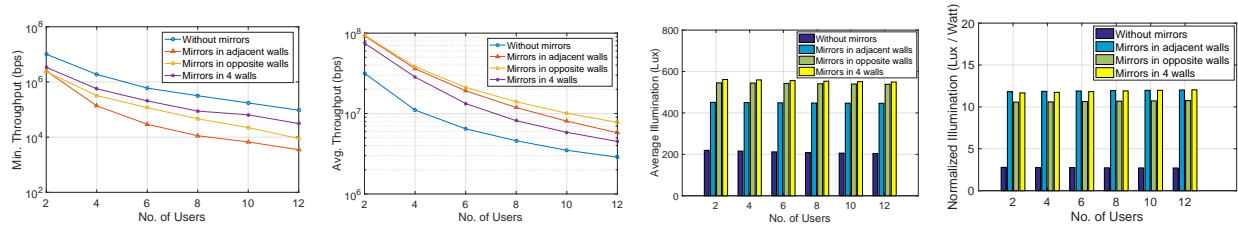
Figure 6.5: Mirror placement heatmaps in four walls for different bulb radiuses and divergence angles.

sults among these randomly generated cases. To gain confidence in our results, we repeated the simulation experiments 100 times for all the results.

We use white LEDs with luminous efficacy  $\alpha_0 = 169$  lumen/watt [71]. The default values of the remaining input parameters used in our simulations are given in Table 5.2. For placing LEDs on the bulb, we followed the method in Section 6.1. In particular, for a bulb with  $R = 40\text{cm}$  radius, we place  $M = 391$  LEDs on 20 layers with  $k_{1..20} = [1, 6, 12, 15, 19, 26, 30, 37, 43, 33, 30, 28, 25, 21, 16, 13, 11, 10, 9, 6]$ .

### 6.3.1 Placement of Mirrors

We solve the design problem in (6.17) using different mirror placement approaches for different scenarios. For  $R = 40\text{cm}$  and  $\theta_d = 30^\circ$ , we solve the design problem considering three separate approaches - 1) Mirror placement in two adjacent walls, 2) Mirror placement in two opposite walls

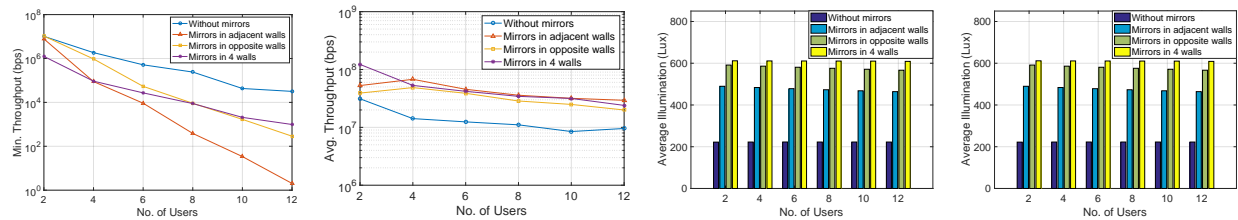


(a) Minimum throughput vs. No. of users. (b) Average throughput vs. No. of users. (c) Average illumination vs. No. of users. (d) Normalized illumination vs. No. of users.

Figure 6.6: Comparison between different mirror placement approaches for *NUA* with  $M = 391$  and  $\theta_d = 30^\circ$ .

and 3) Mirror placement in all four walls. We define the four walls as  $XZ$ ,  $YZ$ ,  $XY + rs$  and  $XZ + rs$  planes, where  $rs$  can be denoted as the room floor size. The mirror placement heatmaps from each of these scenarios are shown in Fig. 6.5. We can see that when we let the optimizer place mirrors in all four walls, it is difficult to establish any concrete pattern from the mirror placement heatmaps although there are some similarities. This happens because when the optimizer considers the sensing points near the corners of the room, there are several options to choose a mirror location from either of the two adjacent walls sharing the corner, and since there is no particular rule do that, the mirrors are chosen randomly from those possible locations which could yield similar performance in terms of illumination level and uniformity, thus breaking the symmetry in the heatmaps. This is not the case when we allow the optimizer to place mirrors in two opposite walls as they do not share any corner, so we can see the same pattern of mirror placement in those two walls. Even in the case of two adjacent walls, the mirror placement follows the same pattern as the optimizer can avoid placing the mirror on the sides of the two walls which share the same corner and place most of the mirrors of the sides which do not share the same corner, as illustrated in the figure.





(a) Minimum throughput vs. No. of users. (b) Average throughput vs. No. of users. (c) Average illumination vs. No. of users. (d) Normalized illumination vs. No. of users.

Figure 6.7: Comparison between different mirror placement approaches for *SSA – User* with  $M = 391$  and  $\theta_d = 30^\circ$ .

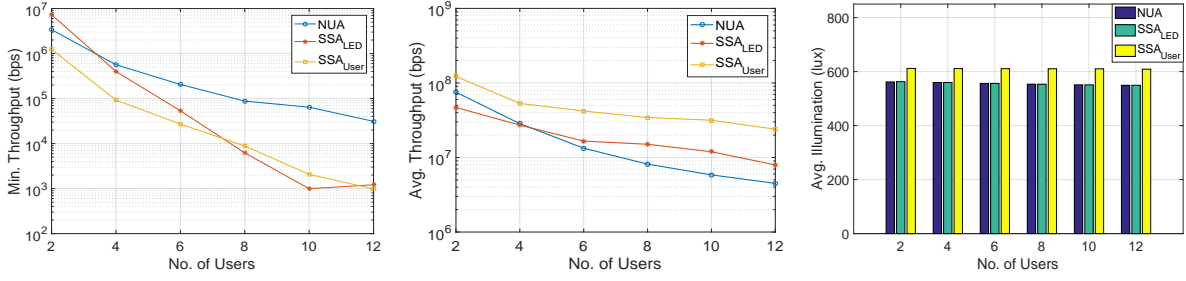
### 6.3.2 Performance Comparison among Mirror Placement approaches

We compare the performance in terms of minimum throughput, average throughput and average illumination for the different mirror placement approaches discussed in the earlier section. We also solve the design problem with no mirror placement at all to determine how much improvement is possible using those mirror placement approaches. The findings are shown in Fig. 6.6 and 6.7. As the solution of the design problem is focused on optimizing the illumination, we see a noticeable three-fold improvement in average illumination level when mirror placement is applied, with the approach of placement in all walls having the most improvement aligning with our expectations. Similar improvements with mirror placement is observed even when we plot the normalized illumination with respect to total amount source power among all LEDs. Although there is no significant improvement in minimum throughput values after employing mirror placement, we can see up to four-fold increment in the average throughput values when comparing the four-wall case with no mirror case. Adjacent walls and opposite walls cases also yield a solid improvement in both of average throughput and illumination level.

Overall, these comparisons provide valuable insights with regard to VLC network design. Since a much higher level of illumination can be obtained in average from the same number of LEDs, either of the three mirror placement approaches can be seen as beneficial. A trade-off between system performance and ease of mirror employment can be observed among the approaches. Among the three approaches, placing mirror in all four walls is the one which can yield maximum performance improvement in terms of illumination. In terms of average throughput, all the three approaches demonstrate better performance compared to the no mirror approach. However, in terms of the ease of mirror employment, placing mirror in the opposite walls is arguably the preferable approach if the mirror placement pattern is such that most of the chosen mirror grids are connected to each other - in that case the group of connected mirrors can be placed as a larger mirror - making the employment much easier. In rest of the simulations for this paper we use the four wall approach to obtain results from the design problems.

### **6.3.3 Comparison between NUA, SSA-LED and SSA-User**

We compare our proposed heuristic approaches, *NUA*, *SSA – LED* and *SSA – User* to see whether one performs significantly better. We compare both minimum and average throughput among the users with average illumination level across the sensing points from 2 to 12 users for these three approaches, as seen in Fig. 6.8(a), 6.8(b) and Fig. 6.8(c). As we can see, minimum throughput and average throughput decreases for all three approaches with increased number of users. For *SSA – User*, minimum throughput has lower value compared to *NUA* because this approach highly



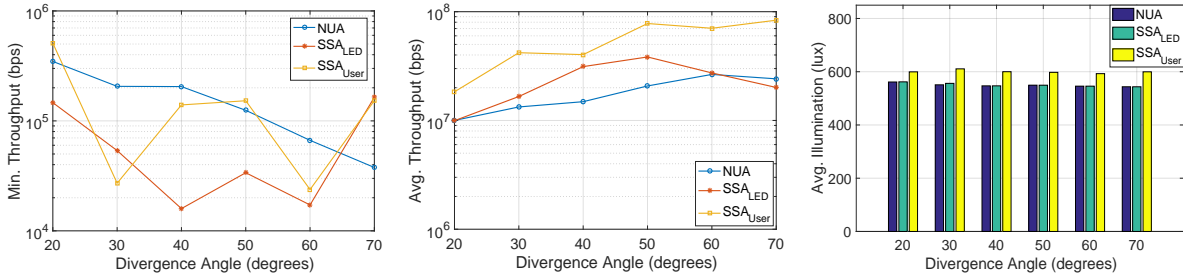
(a) Minimum throughput vs. No. of users. (b) Average throughput vs. No. of users. (c) Average illumination vs. No. of users.

Figure 6.8: Comparison between  $NUA$ ,  $SSA - LED$  and  $SSA - User$  with  $M = 391$  and  $\theta_d = 30^\circ$ .

prioritizes the users chosen first for LED assignments, which largely affects the users chosen at the end.  $SSA - LED$  also has lower values compared to  $NUA$ , as the restriction of assignment for some of the LEDs leads few user to starvation. But the average throughput is better for  $SSA - LED$  than  $NUA$  as that restriction ensures a considerable decline in interference as well.  $SSA - User$  does even better in terms of the average throughput as the high quality service provided to the users assigned first comprehensively overpowers the low quality service provided to the users in the end. In Fig. 6.8(c), we can see that the average illumination values remains steady for all three heuristics with increasing number of users as changes in LED source power allocation for these heuristics are not substantial enough to have any adverse effect on the overall illumination level.

### 6.3.4 Effect of Divergence Angle

For each of our proposed heuristics, we plot minimum and average throughput with average illumination in the room for different divergence angles when there are six users in total, shown in Fig. 6.9. With larger divergence angles, the LED beams get larger, thus there are more chances of a



(a) Minimum throughput vs. Divergence angle. (b) Average throughput vs. Divergence angle. (c) Average illumination vs. Divergence angle.

Figure 6.9: Comparison between  $NUA$ ,  $SSA - LED$  and  $SSA - User$  for different divergence angle with 6 users.  $M = 391$  and  $R = 40cm$ .

particular user to get coverage of an LED, but at the same time the chance of interference increases too. Looking at the average throughput,  $SSA - LED$  and  $SSA - User$  handle the interference better than  $NUA$  for increasing divergence angles as shown in Fig. 6.9(b). Average illumination level is not hampered much with either heuristic in this case as well.

## 6.4 Chapter Summary

In this paper, we have explored a novel mirror employment approach for performance improvement for an MEMD VLC system. In order to maximize the average throughput and illumination, we have formulated an optimization problem to obtain optimum mirror placement, power allocation and LED-user association. As the problem is NP-complete, we have proposed a two-stage solution of the optimization problem. As a part of the solution of the first stage, we have introduced several mirror placement approaches and analyzed their performance. To deal with heavy computation complexity in the second stage with the communication problem, we have presented multiple heuristic approaches to solve it with a detailed analysis on their performance. We have shown that up to threefold increase in average illumination and fourfold increase in average throughput can be achieved using a mirror placement approach.

# **CHAPTER 7**

## **RESOURCE OPTIMIZATION IN VISIBLE LIGHT COMMUNICATION**

### **FOR INTERNET OF THINGS**

In this chapter, we are using a VLC-based architecture for providing scalable communications to Internet-of-Things (IoT) devices where a multi-element hemispherical bulb is used that can transmit data streams from multiple light emitting diode (LED) boards.<sup>1</sup> The essence of this architecture is that it uses a Line-of-Sight (LoS) alignment protocol that handles the hand-off issue created by the movement of receivers inside a room. We start by proposing an optimization problem aiming to minimize the total consumed energy emitted by each LED taking into consideration the LEDs' power budget, users' perceived quality-of-service, LED-user associations, and illumination uniformity constraints. Then, because of the non-convexity of the problem, we propose to solve it in two stages: (1) We design an efficient algorithm for LED-user association for fixed LED powers, and (2) using the LED-user association, we find an approximate solution based on Taylor series to optimize the LEDs' power. We devise a heuristic solution based on this approach. Finally, we illustrate the performance of our method via simulations.

---

<sup>1</sup>Most of the content on this chapter was published in proceedings [13].

## 7.1 System Model

We consider a VLC downlink system model in an indoor setting consisting of a single hemispherical bulb containing  $M$  directional LED transmitters in  $L$  layers to serve  $U$  mobile users using power of  $P_m$  Watt,  $\forall m = 1, \dots, M$  which is already described in section 3.1.

### 7.1.1 Assumptions and Notation

For this chapter, we make assumptions similar to ones made in section 5.1.1.

### 7.1.2 LED-User Association

We propose to use a binary variable  $\varepsilon_{mu}$  that indicates the association between LED  $m$  and user  $u$  which is already described in section 5.1.2.

### 7.1.3 Channel Model

In this chapter, we assume the channel model is similar to the one that is described in section 5.1.3.

#### **7.1.4 SINR Calculation**

We assume that each LED is either associated with one user or used for lighting only. Therefore, SINR at user  $u$  can be expressed as equation 5.5 in section 5.1.4.

#### **7.1.5 Illumination Uniformity**

The illumination uniformity,  $\vartheta$ , is defined as the ratio between the minimum and the average illumination intensity [56] among all  $N$  sensors, is expressed as equation 5.6 in 5.1.5.

### **7.2 Problem Formulation**

We formulate an optimization problem aiming to minimize the total energy consumption of LEDs while satisfying a certain rate threshold for users and taking into consideration the association and illumination uniformity constraints. So, the optimization problem can be written as:



$$\text{(P0): minimize}_{\varepsilon_{mu} \in \{0,1\}, P_m \geq 0} \sum_{m=1}^M P_m \quad (7.1)$$

subject to (6.8) and:

$$P_m \leq \bar{P}, \quad \forall m, \quad (7.2)$$

$$\vartheta \geq \bar{I}_{\min}, \quad (7.3)$$

$$B \log_2(1 + \Gamma_u) \geq \bar{R}_u, \quad \forall u. \quad (7.4)$$

where (6.8) and (7.2) represent the LEDs' power budget and association constraints. (7.3) represents the illumination uniformity constraint, where  $\bar{I}_{\min}$  is defined as the minimum acceptable illumination uniformity threshold which we set to be 0.7 [56]. Finally, (7.4) represents the minimum rate QoS, where  $\bar{R}_u$  is the minimum rate expected for each IoT device.

### 7.3 Problem Solution

The formulated optimization problem given in (7.1)-(7.4) is a non-convex and mixed-integer non-linear programming problem. So, we propose a low complexity two stages heuristic solution. In the first stage, we propose a 'Nearest User Assignment' approach to determine the value of  $\varepsilon_{mu}$ . Then, given the LED-user associations, we optimize the LEDs' power allocations in the second stage.

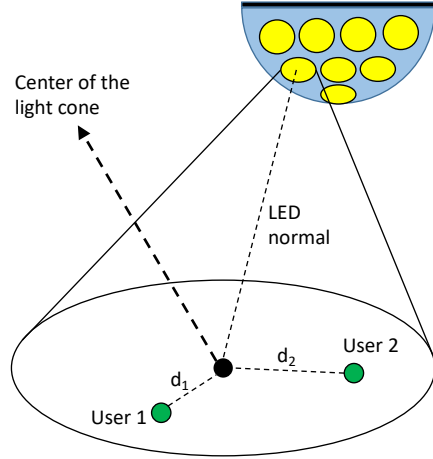


Figure 7.1: Nearest User Assignment Approach in case of interference for an LED on the bulb.

### 7.3.1 Low Complexity Two-Stage Solution (TSS)

Optimizing  $\epsilon_{mu}$  and  $P_m$  at the same time makes our problem really complex specially for IoT scenarios where we have large number of users  $U$  and large number of LEDs  $M$ . In a practical scenario, IoT devices or users will be moving in the room and every time users' locations change the optimization will need to be re-performed. Therefore, we propose a Two-Stage Solution (TSS) as a practical and efficient solution with less complexity.

In order to simplify the problem **P0**, we propose to optimize  $\epsilon_{mu}, \forall m, u$  first, then use  $\epsilon_{mu}$  values to optimize  $P_m$ . To do this, we firstly propose to use a heuristic 'Nearest User Assignment' approach to determine the value of  $\epsilon_{mu}$ . We then optimize  $P_m, \forall m$  by applying a Taylor series approximation to convert the problem into convex one. Finally, Successive Convex Approximation (SCA) approach is used to find the best approximation.

### 7.3.1.1 LED-User Association

In our 'Nearest User Assignment' for obtaining the value of LED-User association matrix  $\varepsilon_{mu}$ , we propose to find the user which is most aligned for each LED  $m$ . That is, for each LED  $m$  into consideration, we firstly, find the light cone of LED  $m$  (Fig. 7.1). After that, knowing the coordinate of each user, we can determine which user is the closest to the center of light cone of LED  $m$ . Let us assume this nearest user to be  $u$ , where the user  $u$  is in the LOS of LED  $m$ , then LED  $m$  gets assigned to user  $u$  (that is, we let  $\varepsilon_{mu} = 1$ ) and  $\varepsilon_{mu'} = 0, \forall u' \neq u$ . In this way, no LED is assigned to more than one user. Finally, we use this LED-User association matrix value while optimizing the LEDs' power, which is discussed in the next subsection.

### 7.3.1.2 Power Optimization

For given LED-user association, the optimization problem **P0** (with some term arrangements) that optimizes LEDs' power can be written as:

$$\text{(P1): } \underset{P_m \geq 0}{\text{minimize}} \quad \sum_{m=1}^M P_m \quad (7.5)$$

subject to (5.8), (7.3) and (7.4).

Notice that in **P1**, the objective function is a convex function and all constraints are convex functions except (7.4). This constraint is neither concave nor convex with respect to the LED transmit

power  $P_m$ . Hence, the goal is to convert constraint (7.4) into a convex one in order to solve the problem efficiently. Therefore, constraint (7.4) can be re-written as

$$\sqrt{C_u \left( N_0 B + \sum_{\substack{k=1 \\ k \neq u}}^U \beta_{ku}^2 \right)} \leq \beta_{uu} \quad (7.6)$$

where  $C_u = 2^{(\bar{R}_u/B)} - 1$ . It can be seen that the RHS of (7.6) is a linear function, thus we only need to approximate the LHS. Therefore, we propose to use same first order Taylor expansion approximation in order to convert the LHS of (7.6) into a convex one as the following:

$$\frac{\sqrt{C_u N_0 B + C_u \sum_{\substack{k=1 \\ k \neq u}}^U (\beta_{ku}(r))^2} + \left[ C_u \sum_{\substack{k=1 \\ k \neq u}}^U \varepsilon_{mk} h_{mk} \beta_{ku}(r) \right] (P_m - P_m(r))}{\sqrt{C_u N_0 B + C_u \sum_{\substack{k=1 \\ k \neq u}}^U (\beta_{ku}(r))^2}} \leq \beta_{uu} \quad (7.7)$$

where  $\beta_{ku}(r) = \sum_{m=1}^M \varepsilon_{mk} h_{mk} P_m(r)$ . After the approximation, the optimization problem **P1** becomes a convex optimization problem and it can be solved using standard convex optimization techniques. Finally, we propose to use SCA approach to find the best Taylor series approximation (in the end of Algorithm 3).

Table 7.1: Simulation Parameters

Parameter	Value
Room Size	6 m x 6 m x 3 m
Radius of the transmitter, $r_t$	1.5 cm
Radius of the receiver, $r_r$	3.75 cm
Divergence angle of the LEDs, $\theta_d$	$40^\circ$
No. of users, U	2-40
No. of sensors, N	100
Luminous efficacy of white LED, $\alpha_0$	60 Lumens / Watt
AWGN spectral density, $N_0$	$2.5 \times 10^{-20}$ W / Hz
Modulation bandwidth, B	20 MHz
Minimum uniformity, $\bar{I}_{min}$	0.7

#### 7.4 Simulation Results

In order to understand the performance of our heuristics, we perform extensive simulations in MATLAB. Table 7.1 shows the default input parameters used in our simulation setup. The room size corresponds to a small size conference room or a large office with a  $6 \text{ m} \times 6 \text{ m}$  floor and 3 m of height. We consider a hemispherical bulb with radius  $R = 40 \text{ cm}$  and the total number of LEDs used is 65 in 6 layers where  $m_{1..6} = [11 \ 14 \ 17 \ 10 \ 7 \ 5]$  and 1 LED exactly at the center point of the bulb. We assume the radius of the LED boards to be  $r_t=1.5 \text{ cm}$  and the radius of the photo-detector receiver at the users to be  $r_r=3.75 \text{ cm}$ .

We assume 20 MHz of bandwidth, which is very conservative for VLC bands and operational limitations since LEDs and PDs can work with much larger bandwidth than this. Finally, in terms of target illumination and communication efficiency, we target a minimum uniformity of  $\bar{I}_{min} = 0.7$  [56] and minimum data rate per user of  $\bar{R}_u = 1 \text{ Mbps}$ .

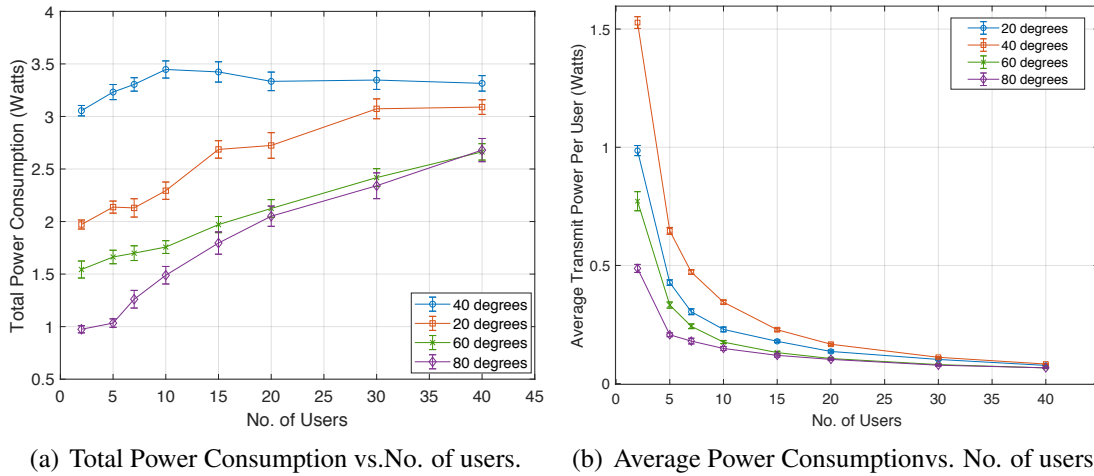


Figure 7.2: Effect on Power Consumption of the System.

To gain confidence in the results, we run the simulations at least 100 times with randomly chosen user locations within the room. For seeding the random number generator in our simulations, we used the prime numbers starting with 11. We show the results with 95% confidence intervals.

#### 7.4.1 Effect on Total Power Consumption of the System

We observe the effect on total power consumption of the system, which is the objective function in our optimization problem, with increasing number of users. The plots for total power consumed by the bulb and average transmit power spent for each user versus the total number of users in the room for different divergence angles are shown in Figure 7.2(a) and 7.2(b), respectively. As we can see, the total power consumption of the bulb is increasing with the number of users, though not too much. This indicates that, as more users are admitted to the room, the LED-user associations are tuned to maintain the minimum data rate a user gets and the illumination uniformity constraint.

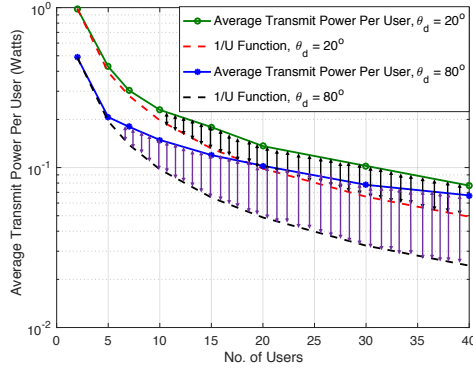


Figure 7.3: Average Transmit Power Decay Per User for  $\theta_d = 20^\circ$  and  $\theta_d = 80^\circ$ .

The average transmit power spent for each user (Figure 7.2(b)) significantly decreases for large number of users in the system. This reveals that more LEDs could be assigned to a user when there are few users in the room, but, as the number of users increases, the LEDs available for a user reduces which causes the aggregate transmit power spent for a user to reduce significantly. So, overall, our algorithm is able to keep the total power consumption to a satisfactory level which is the main objective of this work, and the cost-effectiveness is improved significantly for a very high number of users, as the amount of average transmit power spent for each user becomes very low while satisfying the minimum data rate and illumination uniformity constraints.

For a stronger analysis on the decays of average transmit powers per user with increasing number of users, we plot the  $\frac{1}{U}$  function along with them for the cases of  $\theta_d = 20^\circ$  and  $\theta_d = 80^\circ$  in log scale. Although in both cases the power decays are slower than their respective  $\frac{1}{U}$  functions, the decay for  $\theta_d = 80^\circ$  is much slower than the decay for  $\theta_d = 20^\circ$  (Figure 7.3). As we know, the possibility of interference is much higher for wider divergence angles as there is more possibility of having more than one user in an LED's beam. To counter this extra interference, more transmit

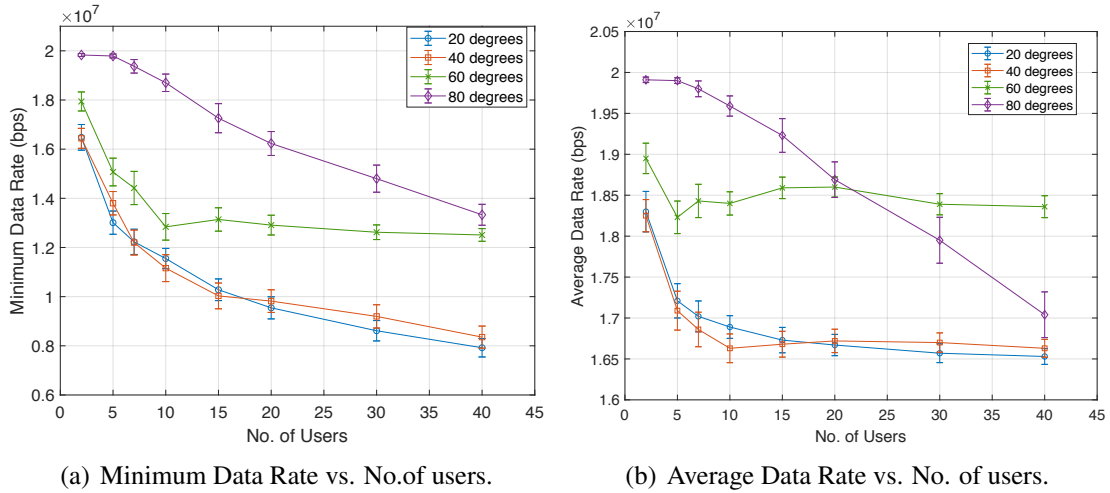


Figure 7.4: Effect on User Data Rate of the System.

power is needed to increase the signal portion of SINR and the average transmit power needed is also higher as a result.

### 7.4.2 Effect on Data Rate

Another important goal of our optimization problem is to provide a minimum data rate to each user of the system to maintain a good QoS, and for that we analyze the minimum and average throughput of the system with respect to the number of users, which is demonstrated in Figure 7.4(a) and 7.4(b). From these plots, we can see that our approach can maintain a very good data rate, both average and minimum, even for a large number of users, though both of these rates drop with increasing number of users, which is expected.



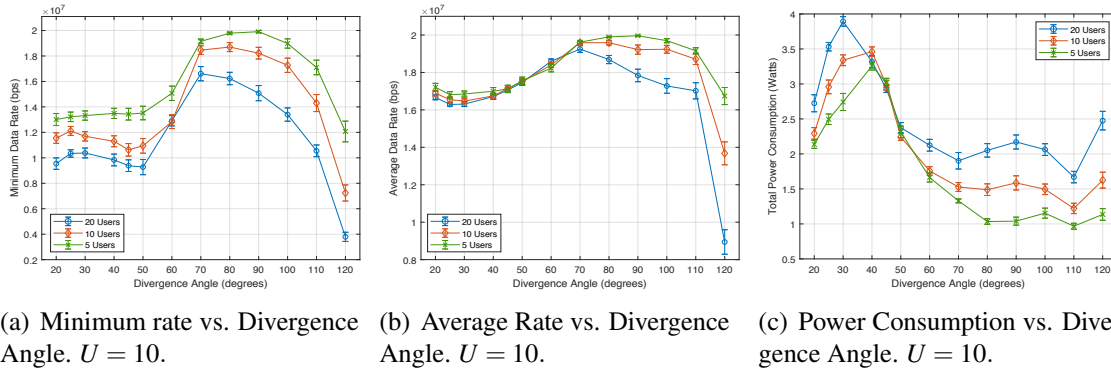


Figure 7.5: System Analysis for different LED Divergence Angles.

Interestingly, we can observe a clear trade-off between the interference caused by large divergence angles and the high data rate opportunities when the number of users is low. We observe that  $80^\circ$  provides notably higher minimum and average data rates for up to 20 users, but it cannot maintain a good data rate for more users. On the other hand, narrower divergence angles offer lower data rates for few-users cases but can maintain a good data rate even though the number of users increases.

### 7.4.3 System Analysis for different LED Divergence Angles

We also look at different divergence angles of the LEDs to see the effect on total power consumption, and minimum and average data rates. We look at this case for  $U = 5, 10$  and 20 to compare the data rate for different number of users and obtain total power consumption, minimum rate and average rate for  $\theta_d$  from  $20^\circ$  to  $120^\circ$  in  $10^\circ$  intervals which is shown in Figure 7.5. We observe that after a certain point (with divergence angle  $60^\circ$ ), less power is needed for maintaining the required

data rate for the users. Also, the average data rate is increasing with angles more than  $40^\circ$ , more specifically at  $70^\circ$ . That indicates the improvement of the overall system performance if the system is designed with LEDs having divergence angle more than  $60^\circ$ . However, with divergence angle greater than  $90^\circ$ , the system performance reduces signifying that our algorithm works best with divergence angle in the range  $60^\circ$  to  $90^\circ$ .

---

**Algorithm 3** Algorithm for TSS

---

```
1: Let  $\varepsilon_{mu} = 0$  for  $m = 1..M$  and  $u = 1..U$ .
2: Let  $d \rightarrow 0, d_{min} \rightarrow 0, n \rightarrow 0$ 
3: for  $m = 1$  to  $M$  do
4:   for  $u = 1$  to  $U$  do
5:     if user  $u$  is inside the cone of LED  $m$  then
6:       if  $d == 0$  then
7:          $d \rightarrow$  distance between center of the cone and user  $u$ 
8:          $d_{min} \rightarrow d$ 
9:          $n \rightarrow u$ 
10:      end if
11:     else
12:        $d \rightarrow$  distance between center of the cone and user  $u$ 
13:       if  $d < d_{min}$  then
14:          $d_{min} \rightarrow d$ 
15:          $n \rightarrow u$ 
16:       end if
17:     end if
18:   end for
19:   if  $n! = 0$  then
20:      $\varepsilon_{mn} \rightarrow 1$ 
21:      $n \rightarrow 0$ 
22:   end if
23: end for
24: Select feasible initial values  $P_m^{(0)}$ .
25: repeat
26:    $r=1$ .
27:   Solve the optimization problem with calculated  $\varepsilon_{mu}$  using the interior-point method to determine the
   new approximated solution  $P_m^{(r)}$ .
28: until Convergence ( $|\chi^{(r+1)} - \chi^{(r)}| \leq \xi$ ).
```

---

## **CHAPTER 8**

### **SUMMARY AND FUTURE DIRECTIONS**

We introduced a multi-element VLC architecture that employs a hemispherical bulb with multiple narrow FOV LEDs. The mobile receivers use VLC for download and RF for upload, and the multi-element bulb uses a software-defined approach to manage LOS alignment with receivers. We modeled the bulb structure, and presented preliminary results showing that the architecture can offer high spatial reuse while keeping a desired illumination level. Also, we presented a framework for optimizing the multi-element bulb design not only taking the signal quality into consideration but also the evenness of lighting across the room. To further improve the performance of the framework, we proposed a mirror employment approach to redirect the reflected LED beams on the wall to darker spots in the room floor. We compared the performance of our heuristic approaches to solve the proposed two-stage optimization problem and showed that about threefold increase in average illumination and fourfold increase in average throughput could be achieved when the mirror placement is applied which was a significant performance improvement.

In addition, we proposed an optimization problem that successfully minimizes the total energy consumed by each LED bulb considering the LED's power budget maintaining certain illumination uniformity constraints, considering the users' QoS and the LED-user association and used the Taylor series approximation to optimize the total power of the LEDs. We successfully built a

framework corresponding to transmission power and rate optimization based on a certain lighting constraints. We believe that the software-defined VLC framework will greatly contribute to the field of VLC, particularly for the IoT applications.

The presented framework can serve as a basis for future studies for better understanding and further improvement. For instance, the optimization could be done over different room sizes and bulb parameters. We are considering the hemispherical shape of the bulb, but experimenting with some other shapes (triangular, square etc.) can be an interesting future work as well. Further, multiple such bulbs in a room could be considered to optimize the overall room's SINR as well as lighting quality. For our proposed mirror placement approach, it is worth exploring different mirror sizes and shapes which might yield further improvement in throughput or illumination level. For the LED assignment problem, other heuristic algorithms may be explored to attain results that could be closer to the optimal solution. It would also be worth observing how the proposed algorithms and mirror placement approaches perform with different system parameters (e.g., room shape, shape of the bulb) and whether there are any relationship between them. In our work, we considered a single bulb in a standard size room. Designing an MEMD VLC system for a much larger indoor environment with multiple such bulbs is definitely a challenging and promising direction. We have assumed all the signals driving the LEDs are using same frequency, although using different frequencies could possibly improve the overall throughput of the system as there would be less interference. However, the additional challenge of changing the LED-user association with these different frequencies will have to be tackled. And, the last but not the least,

a proof-of-concept prototype of the architecture can surely ameliorate the understanding of the optimally designed bulb characteristics.

**APPENDIX A**  
**LIST OF ABBREVIATIONS**

BER	Bit Error Rate
CSK	Color Shift Keying
FOV	Field Of View
FSO	Free Space Optics
IFFT	Inverse Fast Forrier Transform
IM	Instant Messaging
IoT	Internet of Things
LED	Light Emitting Diode
LLC	Logic Link Control
L-PPM	L-Pulse Position Modulation
LOS	Line Of Sight
MCU	Microcontroller Unit
MIMO	Multi Input Multi Output
NRZ	Non-return-to Zero
OFDM	Orthogonal Frequency Division Multiplexing
OOK	On-Off Keying
PD	Photodiode
PPM	Pulse Position Modulation
RF	Radio Frequency
RGB	Red Green Blue
RLL	Run-length Limited



SIR	Signal-to-Interference Ratio
SLM	Spatial Light Modulator
VLC	Visible Light Communication
VPPM	Variable Pulse Position Modulation
WDM	Wavelength-division Multiplexing
Wi-Fi	Wireless Fidelity

**APPENDIX B**  
**LIST OF SYMBOLS**

$V$	Visibility (km)
$\lambda$	Optical signal wavelength (nm)
$\sigma$	Coefficient of absorption and scattering
$\theta_d$	Divergence angle (radian)
$r_t$	Transmitter radius (cm)
$R$	Radius of the bulb (cm)
$\theta_i$	Layer $i$ 's angle with the normal (radian)
$\vec{LP}_i$	Vector between $i$ th LED on the bulb and its normal point on the floor
$\vec{LP}_0$	Vector of the central LED facing down
$P_L(i)$	Power on the normal $i$ th LED (W)
$r_r$	Receiver radius (cm)
$H_i$	Slanted normal length of LED $i$ (cm)
$N_t$	The number of search frames without acknowledgment from a receiver after which the bulb will consider the connection between that receiver and itself is timed out
$N_{rcv}$	Number of receivers in the room
$S_{ij}$	Average power received for receiver $i$ at section $j$
$SIR_j$	Average Signal-to-Interference-Ratio at section $j$
$SIR_a$	Average Signal-to-Interference-Ratio of the two receivers
$k_{i=1..l}$	Array of LED count in each layer
$K_{i=1..l}$	Array of maximum possible LED count in each layer
$\theta_{LB}$	Angle created with the center point of the bulb by all the LEDs in the same layer

$r_{li}$	The radius of circle created by the LEDs in the $i$ -th layer
$\theta_{li}$	The angle created by each LED with the center of the circle created by its respective layer
$P_{LED}$	Source power of each LED (W)
$P_{total}$	Total power generated by the bulb (W)
$M$	Number of LEDs in total
$U$	Number of users in total
$B$	Communication bandwidth
$P_m$	Transmit power of LED $m$
$\bar{P}$	Maximum LED's transmit power
$\varepsilon_{mu}$	Association between LED $m$ and user $u$
$h_{mu}$	Channel gain between LED $m$ and user $u$
$A_u$	User PD area
$d_{mu}$	Distance between LED $m$ and user $u$
$\varphi_{mu}, \phi_{mu}$	Irradiance and incidence angles, respectively
$\phi_c$	FOV angle of the PD
$Q_0(\varphi_{mu})$	Lambertian radiant intensity
$q$	The order of Lambertian emission
$\varphi_{1/2}$	The transmitter semiangle at half power
$\Gamma_u$	SINR at user $u$
$\vartheta$	Illumination uniformity
$\alpha_0$	The luminous efficiency

$\mu$  Minimum acceptable illumination uniformity

## LIST OF REFERENCES

- [1] R. Wood, “Wireless network traffic worldwide: forecasts analysis 2014-2019,” Research Forecast Report, October 2014. [Online]. Available: <https://www.marketresearch.com/product/sample-8471957.pdf>
- [2] D. Karunatilaka, F. Zafar, V. Kalavally, and R. Parthiban, “Led based indoor visible light communications: State of the art.” *IEEE Commun. Surveys and Tutorials*, vol. 17, no. 3, pp. 1649–1678, Aug. 2015.
- [3] U. Department of Energy, “How energy-efficient light bulbs compare with traditional incandescents — department of energy,” <https://www.energy.gov/energysaver/save-electricity-and-fuel/lighting-choices-save-you-money/how-energy-efficient-light>, (Accessed on 04/25/2020).
- [4] A. Sevincer, A. Bhattarai, M. Bilgi, M. Yuksel, and N. Pala, “LIGHTNETs: Smart lighting and mobile optical wireless networks – A survey,” *IEEE Communications Surveys & Tutorials*, vol. 15, no. 4, pp. 1620–1641, April 2013.
- [5] “Wireless data from every light bulb,” TED Talk, July 2011. [Online]. Available: [http://www.ted.com/talks/harald\\_haas\\_wireless\\_data\\_from\\_every\\_light\\_bulb.html](http://www.ted.com/talks/harald_haas_wireless_data_from_every_light_bulb.html)
- [6] D. Wu, Z. Ghassemlooy, H. LeMinh, S. Rajbhandari, and Y. S. Kavian, “Power distribution and Q-factor analysis of diffuse cellular indoor visible light communication systems,” in *Proc. of Eur. Conf. on Networks and Optical Communications*, July 2011, pp. 28–31.
- [7] A. Tsiatmas, F. M. J. Willems, and S. Baggen, “Optimum diversity combining techniques for VLC systems,” in *Proc. IEEE GC Wkshps*, Austin, TX, Dec. 2014.
- [8] J. B. Carruther and J. M. Kahn, “Angle diversity for nondirected wireless infrared communication,” *IEEE Tran. on Comm.*, vol. 48, no. 6, pp. 960–969, 2000.
- [9] H. Willebrand and B. S. Ghuman, *Free Space Optics*. Sams Pubs, 2001.
- [10] H. Minh, D. O’Brien, G. Faulkner, and M. Wolf, “Bidirectional gigabit ethernet optical wireless communications system for home access networks,” *IET Commun.*, vol. 6, no. 11, pp. 1529–1536, 2012.

- [11] S. I. Mushfique and M. Yuksel, "Optimal multi-element VLC bulb design with power and lighting quality constraints," in *Proc. ACM Visible Light Communication Systems Workshop (VLCS)*, New York, NY, Dec. 2016, pp. 7–12. [Online]. Available: <https://doi.org/10.1145/2981548.2981553>
- [12] S. I. Mushfique, P. Palathingal, Y. S. Eroglu, M. Yuksel, I. Guvenc, and N. Pala, "A software-defined multi-element VLC architecture," *IEEE Communications Magazine*, vol. 56, no. 2, pp. 196–203, Feb 2018. [Online]. Available: <https://doi.org/10.1109/MCOM.2018.1700306>
- [13] S. I. Mushfique, A. Dey, A. Alsharoa, and M. Yuksel, "Resource optimization in visible light communication for Internet of Things," in *2019 IEEE International Symposium on Local and Metropolitan Area Networks (LANMAN)*. IEEE, 2019, pp. 1–6. [Online]. Available: <https://doi.org/10.1109/LANMAN.2019.8846992>
- [14] S. I. Mushfique, A. Alsharoa, and M. Yuksel, "Optimization of SINR and illumination uniformity in multi-LED multi-datastream VLC networks," *IEEE Transactions on Cognitive Communications and Networking*, 2020. [Online]. Available: <https://doi.org/10.1109/TCCN.2020.2972310>
- [15] P. Palathingal, M. Yuksel, I. Guvenc, and N. Pala, "A multi-element VLC architecture for high spatial reuse," in *Proceedings of the 2Nd International Workshop on Visible Light Communications Systems*, ser. VLCS '15. New York, NY, USA: ACM, 2015, pp. 21–26. [Online]. Available: <http://doi.acm.org/10.1145/2801073.2801077>
- [16] H. Minh, D. O'Brien, G. Faulkner, and M. Wolf, "Bidirectional gigabit Ethernet optical wireless communications system for home access networks," *IET Commun.*, vol. 6, no. 11, pp. 1529–1536, 2012.
- [17] E. Ciaramella, Y. Arimoto, G. Contestabile, M. Presi, A. D'Errico, V. Guarino, and M. Matsumoto, "1.28 terabit/s (32x40 gbit/s) wdm transmission system for free space optical communications," *IEEE Journal on selected areas in communications*, vol. 27, no. 9, 2009.
- [18] Z. Wu and T. Little, "Network solutions for the LOS problem of new indoor free space optical system," in *Communication Systems Networks and Digital Signal Processing (CSNDSP), 2010 7th International Symposium on*. IEEE, 2010, pp. 582–587.
- [19] T. Borogovac, M. Rahaim, and J. B. Carruthers, "Spotlighting for VLC and illumination," in *Proc. IEEE GC Wkshps*, 2010, pp. 1077–1081.
- [20] X. Deng, K. Arulandu, Y. Wu, G. Zhou, and J. P. M. G. Linnartz, "Performance analysis for joint illumination and visible light communication using buck driver," *IEEE Transactions on Communications*, vol. PP, no. 99, pp. 1–1, 2018.
- [21] S. Rajagopal, R. D. Roberts, and S. K. Lim, "IEEE 802.15.7 visible light communication: modulation schemes and dimming support," *IEEE Communications Magazine*, vol. 50, no. 3, pp. 72–82, March 2012.

- [22] N. Fujimoto and H. Mochizuki, "477 Mbit/s visible light transmission based on OOK-NRZ modulation using a single commercially available visible led and a practical led driver with a pre-emphasis circuit," in *2013 Optical Fiber Communication Conference and Exposition and the National Fiber Optic Engineers Conference (OFC/NFOEC)*, March 2013, pp. 1–3.
- [23] S. Zhao, J. Xu, and O. Trescases, "A dimmable LED driver for visible light communication (vlc) based on LLC resonant DC-DC converter operating in burst mode," in *2013 Twenty-Eighth Annual IEEE Applied Power Electronics Conference and Exposition (APEC)*, March 2013, pp. 2144–2150.
- [24] J. Luna-Rivera, R. Perez-Jimenez, J. Rabadan-Borjes, J. Rufo-Torres, V. Guerra, and C. Suarez-Rodriguez, "Multiuser CSK scheme for indoor visible light communications," *Optics express*, vol. 22, no. 20, pp. 24 256–24 267, 2014.
- [25] A. H. Azhar, T. A. Tran, and D. O'Brien, "A gigabit/s indoor wireless transmission using MIMO-OFDM visible-light communications," *IEEE Photonics Technology Letters*, vol. 25, no. 2, pp. 171–174, Jan 2013.
- [26] T. Borogovac, M. B. Rahaim, M. Tuganbayeva, and T. D. Little, "Lights-off visible light communications," in *GLOBECOM Workshops (GC Wkshps), 2011 IEEE*. IEEE, 2011, pp. 797–801.
- [27] A. Kashyap and M. Shayman, "Routing and traffic engineering in hybrid RF/FSO networks," in *IEEE International Conference on Communications, 2005. ICC 2005. 2005*, vol. 5, May 2005, pp. 3427–3433 Vol. 5.
- [28] H. Chowdhury, I. Ashraf, and M. Katz, "Energy-efficient connectivity in hybrid radio-optical wireless systems," in *ISWCS 2013; The Tenth International Symposium on Wireless Communication Systems*, Aug 2013, pp. 1–5.
- [29] D. Nguyen-Huu, T. Duong, and T. Nguyen, "Location-assisted coding for FSO communication," *IEEE Transactions on Communications*, vol. 65, no. 10, pp. 4360–4370, Oct 2017.
- [30] D. A. Basnayaka and H. Haas, "Design and analysis of a hybrid radio frequency and visible light communication system," *IEEE Transactions on Communications*, vol. 65, no. 10, pp. 4334–4347, Oct 2017.
- [31] S. Shao, A. Khreishah, M. Ayyash, M. B. Rahaim, H. Elgala, V. Jungnickel, D. Schulz, T. D. C. Little, J. Hilt, and R. Freund, "Design and analysis of a visible-light-communication enhanced WiFi system," *IEEE/OSA Journal of Optical Communications and Networking*, vol. 7, no. 10, pp. 960–973, October 2015.
- [32] P. Hu, P. H. Pathak, A. K. Das, Z. Yang, and P. Mohapatra, "Plifi: Hybrid WiFi-VLC networking using power lines," in *Proceedings of the 3rd Workshop on Visible Light Communication Systems*, ser. VLCS '16. New York, NY, USA: ACM, 2016, pp. 31–36. [Online]. Available: <http://doi.acm.org/10.1145/2981548.2981549>



- [33] A. Aldabahi, M. Rahaim, A. Khreishah, M. Ayyash, R. Ackerman, J. Basuino, W. Berreta, and T. D. C. Little, “Extending ns3 to simulate visible light communication at network-level,” in *2016 23rd International Conference on Telecommunications (ICT)*, May 2016, pp. 1–6.
- [34] J. Grubor, S. C. J. Lee, K. Langer, T. Koonen, and J. W. Walewski, “Wireless high-speed data transmission with phosphorescent white-light LEDs, berlin, germany,” in *Proc. of the 33rd European Conference and Exhibition of Optical Communication*, Sep. 2007, pp. 1–2.
- [35] Y. Yang, X. Chen, L. Zhu, B. Liu, and H. Chen, “Design of indoor wireless communication system using LEDs,” in *Proc. of the Communications and Photonics Conference and Exhibition, Shanghai, China*, Nov. 2009, pp. 1–2.
- [36] Z. Wang, C. Yu, W.-D. Zhong, J. Chen, and W. Chen, “Performance of a novel led lamp arrangement to reduce snr fluctuation for multi-user visible light communication systems,” *Optics express*, vol. 20, no. 4, pp. 4564–4573, 2012.
- [37] J.-H. Liu, Q. Li, and X.-Y. Zhang, “Cellular coverage optimization for indoor visible light communication and illumination networks,” *Journal of Communications*, vol. 9, no. 11, pp. 891–898, 2014.
- [38] A. M. Abdelhady, O. Amin, A. Chaaban, and M.-S. Alouini, “Resource allocation for outdoor visible light communications with energy harvesting capabilities,” in *Proc. of the IEEE Global Communications Conference Workshops (GLOBECOM Workshop)*, Singapore, Singapore, Dec. 2017, pp. 1–6.
- [39] P. F. Mmbaga, J. Thompson, and H. Haas, “Performance analysis of indoor diffuse VLC MIMO channels using angular diversity detectors,” *IEEE Journal of Lightwave Technology*, vol. 34, no. 4, pp. 1254–1266, Feb. 2016.
- [40] M. K. Jha, A. Addanki, Y. Lakshmi, and N. Kumar, “Channel coding performance of optical mimo indoor visible light communication,” in *2015 International Conference on Advances in Computing, Communications and Informatics (ICACCI)*. IEEE, 2015, pp. 97–102.
- [41] G. B. Prince and T. D. C. Little, “On the performance gains of cooperative transmission concepts in intensity modulated direct detection visible light communication networks, valencia, spain,” in *Proc. of the 6th IEEE International Conference on Wireless and Mobile Communications*, Sept. 2010, pp. 297–302.
- [42] P. M. Butala, H. Elgala, and T. D. Little, “SVD-VLC: A novel capacity maximizing VLC MIMO system architecture under illumination constraints,” in *Proc. of the IEEE Global Communication Conference Workshops (GLOBECOM Wkshps)*, Atlanta, GA, USA, Dec. 2013, pp. 1087–1092.
- [43] T. V. Pham, H. Le Minh, and A. T. Pham, “Multi-cell VLC: Multi-user downlink capacity with coordinated precoding,” in *Proc. of the IEEE International Conference on Communications Workshops (ICC Workshops)*, Paris, France, May 2017, pp. 469–474.

- [44] D. Bykhovsky and S. Arnon, “Multiple access resource allocation in visible light communication systems,” *IEEE Journal of Lightwave Technology*, vol. 32, no. 8, pp. 1594–1600, Apr. 2014.
- [45] Y. S. Eroğlu, İ. Güvenç, A. Şahin, Y. Yapıcı, N. Pala, and M. Yüksel, “Multi-element VLC networks: LED assignment, power control, and optimum combining,” *IEEE Journal on Selected Areas in Communications*, vol. 36, no. 1, pp. 121–135, Jan. 2018.
- [46] Z. Chen, D. Tsonev, and H. Haas, “Improving SINR in indoor cellular VLC networks,” in *Proc. IEEE Int. Conf. Commun. (ICC)*, Sydney, Australia, June 2014, pp. 3383–3388.
- [47] A. Tsiatmas, F. M. J. Willems, and S. Baggen, “Optimum diversity combining techniques for VLC systems,” in *Proc. IEEE Globecom Workshops*, Austin, TX, USA, Dec. 2014, pp. 456–461.
- [48] P. H. Pathak, X. Feng, P. Hu, and P. Mohapatra, “Visible light communication, networking and sensing: A survey, potential and challenges,” *IEEE Commun. Surveys and Tutorials*, vol. 17, no. 4, pp. 2047–2077, Oct. 2015.
- [49] T. Q. Wang, Y. A. Sekercioglu, and J. Armstrong, “Analysis of an optical wireless receiver using a hemispherical lens with application in MIMO visible light communications,” *J. Lightwave Technol.*, vol. 31, no. 11, pp. 1744–1754, Jun 2013.
- [50] J. Alarcn-Salazar, I. Zaldvar-Huerta, and M. Aceves-Mijares, “An optoelectronic circuit with a light source, an optical waveguide and a sensor all on silicon: Results and analysis of a novel system,” *Optics and Laser Technology*, vol. 84, pp. 40 – 47, 2016. [Online]. Available: <http://www.sciencedirect.com/science/article/pii/S0030399215306654>
- [51] A. Burton, H. L. Minh, Z. Ghassemlooy, S. Rajbhandari, and P. A. Haigh, “Smart receiver for VLC: Design and analysis,” in *Proc. IEEE Int. Symp. CSNDSP*, Poznan, Poland, Jul. 2012, pp. 1–5.
- [52] H. C. Hulst and H. C. van de Hulst, *Light scattering by small particles*. Courier Corp., 1957.
- [53] T. Ye, H. T. Kaur, S. Kalyanaraman, and M. Yuksel, “Large-scale network parameter configuration using an on-line simulation framework,” *IEEE/ACM Tran. on Networking*, vol. 16, no. 4, pp. 777–790, 2008.
- [54] I. Moreno and C.-C. Sun, “Modeling the radiation pattern of LEDs,” *Optics Express Journal*, vol. 16, no. 3, pp. 1808–1819, Feb. 2008.
- [55] H. Marshoud, P. C. Sofotasios, S. Muhaidat, G. K. Karagiannidis, and B. S. Sharif, “On the performance of visible light communication systems with non-orthogonal multiple access,” *IEEE Transactions on Wireless Communications*, vol. 16, no. 10, pp. 6350–6364, Oct. 2017.

- [56] I. Standardization, “Lighting for work places part 1: Indoor (ISO: 8995-1: 2002 e),” *International Commission on illumination, Vienna*, 2002.
- [57] X. Bi, J. Zhang, Y. Wang, and P. Viswanath, “Fairness improvement of maximum C/I scheduler by dumb antennas in slow fading channel,” in *IEEE 72nd Vehicular Technology Conference-Fall*, 09 2010, pp. 1–4.
- [58] Y. Song and G. Li, “Cross-layer optimization for OFDM wireless networks-Part I: Theoretical framework,” *IEEE Transactions on Wireless Communications*, vol. 4, no. 2, pp. 614–624, Apr. 2005.
- [59] H. Wu, Q. Wang, J. Xiong, and M. Zuniga, “SmartVLC: When smart lighting meets VLC,” in *Proceedings of the 13th International Conference on emerging Networking EXperiments and Technologies*. ACM, 2017, pp. 212–223.
- [60] O. Goldschmidt and D. S. Hochbaum, “Polynomial algorithm for the k-cut problem,” in *Proc. of the 29th IEEE Annual Symposium on Foundations of Computer Science*, 1988, pp. 444–451.
- [61] A. Alsharoa, H. Ghazzai, A. E. Kamal, and A. Kadri, “Optimization of a power splitting protocol for two-way multiple energy harvesting relay system,” *IEEE Transactions on Green Communications and Networking*, vol. 1, no. 4, pp. 444–457, Dec. 2017.
- [62] S. Boyd and L. Vandenberghe, *Convex Optimization*. New York, NY, USA: Cambridge University Press, 2004.
- [63] M. Grant and S. Boyd, “CVX: MATLAB software for disciplined convex programming, version 2.1,” <http://cvxr.com/cvx>, Mar. 2014.
- [64] B. music Netherlands. (2017) Lite gear LED PAR 30 7w lamp WW Edison 45gn. [Online]. Available: <https://www.bax-shop.nl/producten-uit-assortiment/lite-gear-led-par-30-7w-lamp-ww-edison-45g>
- [65] S. I. Mushfique, A. Alsharoa, and M. Yuksel, “MirrorVLC: Optimal mirror placement for multi-element VLC networks,” submitted 2020.
- [66] Z. Ghassemlooy, W. Popoola, and S. Rajbhandari, *Optical wireless communications: system and channel modelling with MATLAB®*. CRC press, 2019.
- [67] M. Saadi, T. Ahmad, Y. Zhao, and L. Wuttistikulkij, “An LED based indoor localization system using k-means clustering,” in *2016 15th IEEE International Conference on Machine Learning and Applications (ICMLA)*. IEEE, 2016, pp. 246–252.
- [68] S.-H. Yang, E.-M. Jung, and S.-K. Han, “Indoor location estimation based on led visible light communication using multiple optical receivers,” *IEEE Communications Letters*, vol. 17, no. 9, pp. 1834–1837, 2013.

- [69] K.-H. Park, H. M. Oubei, W. G. Alheadary, B. S. Ooi, and M.-S. Alouini, "A novel mirror-aided non-imaging receiver for indoor 2 x 2 mimo-visible light communication systems," *IEEE Transactions on Wireless Communications*, vol. 16, no. 9, pp. 5630–5643, 2017.
- [70] "Gurobi optimizer reference manual," 2016. Available [online]: <http://www.gurobi.com/>.
- [71] P. M. Pattison, M. Hansen, and J. Y. Tsao, "LED lighting efficacy: Status and directions," *Comptes Rendus Physique*, vol. 19, no. 3, pp. 134–145, 2018.